Analysis of supramolecular assemblies of NE81, the first lamin protein in a non-metazoan organism

DISSERTATION

Marianne Erika Grafe

Zur Erlangung des akademischen Grades

“doctor rerum naturalium“

(Dr. rer. nat.)

in der Wissenschaftsdisziplin “Zellbiologie“

eingereicht an der

Mathematisch-Naturwissenschaftlichen Fakultät

Institut für Biochemie und Biologie

Universität Potsdam

August 2019

Disputation: 18.12.2019

Betreuer:

Prof. Dr. Ralph Gräf (Hauptbetreuer), Universität Potsdam
Prof. Dr. Carsten Beta, Universität Potsdam

Gutachter:

Prof. Dr. Ralph Gräf, Universität Potsdam
Prof. Dr. Salvatore Chiantia, Universität Potsdam
Prof. Dr. Georg Krohne, Universität Würzburg

Kommission:

Prof. Dr. Otto Baumann (Vorsitz), Universität Potsdam
Prof. Dr. Carsten Beta, Universität Potsdam
Prof. Dr. Salvatore Chiantia, Universität Potsdam
Prof. Dr. Ralph Gräf, Universität Potsdam
Prof. Dr. Markus Grebe, Universität Potsdam

Published online at the
Institutional Repository of the University of Potsdam:
https://doi.org/10.25932/publishup-44180
https://nbn-resolving.org/urn:nbn:de:kobv:517-opus4-441802

Teile dieser Arbeit wurden bereits veröffentlicht:

M. Grafe[1], P. Batsios[1], I. Meyer[1], D. Lisin[1], O. Baumann[1], M. Goldberg[2], R. Gräf[1] (2019). "Supramolecular Structures of the *Dictyostelium* Lamin NE81". Cells. 2019 Feb 16;8(2). pii: E162. doi: 10.3390/cells8020162.

Teile dieser Arbeit wurden bereits auf Tagungen vorgestellt:

„International *Dictyostelium* Conference" in Eggmond aan Zee (Amsterdam), 2018.
Analysis of supramolecular assemblies of NE81, the first lamin-like protein in a unicellular organism Marianne Grafe[1], Petros Batsios[1], Otto Baumann[1], Martin W. Goldberg[2], Daria Lisin[1], Irene Meyer[1], Reimer Stick[4] and Ralph Gräf[1]

DGZ Meeting "Life at the edge: The nuclear envelope in nucleocytoplasmic transport and genome organization" in Potsdam, 2018.
Analysis of supramolecular assemblies of NE81, the first lamin-like protein in a unicellular organism Marianne Grafe[1] , Petros Batsios[1] , Otto Baumann[1] , Martin W. Goldberg[2] , Daria Lisin[1], Irene Meyer[1] , Reimer Stick[4], Ralph Gräf[1]

„International *Dictyostelium* Conference" in Geneva (Chavannes-de-Bogis), 2017.
Nuclear envelope proteins in the amoebozoan Dictyostelium discoideum
Petros Batsios[1], Otto Baumann[1], Martin W. Goldberg[2], Marianne Grafe[1], Denis A. Larochelle[3], Daria Lisin[1], Irene Meyer[1], Kristina Mitic[1] , Xiang Ren[3], Reimer Stick[4] and Ralph Gräf[1]

„International *Dictyostelium* Conference" in Tucson, Arizona, 2016.
Nuclear envelope organization in the amoebozoan Dictyostelium discoideum
Petros Batsios[1], Otto Baumann[1], Martin W. Goldberg[2], Marianne Grafe[1], Denis A. Larochelle[3], Daria Lisin[1], Irene Meyer[1], Xiang Ren[3], Reimer Stick[4] and Ralph Gräf[1]

[1]Institut für Biochemie und Biologie, Universität Potsdam, Karl-Liebknecht-Str. 24-25,14476 Potsdam, Germany

[2] School of Biological and Biomedical Sciences, The University of Durham, UK

[3] Department of Biology, Clark University, Worcester, MA, USA

[4] Institut für Zellbiologie, Universität Bremen, Germany

Abschlussarbeiten die aus dieser Arbeit hervorgegangen sind:

Thomas Suckau, 2016. *Isolierung und Lokalisation von rekombinanten Lamin Mutanten in Dictyostelium discoideum und zellfreien System.* Master Thesis, Universität Potsdam.

Daria Lisin, 2017. *Reinigung und Analyse von IF-Familie Proteinen aus Dictyostelium Amöben.* Bachelor Thesis, Universität Potsdam.

Oda-Emilia Meyfarth, 2017. *Heterologe Expression von Xenopus Lamin LIII in Dictyostelium discoideum.* Bachelor Thesis, Universität Potsdam.

Phillip Hofmann, 2019. *Lichtsensitive Regulation der Lamin-Polymerisation bei Dictyostelium discoideum.* Bachelor Thesis, Universität Potsdam.

Table of Contents

LIST OF ABBREVIATIONS

APS	ammonium peroxydisulfate
BAF	barrier-to-autointegration factor
BCIP	5-bromo-4-chloro-3-indolyl-phosphate
BLAST	basic local alignment search tool
BLUF	sensors of blue light using flavin adenine dinucleotide
bp	base pairs
cAMP	cyclic adenosine monophosphate
CDK	cyclin dependent kinase
Cryo-EM	cryogenic electron microscopy
DAPI	4′,6-diamidin-2-phenylindol
DNA	Deoxyribonucleic acid
ECL	enhanced chemiluminescence
ER	endoplasmic reticulum
ESCRT	endosomal sorting complexes required for transport
ExM	expansion fluorescence microscopy
FACE1	farnesylated-proteins converting enzyme
FCS	fluorescence correlation spectroscopy
feSEM	field-emission scanning electron microscopy
FL	full length
FRAP	fluorescence recovery after photobleaching
GFP	green fluorescent protein
GUV	giant unilamellar vesicle
IF	intermediate filament
INM	inner nuclear membrane
Ig-fold	immunoglobulin fold
KASH	Klarsicht/ANC-1/Syne/homology
kDa	kilo Dalton
KO	knockout
LBR	lamin B receptor
LEM	LAP2/emerin/MAN1

LINC	linker of nucleoskeleton and cytoskeleton
LOV	light-oxygen-voltage
LTD	lamin tail domain
MEF	mouse embryonic fibroblasts
MSC	MAN1–Src1p–C-terminal
MTOC	microtubule organizing center
NBT	nitroblue tetrazoliumchlorid
NE	nuclear envelope
NEBD	nuclear envelope breakdown
Ni-NTA	Nickel nitrilotriacetic acid
NLS	nuclear localization signal
NPC	nuclear pore complex
ONM	outer nuclear membrane
PAGE	polyacrylamide gel electrophoresis
PBS	phosphate buffered saline
PCR	polymerase chain reaction
PenStrep	penicillin/streptomycin
POD	horseradish peroxidase
PSF	point spread function
Rce1	Ras converting enzyme 1
Rpm	revolutions per minute
SAR	Stramenopila, Alveolata, and Rhizaria
SD	standard deviation
SDS	sodium dodecyl sulfate
SIM	structured illumination microscopy
SLiCE	seamless ligation cloning extract
STED	stimulated emission depletion
TBS	Tris buffered saline
TEM	transmission electron microscopy
TEMED	N,N,N',N'-tetramethylethylendiamin
Tris	Tris(hydroxymethyl)-aminomethan
Triton X-100	t-Octylphenoxypolyethoxyethanol
UTR	untranslated region
WT	wild type
Zmpste24	zinc metallopeptidase STE24

ZUSAMMENFASSUNG

Lamine sind Proteine an der inneren Kernhülle und bilden zusammen mit verbundenen Proteinen die nukleäre Lamina. Dieses Netzwerk sorgt für die Stabilität des Zellkerns und unterstützt die Organisation des Zell-Zytoskeletts. Zusätzlich sind Lamine und ihre verbundenen Proteine in viele Prozesse wie Genregulation und Zelldifferenzierung involviert. Bis 2012 war der Stand der Forschung, dass nur bei mehrzelligen Organismen eine nukleäre Lamina zu finden ist. NE81 ist das erste lamin-ähnliche Protein, das in einem nicht-mehrzelligen Organismus (*Dictyostelium discoideum*) entdeckt wurde. Es hat viele Eigenschaften und Strukturmerkmale mit Laminen gemeinsam. Dazu zählt der dreiteilige Aufbau des Proteins, eine Phosphorylierungsstelle für ein Zellzyklus-abhängiges Enzym, ein Kernlokalisationssignal, wodurch das Protein in den Kern transportiert wird, sowie eine C-terminale Sequenz zur Verankerung des Proteins in der Kernhülle. In dieser Arbeit wurden verschiedene Methoden zur vereinfachten Untersuchung von Laminstrukturen getestet, um zu zeigen, dass sich NE81 wie bereits bekannte Lamin-Proteine verhält und supramolekulare Netzwerke aus Laminfilamenten bildet. Zur Analyse der Struktur supramolekularer Anordnungen wurde das Protein durch Entfernen des Kernlokalisationssignals auf der äußeren Kernhülle von *Dictyostelium* gebildet. Die anschließende Untersuchung der Oberfläche der Kerne mit einem Rasterelektronenmikroskop zeigte, dass NE81 Strukturen in der Größe von Laminen bildet, allerdings nicht in regelmäßigen filamentösen Anordnungen. Um die Entstehung der Laminfilamente zu untersuchen, wurde lösliches NE81 aus *Dictyostelium* aufgereinigt und mit verschiedenen mikroskopischen Methoden untersucht. Dabei wurde festgestellt, dass NE81 unter Niedrigsalz-Bedingungen dünne, fadenförmige Strukturen und Netzwerke ausbildet, die denen von Säugetier-Laminen sehr ähnlich sind. Die Mutation der Phosphorylierungsstelle von NE81 zu einer imitierenden dauerhaften Phosphorylierung von NE81 in der Zelle, zeigte zunächst ein gelöstes Protein, das überraschenderweise unter Blaulichtbestrahlung der Zelle wieder lamin-ähnliche Anordnungen formte.

Die Ergebnisse dieser Arbeit zeigen, dass NE81 echte Laminstrukturen ausbilden kann und hebt *Dictyostelium* als Nicht-Säugetier-Modellorganismus mit einer gut charakterisierten Kernhülle, mit allen relevanten, aus tierischen Zellen bekannten Proteinen, hervor.

ABSTRACT

Nuclear lamins are nucleus-specific intermediate filaments forming a network located at the inner nuclear membrane of the nuclear envelope. They form the nuclear lamina together with proteins of the inner nuclear membrane regulating nuclear shape and gene expression, among others. The amoebozoan *Dictyostelium* NE81 protein is a suitable candidate for an evolutionary conserved lamin protein in this non-metazoan organism. It shares the domain organization of metazoan lamins and is fulfilling major lamin functions in *Dictyostelium*. Moreover, field-emission scanning electron microscopy (feSEM) images of NE81 expressed on *Xenopus* oocytes nuclei revealed filamentous structures with an overall appearance highly reminiscent to that of metazoan *Xenopus* lamin B2. For the classification as a lamin-like or a *bona fide* lamin protein, a better understanding of the supramolecular NE81 structure was necessary. Yet, NE81 carrying a large N-terminal GFP-tag turned out as unsuitable source for protein isolation and characterization; GFP-NE81 expressed in *Dictyostelium* NE81 knock-out cells exhibited an abnormal distribution, which is an indicator for an inaccurate assembly of GFP-tagged NE81. Hence, a shorter 8×HisMyc construct was the tag of choice to investigate formation and structure of NE81 assemblies. One strategy was the structural analysis of NE81 *in situ* at the outer nuclear membrane in *Dictyostelium* cells; NE81 without a functional nuclear localization signal (NLS) forms assemblies at the outer face of the nucleus. Ultrastructural feSEM pictures of NE81ΔNLS nuclei showed a few filaments of the expected size but no repetitive filamentous structures. The former strategy should also be established for metazoan lamins in order to facilitate their structural analysis. However, heterologously expressed *Xenopus* and *C. elegans* lamins showed no uniform localization at the outer nuclear envelope of *Dictyostelium* and hence, no further ultrastructural analysis was undertaken. For *in vitro* assembly experiments a *Dictyostelium* mutant was generated, expressing NE81 without the NLS and the membrane-anchoring isoprenylation site (HisMyc-NE81ΔNLSΔCLIM). The cytosolic NE81 clusters were soluble at high ionic strength and were purified from *Dictyostelium* extracts using Ni-NTA Agarose. Widefield immunofluorescence microscopy, super-resolution light microscopy and electron microscopy images of purified NE81 showed its capability to form filamentous structures at low ionic strength, as described previously for metazoan lamins. Introduction of a phosphomimetic point mutation (S122E)

into the CDK1-consensus sequence of NE81 led to disassembled NE81 protein *in vivo*, which could be reversibly stimulated to form supramolecular assemblies by blue light exposure.

The results of this work reveal that NE81 has to be considered a *bona fide* lamin, since it is able to form filamentous assemblies. Furthermore, they highlight *Dictyostelium* as a non-mammalian model organism with a well-characterized nuclear envelope containing all relevant protein components known in animal cells.

1 Introduction

1.1 Nuclear envelope organization

1.1.1 The metazoan nuclear envelope

The nuclear envelope consists of two lipid bilayers: the outer nuclear membrane is associated with the endoplasmic reticulum (ER) whereas the inner nuclear membrane is bound to an underlying protein meshwork. These membranes separate the cytoplasm with its protein synthesis machinery from the cellular DNA and the gene expression organization. Both nuclear membranes are contiguous at the nuclear pore complexes. The latter are channels spanning the membranes. They are composed of nucleoporins and allow bidirectional trafficking via Ran-GTPase-dependent transport (Beck and Hurt, 2017). The inner nuclear membrane is associated with the nuclear lamina, mainly consisting of specialized intermediate filaments called lamins and nuclear envelope transmembrane proteins (NETs). The lamin network is directly bound to chromatin, LEM proteins (LAP1, Emerin and MAN1), BAF (barrier-to-autointegration factor) as well as the lamin B receptor (LBR), and to the LINC complex that connects it with protein filaments in the cytoplasm (cytoskeleton)(Figure 1). The LINC complex includes the Sun proteins at the nucleoplasmic side which are bound to KASH domain proteins, connected to the centrosome and to Nesprins, attached to the cytoskeleton (Tapley and Starr, 2013). The centrosome is the microtubule organizing center or MTOC. The non-membranous organelle nucleates and organizes microtubules and supports the coordination of the mitotic spindle. In metazoan cells, usually undergoing an open mitosis with cytoplasmic spindle assembly, it starts with the nuclear envelope breakdown (NEBD). The phosphorylation of nucleoporin and lamins by cyclin dependent kinases (CDKs) leads to nuclear pore complex disassembly and depolymerization of the lamin meshwork (Laurell et al., 2011, Torvaldson et al., 2015). After cell division, the ESCRT machinery, that is also involved in membrane fusion during cytokinesis, helps in nuclear envelope reformation and mitotic spindle disassembly (Vietri et al., 2015).

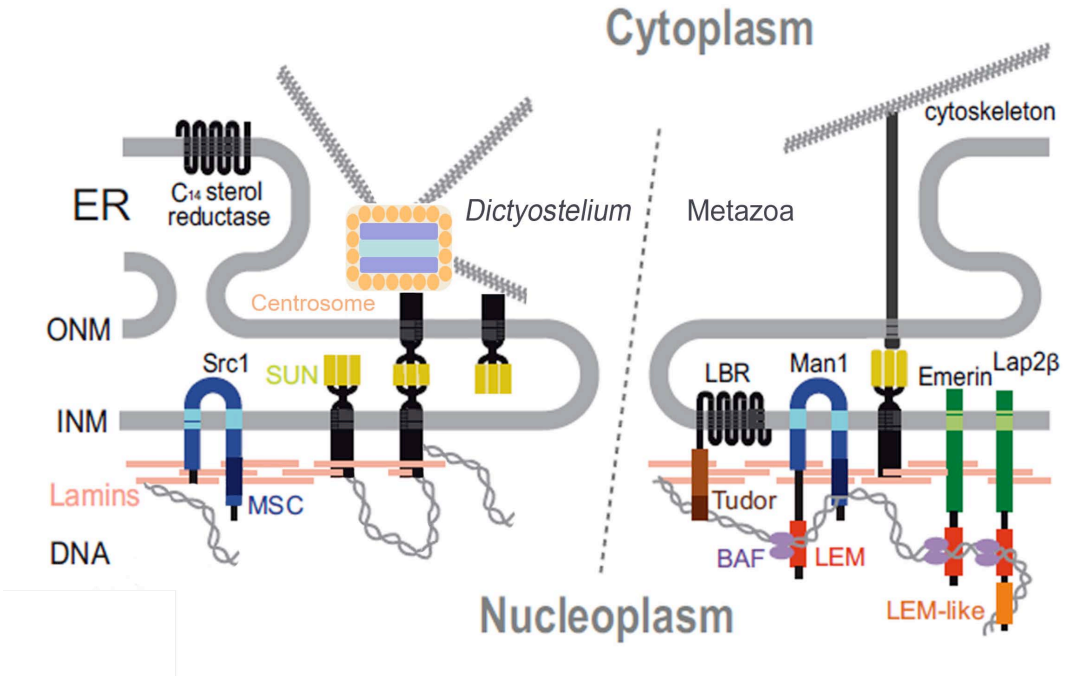

Figure 1 Nuclear envelope organization in *Dictyostelium* (left) and metazoans (right), adapted from Koreny and Field (2016). A part of a simplified nucleus is shown with substantial proteins drawn as cartoons. The proteins are embedded within the nuclear envelope or associated with it. ER: endoplasmic reticulum. ONM: outer nuclear membrane. INM: inner nuclear membrane. The structures and proteins are not shown in an exact scale.

1.1.2 The nuclear envelope in Dictyostelium discoideum

The model organism *Dictyostelium discoideum* (*D. discoideum*) is a non-metazoan eukaryote. As in all eukaryotes, the *Dictyostelium* nuclear envelope consists of two nuclear membranes. Other than in Metazoa, the LINC complex protein Sun1 is associated with both nuclear membranes and connects the nucleus with the centrosome (Gräf et al., 2015)(Figure 1). At the inner nuclear membrane, it interacts with NE81 and is associated with centromere proteins to help clustering the centromeres in the pericentrosomal region. NE81 is part of a nuclear lamina and was the first lamin protein discovered in a unicellular organism (Krüger et al., 2012). The indirect linkage of centrosome to the nuclear lamina could be mediated by self-interaction between SUN-domains, by another unknown protein and/or the unusual kinesin Kif9, which resides in the outer nuclear membrane. Another protein found at the outer nuclear membrane is the C_{14} sterol reductase Erg24. Although *Dictyostelium* has no lamin B receptor itself, the C_{14} sterol reductase domain of Erg24 is a C-terminal part of the lamin B receptor. The domain is common among all eukaryotes (Koreny and Field, 2016).

However, Erg24 is missing the N-terminal tudor domain of the lamin B receptor that binds to lamin and chromatin in metazoan nuclei. Unlike Erg24, the LEM-like protein Src1 does bind to NE81, which contributes to formation of the nuclear lamina and stabilization of the inner nuclear membrane (Batsios et al., 2016). The C-terminal MSC (MAN1–Src1p–C-terminal) domain of the LEM-domain proteins is well conserved and contains a helix-turn-helix motif. Usually the LEM-like and MSC domains bind directly to chromatin, whereas the LEM domain binds the DNA via BAF, which is not present in the *Dictyostelium* nuclear envelope.

Dictyostelium cells undergo a semi-closed mitosis without a nuclear envelope breakdown. Nevertheless, the nuclear lamina gets phosphorylated by CDK1, leading to a better nucleoplasmic deformability (Krüger et al., 2012). It is assumed that simultaneous phosphorylation of nuclear pore complexes causes an enhanced permeability that allows the centrosomal spindle-assembly to be incorporated into the nuclear envelope, as it has been shown to be the case in semi-closed mitosis of *Aspergillus* (Osmani et al., 2006).

1.2 Lamins

1.2.1 Lamin sequence organization

Lamins are nucleus-specific intermediate filaments building the nuclear lamina, a dense protein network localized at the inner nuclear membrane. Lamins are classified as type V intermediate filament proteins and share a typical tripartite domain organization, containing a central rod domain flanked by head and tail domains (Gruenbaum and Foisner, 2015)(Figure 2). The head domain has a CDK1 consensus sequence for phosphorylation right before the coiled-coil rod domain usually containing four α-helical segments. The tail domain includes a nuclear localization signal (NLS) at its beginning, followed by a lamin tail domain (LTD) and a CaaX box (=cysteine, two aliphatic amino acids and X for any amino acid specifying the type of isoprene moiety) for prenylation at the C-terminal end. The LTD is highly conserved among metazoans and folds into an immunoglobulin-like domain (Dhe-Paganon et al., 2002).

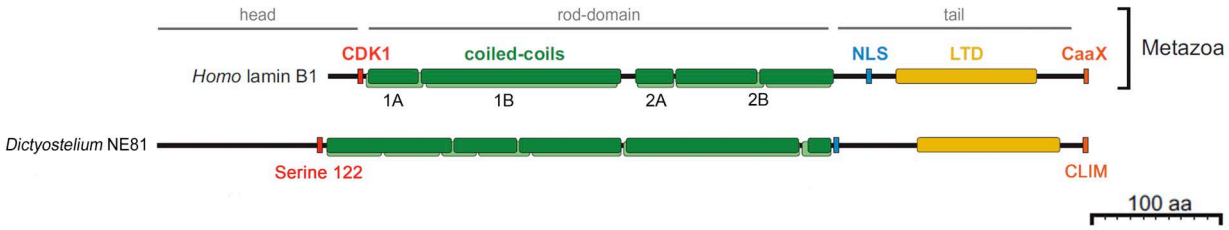

Figure 2 Lamin sequence organization of eukaryotes, adapted from Koreny and Field (2016). Lamins have a tripartite domain organization similar to intermediate filaments containing a central rod domain flanked by head and tail domains. Sequence motifs and structural elements are indicated: CDK1 phosphorylation consensus sequence (red), nuclear localization signal = NLS (blue), lamin tail domain = LTD (yellow), CaaX box motif (orange). Coiled-coil regions and gaps in the α-helical segments (1A, 1B, 2A, and 2B) were predicted in Marcoil (dark green) and Pcoils (light green). *Dictyostelium* lamin NE81 shares all relevant sequence motifs and structural elements of metazoan lamins. The main CDK1 site of NE81 is at amino acid 122 (serine) and the CaaX box consists of cysteine, leucine, isoleucine, and methionine (CLIM).

1.2.2 Lamin genes

Lamins can be subdivided into A- and B-types, based on their sequence homologies and biochemical properties. All metazoan cells express at least one B-type lamin, whereas A-type lamins are mainly expressed in differentiated cells. The mammalian genome has three lamin genes encoding four major and three minor lamin isoforms (Dittmer and Misteli, 2011). *LMNA* codes for the two major isoforms lamins A and C. Lamin C is an A-type lamin and arises by alternative splicing. The two major B-type isoforms B1 and B2 are derived from the two genes *LMNB1* and *LMNB2*, the minor isoform lamin B3 is only expressed in germ cells. Vertebrates like *Xenopus laevis* share an additional B-type gene *LIII*, coding for lamin LIII that is likewise exclusively expressed in oocyte nuclei. Although invertebrate lamins share the general sequence organization of vertebrate lamins, they are more divergent. The nematode *Caenorhabditis elegans* (*C. elegans*) has one B-type gene, *lmn1* coding for Ce-lamin, whereas *Drosophila melanogaster* has two lamin genes expressing the A-type lamin LmC and a B-type lamin Dm0 (Riemer and Weber, 1994, Dechat et al., 2010).

1.2.3 Lamin processing

After translation the pre-lamin A, B1 and B2 proteins undergo post-translational modification. The processing follows a sequence of highly regulated steps starting with attachment of an isoprenoid group to cysteine of the CaaX box by a farnesyltransferase. The last amino acid

(X) specifies whether a farnesyl (X is a serine, alanine, methionine, or glutamine) or a geranylgeranyl (X is a leucine) group will be covalently attached (Barton and Worman, 1999). In the next step, the last three residues (-aaX) are removed by a prenyl protease that is a zinc metalloproteinase. In humans, two proteins have been identified: RCE1 (Ras-converting enzyme 1) and Zmpste24/FACE1 (farnesylated-proteins converting enzyme). Hereafter, the carboxylic acid group gets methylated by the isoprenylcysteine carboxyl methyltransferase (ICMT). Since B-type lamins remain isoprenylated and bind to the nuclear membrane through their lipid anchor, the latter step leads to mature lamin B1 and B2. In case of pre-lamin A, additional 15 C-terminal residues including the modified cysteine, are cleaved off by Zmpste24/FACE1 resulting in mature lamin A. The splicing variant lamin C is 74 residues shorter containing no CaaX box and is therefore not processed (Dechat et al., 2008).

1.2.4 Lamin assembly and supramolecular structure

All intermediate filaments including lamins share an α-helical rod domain, which promotes the formation of higher-order polymers. The domain contains four subhelical segments (1A, 1B, 2A, and 2B) forming heptad-repeats that are typical for coiled-coil proteins (Figure 2). The heptad consists of a seven amino acid repeating unit (a-b-c-d-e-f-g) with hydrophobic residues in first (a) and fourth (d) position (Strelkov et al., 2003)(Figure 3 A). Experiments with *in vitro* purified lamins have shown that lamin monomers form a coiled-coil dimer (Karabinos et al., 2003), by association of two α -helical rod domains into a left handed superhelix. The dimers polymerize into a polar head-to-tail structure, arranged in a staggered conformation with a short overlapping tetrameric region. Next, the lateral assembly of two head-to-tail polymers forms a protofilament. In case of Ce-lamin three or four protofilaments assemble into 10 nm thick filaments (Ben-Harush et al., 2009). Since most lamin filaments do not form stable 10-nm filament populations, but assemble into paracrystalline arrays *in vitro*, most *in vitro* studies were undertaken with Ce-lamin.

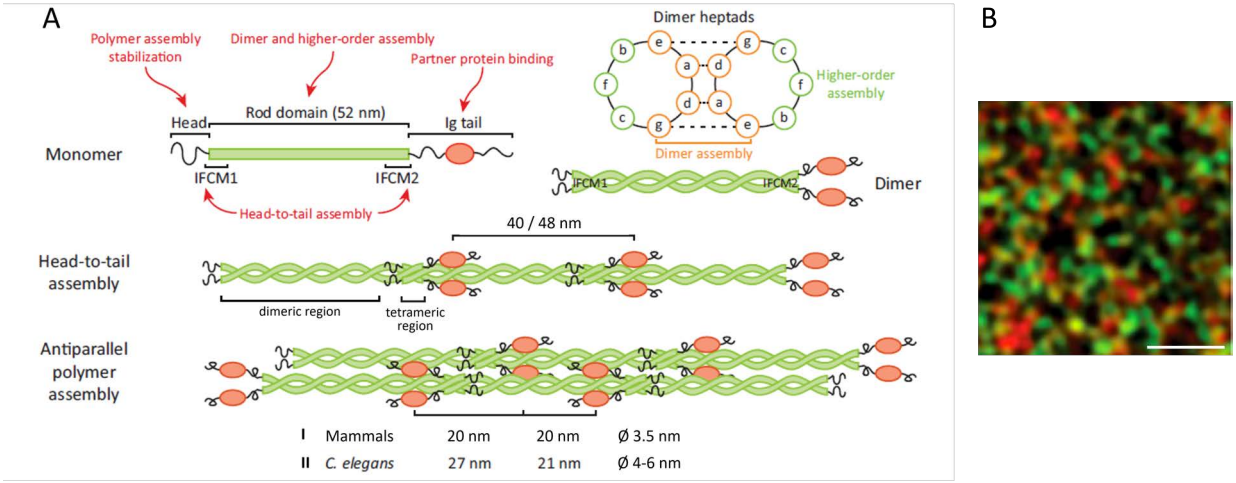

Figure 3 Lamin assembly and supramolecular structure. **A**: Lamin assembly scheme adapted from Davidson and Lammerding (2014). IFCM = intermediate filament consensus motif. Dimers assemble into dimeric head-to-tail polymers with short overlapping tetrameric regions; two head-to-tail polymers build a protofilament. I: Diameter of a lamin filament in mammalian cells is taken from Turgay et al. (2017). II: Diameter of a filament of *C. elegans* lamin in *Xenopus* oocyte is taken from Grossman et al. (2012). **B**: Lamin meshwork of different lamin isoforms in mouse embryonic fibroblasts, shown with indirect immunofluorescence in a high resolution 3D-SIM image, taken from Shimi et al. (2015); Red: Lamin B1, green: Lamin A; Scale bar = 1 µm.

The first *in vivo* determinations showing the supramolecular structure of lamins were done by Aebi and co-workers (1986). Electron microscopy images of the nuclear envelope from *Xenopus* oocytes revealed a lamin meshwork at the inner nuclear membrane that appeared highly ordered with orthogonally arranged filaments exhibiting a thickness of ~10.5 nm and a spacing of ~52 nm. Since lamins are tightly bound to chromatin at the inner nuclear membrane, a dissection of the nuclear lamina without disruption of the network is hampered in most cell types. Therefore, the *Xenopus* system was chosen to examine different lamins. Due to the large size of *Xenopus* egg nuclei, the nuclear envelope can easily manually be dissected. Somatic B-type lamins expressed in *Xenopus* oocytes and analyzed by field-emission scanning electron microscopy (feSEM) formed 10-nm filaments arranged in a two-dimensional lattice, displaying a narrower spacing than measured for lamin LIII. A-type lamins formed even thicker filaments arranged in a more irregular, three-dimensional pattern (Goldberg et al., 2008). The *Dictyostelium* lamin NE81 expressed in *Xenopus* oocytes and analyzed by feSEM revealed short filaments, with an overall appearance very reminiscent of *Xenopus* lamin B2. (Grafe et al., 2019). These studies underline, that filament size and lamin network organization varies widely between organisms.

1.2.5 Lamin function and laminopathies

Lamins are associated with the inner nuclear membrane and assemble into a fibrous meshwork together with transmembrane proteins. The different lamin types have distinct locations in the nucleus. Super-resolution light microscopy analysis disclosed the distinct composition of the mammalian nuclear lamina (Figure 3 B). The images revealed that A- and B-type lamins form a non-homogenous composite meshwork where distinct lamins self-assemble into independent protein complexes (Xie et al., 2016, Shimi et al., 2015). B-type lamins are mainly found at the inner nuclear membrane and are expressed in every cell independently of it differentiation state. They are involved in cellular differentiation, cell proliferation and developmental processes (Dechat et al., 2010). Analyses of nuclear mechanics indicated that B-type lamins provide elastic properties and contribute to nuclear integrity, whereas A-type lamins are important for deformation-resistant stiffness of the nuclei (Lammerding et al., 2006). In addition, lamins are linked to chromatin and are involved in the formation of lamina-associated heterochromatin domains. Thus, they also control epigenetic gene regulation and differentiation (Van Bortle and Corces, 2013). These differences in expression patterns, structural features and dynamic properties were determined *in vivo* by FRAP analyses as well as fluorescence correlation spectroscopy (FCS) (Shimi et al., 2008).

Mutations in the lamin genes disrupt the numerous lamin functions in cells causing various human diseases called laminopathies. More than 600 mutations have been linked to at least fifteen diseases (de Leeuw et al., 2017). Mutations in the *LMNA* gene are more common, since A-type lamins are not essential. The emerging defects in expression and post-transcriptional processing cause disruptions of the lamin network or its interactions with LINC complexes (Lochs et al., 2019). Laminopathies can affect all tissue leading e.g. to muscular dystrophies (Emery–Dreyfuss muscular dystrophy), progeroid syndromes (Hutchinson–Gilford progeria syndrome), neuropathies (Charcot–Marie–Tooth disease), cardiomyopathies and lipodystrophies. In addition many cancer cells show an altered lamin expression, resulting in enhanced deformability of the nuclei, which facilitates metastasis (Davidson and Lammerding, 2014). There are two forms of laminopathy disease phenotypes. In the gene-

expression model, the mutations disable binding sites from lamin A/C that are important for epigenetic gene regulation and therefore provoke alterations in the gene expression pattern of A-type lamins. The structural-mechanical model links the disrupted nuclear lamina to a disrupted cytoplasmic filament formation, causing a change in nuclear morphology and 3D structure (Tatli and Medalia, 2018). The remarkable deformation of tissues under mechanical stress (e.g., blood vessels, muscle, skin) highlights the importance of lamins in mechanobiology (Isermann and Lammerding, 2013). Thus, the supramolecular structures formed by lamins and its organization *in vivo* is important to understand the etiology of these diseases.

1.2.6 Lamins in evolution

Lamins are the major cytoskeletal component of metazoan nuclei with every metazoan cell expressing at least one B-type lamin. Since they are even present in organisms possessing no cytoplasmic intermediate filaments, they are considered the most ancient form of intermediate filaments (Peter and Stick, 2015). The phylogenetic distribution was believed to be restricted to animals; for a long time, no lamins were found in unicellular organisms like fungi and amoebozoans or in plants. Recently, various fibrous protein assemblies associated with the nuclear membrane have been detected in non-metazoan organisms. While higher plants (Archaeplastida) and some unicellular Excavata such as *Trypanosoma* have specialized filamentous proteins that solely contain a coiled-coil domain, the model organism *Dictyostelium discoideum* expresses the lamin homologue NE81 that contains a tripartite domain organization similar to metazoan nuclear lamins (Figure 2). NE81 consist of 716 amino acids with a predicted 370 amino acid long α-helical coiled-coil region. The head domain has a CDK1 consensus sequence for phosphorylation positioned at amino acid 122 right before the rod domain. The tail domain includes a nuclear localization signal at its beginning, followed by a lamin tail domain and a CaaX box (-CLIM). NE81 gets isoprenylated and is tethered to the inner nuclear membrane by its prenyl anchor. It assembles along it in a two-dimensional manner as proposed for B-type lamins. Furthermore, NE81 fulfills major lamin functions in this organism (Krüger et al., 2012, Batsios et al., 2012). The identification of a lamin in the eukaryotic supergroup Amoebozoa led to the identification of other lamin-like proteins in

other eukaryotic clades previously thought to have no lamins. Bioinformatic sequence analyses found homologs of metazoan lamins in Opisthokonta including Choanoflagellata, Filasteria, and Ichtyosporea, in Amoebozoa, and in Dinoflagellata, Rhizaria, and Stramelopila of the SAR group (Kollmar, 2015). The correlation between the phylogenetic tree of identified lamins with the eukaryotic species topology supports the idea of a vertical evolution from the last eukaryotic common ancestor (Koreny and Field, 2016).

1.3 *Dictyostelium discoideum* as model organism

D. discoideum is a social amoeba that can exist in a unicellular and multicellular stage. The haploid eukaryote belongs to the supergroup Amoebozoa, which evolved together with the sister-group Opisthokonta (including Fungi and Metazoa) from the last eukaryotic common ancestor. Opisthokonta and Amoebozoa are sometimes also summarized under the term Amorphea (Adl et al., 2019). Dictyostelium amoebae live in forest soil and feed on bacteria, which are tracked through chemotaxis. On starvation the cells release cAMP as a chemoattractant and aggregate through chemotaxis. A slug is formed from the aggregate and orientates towards light. Although the slug phototaxis has been studied intensively for many decades (Fisher, 2001), its molecular basis is still unknown. The final stage of development of the multicellular structure is a fruiting body composed of stalk and spore cells. The spores can be harvested and are used e.g. for long-term storage of mutant strains. Since the natural NC4 isolate could grow only by phagocytosis of bacteria, new strains were generated capable of axenical growth in liquid media through macropinocytosis of nutrients (AX-strains) (Sussman and Sussman, 1967, Loomis, 1971). In complex nutrient medium (e.g. HL5C) the axenic mutants double every eight hours under optimal conditions. The cell cycle consists of a short S phase, no detectable G1 phase and a long G2 phase followed by a short M phase of 10-20 min (Weeks and Weijer, 1994). Numerous established molecular genetic techniques allow a direct manipulation of specific genes (Hirth et al., 1982). In transformations with common overexpression plasmids the DNA gets integrated ectopically, sometimes in tandem

repeats with varying repetitions (depending on the selection marker used) (Pang et al., 1999). Additionally, different methods are available for direct manipulation of specific genes by homologous recombination creating knockout or knockin mutants (Kuspa et al., 1995, Wiegand et al., 2011). Since *Dictyostelium* is haploid, these transformations are very efficient and effects of the mutation can be detected directly. Moreover, the tool of tagging genes with genetically encoded fluorescent proteins or epitope tags is commonly used for live cell imaging or in fluorescence microscopy (Levi et al., 2000).

The speed and low cost of cell culture and the easiness to create genetic manipulation makes *D. discoideum* a convenient model system to study fundamental cellular processes as well as general biomedical questions, including a wide-range of human diseases. The 34 megabases genome is organized in six chromosomes encoding a predicted number of 12,500 proteins. The genome size is comparable to the genome of the yeast model *Saccharomyces cerevisiae,* however *D. discoideum* amoebae share several homologous genes with higher eukaryotes that are absent in *Saccharomyces* (Eichinger et al., 2005). The high conservation of some proteins indicates their important role in evolution and could improve understanding the basis of many human diseases. *Dictyostelium* research fields include pathogen–host interactions, pathobiology of cell motility and chemotaxis, autophagy and protein aggregation disorders (e.g. ubiquitinated protein aggregates, which are also common features in pathologies like Alzheimer's and Parkinson's disease), complex mitochondrial diseases (e.g. blindness, epilepsy, muscle disorders) and neurological disorders (e.g. lissencephaly) (reviewed in Muñoz-Braceras et al., 2013; Meyer et al., 2011).

1.4 Aim of study

With the identification and characterization of NE81 as the first lamin protein in a non-metazoan organism it is likely that lamins have evolved much earlier in the Amorphea branch of the tree of life. To confirm NE81 as a *bona fide* lamin protein, it is necessary to determine if NE81 forms supramolecular structures similar to those of metazoan lamins. In this work, formation and structure of supramolecular NE81 assemblies will be investigated by different super-resolution light microscopy and electron microscopy methods and compared with well-examined metazoan lamin data. One strategy will be the structural analysis of NE81 *in situ* at the outer nuclear membrane of *Dictyostelium* nuclei. This method should also be established for metazoan lamins in order to facilitate their structural analysis and resolve their formation, since it is still unknown in most organisms. Secondly, supramolecular NE81 assemblies will be researched by *in vitro* studies with native, assembly-competent NE81.

2 Results

2.1 The small HisMyc-tag does not interfere with NE81 protein assembly

In order to investigate NE81, a protein tag is needed for visualization and purification. Published data and previous experiments on the NE81 protein were done with GFP as protein tag (Krüger et al., 2012, Batsios et al., 2016). Prior to using GFP as fluorescence and affinity tag it was necessary to exclude that the large N-terminal GFP-tag would interfere with NE81 assembly, as shown for other intermediate filaments such as human GFP-vimentin; when expressed with an NLS, the GFP-fusion protein was unable to form filaments in the nucleus but the filament formation could be rescued by co-expression of untagged vimentin (Kreplak et al., 2008).

The engineered small 8xHisMyc-tag (HHHHHHHH-AEEQKLISEEDL) with a size around 2.5 kDa consists of eight histidine (His) residues to facilitate purification of the NE81 protein, and a part of the *c-myc* gene sequence recognized by monoclonal 9E10 antibody for labeling. The HisMyc-tag like the 26.8 kDa sgGFP was used as N-terminal tag. The C-terminal coded CaaX box gets processed during post-translational modifications and hence, a C-terminal tag would get cleaved off. Overexpression plasmids were transformed in wild type AX2 cells and stable clones were identified by immunofluorescence and Western blot analysis. In GFP-NE81^{WT} and HisMyc-NE81^{WT} the endogenous *NE81* gene was disrupted by homologous recombination using a knockout cassette, creating NE81 knockout strains only expressing the NE81 fusion protein.

The transformed *Dictyostelium* cells were tested for expression of the respective fusion construct and moreover for knockout of the *NE81* gene by immunoblotting using a polyclonal anti-NE81/anti-rabbit antibody. Whole cell extracts of identical cell numbers were analyzed (Figure 4).

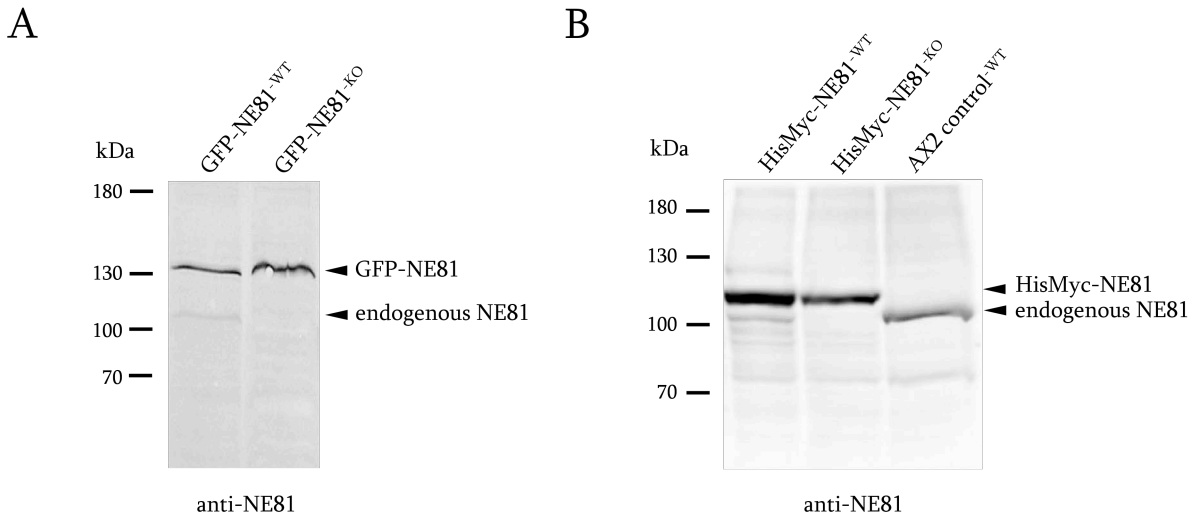

Figure 4 Expression of tagged and endogenous NE81 in wild type (WT) cells and NE81 knockout (KO) cells. Whole-cell extracts of $4{\cdot}10^5$ cells lysed in 10 µl urea buffer were loaded. Immunoblots labeled with anti-NE81, either made from **A**: 10% acrylamide gel and stained with anti-rabbit-alkaline phosphatase/NBT/BCIP (GFP tagged strains) or **B**: 8% PDA gel and visualized with anti-rabbit-horseradish peroxidase/ECL (AX2 control & HisMyc-tagged strains). Both knockout strains show the absence of endogenous NE81 in contrast to the wild type strains. All mutant strains show a band shift of the tagged protein compared to endogenous NE81.

NE81 has a size of 81 kDa but is typically visualized around 100 kDa in Western blot analysis. This could be caused by the post-translational modifications of NE81. The overexpression GFP-NE81^{WT} strain and HisMyc-NE81^{WT} strain showed a band shift of the tagged protein compared to endogenous NE81, that runs below the fusion proteins. Both knockout strains showed no band at the size of endogenous NE81 in contrast to the wild type strains. The mutants with the NE81 fusion protein expressed in wild type background had a weak endogenous NE81 band indicating its down regulation compared to AX2 control cells. Due to the small size difference between the endogenous NE81 protein and the HisMyc-NE81 fusion protein as well as the down regulation of the endogenous NE81 in this mutant, a specific PCR was necessary proving the correct insertion of the knockout cassette (Figure 5).

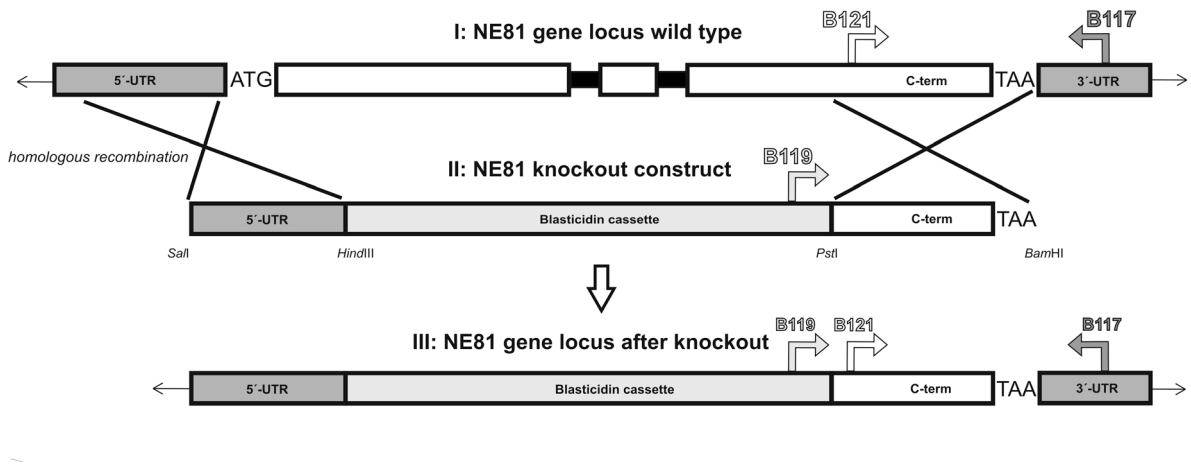

Figure 5 Scheme of (I) endogenous NE81 locus and (II) a knockout construct (plasmid containing a blasticidin cassette) for generating (III) a NE81 knockout strain. Verification of knockout strains: Positive control PCR1 for validation of genomic DNA with primers B121 binding inside the coding region (endogenous & plasmid DNA) and B117 binding in 3'UTR region (824 bp product). Knockout verification PCR2 with primer B119 binding exclusively in plasmid DNA region and primer B117 binding in 3'UTR region (845 bp product).

The NE81 knockout construct contains an 820 bp genomic DNA fragment from the 5´UTR region and a 680 bp fragment from the C-terminal coding region of the gene. Transformation of the linearized construct led to replacement of the chromosomal NE81 coding sequence through the blasticidin cassette. Additionally, the shortening of the promotor prevents expression of the C-terminal coding fragment. For a knockout verification (PCR2) that proves the correct integration of the construct, the PCR product need to start inside the blasticidin cassette (primer B119) and end outside in the 3'UTR region (B117). Secondly, to exclude false negative results by damaged genomic DNA, a positive control is required (PCR1). Here the forward primer B121 binds inside the C-terminal coding sequence (present in construct and endogenous DNA) and the same reverse primer B117 in the 3'UTR region resulting in an 824 bp product. All strains should be positive in PCR 1 (positive control) and just the knockout strains should have a product in PCR 2 (knockout verification). Genomic DNA was extracted from designated strains and verified with indicated PCR protocols (see 4.2.1). Results were visualized on Ethidium bromide stained agarose gel (Figure 6).

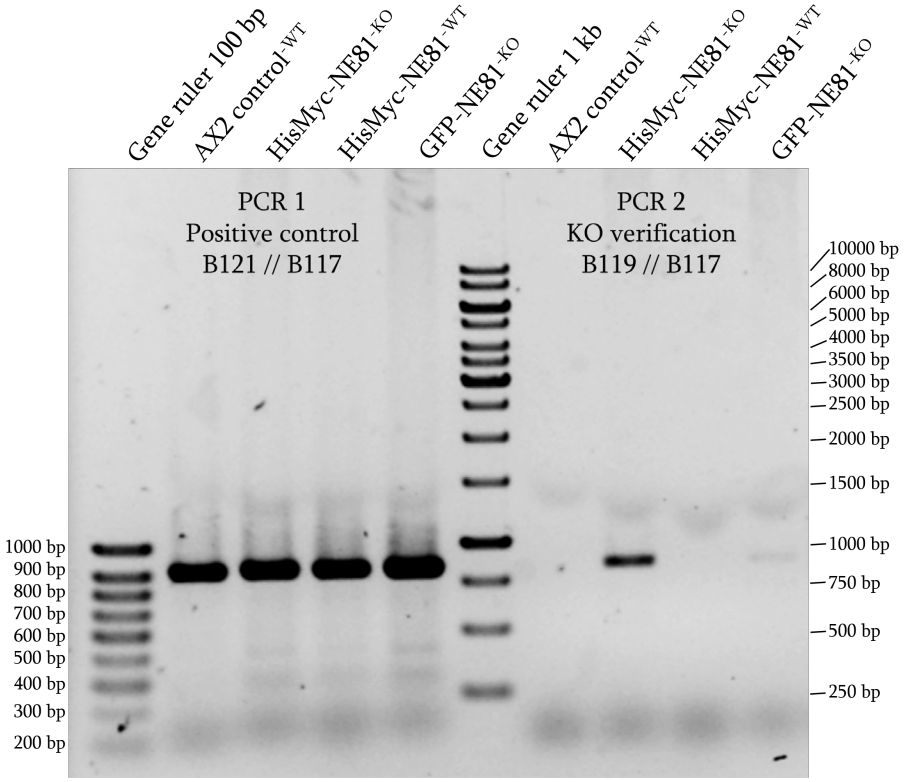

Figure 6 Knockout verification PCR with genomic DNA purified from wild type and mutant strains visualized on agarose gel. PCR1 (positive control): all strains show a PCR product in the right size around 824 bp. PCR 2 (knockout verification): only the knockout strains show a product in the right size around 845 bp.

The wild type control and HisMyc-NE81-^{WT} strain were positive in PCR 1, which confirmed an intact genomic DNA, and due to the lack of the blasticidin cassette they were negative in PCR 2. As expected, the two knockout strains had a product in both PCRs. In PCR 2 where the forward primer binds exclusively in a plasmid DNA region, the GFP-NE81^{-KO} and the HisMyc-NE81^{-KO} had a product around 845 bp, whereas the GFP-knockout strain was just weak positive. Hence, both knockout strains inserted the knockout construct and the endogenous *NE81* gene was disrupted.

Former experiments with identical genomic DNA and in some cases identical primer pairs, were constantly negative for no obvious reason. Su and colleagues (1996) discovered that lowering the extension temperature to 60°C is favorable for amplification of AT-rich regions as in *Plasmodium falciparum*. Since *Dictyostelium* terminators and 3'UTR regions are also AT-rich, reducing the extension temperature from 68°C to 60°C delivered the intended PCR results.

After verification of the knockout of endogenous NE81 it was tested, if the tags interfere with NE81 localization and function. For comparison wild type AX2 cells, HisMyc-NE81^{WT} and both NE81 knockout variants GFP-NE81^{KO} and HisMyc-NE81^{KO} were fixed on cover slip and stained with designated antibodies for fluorescence microscopy.

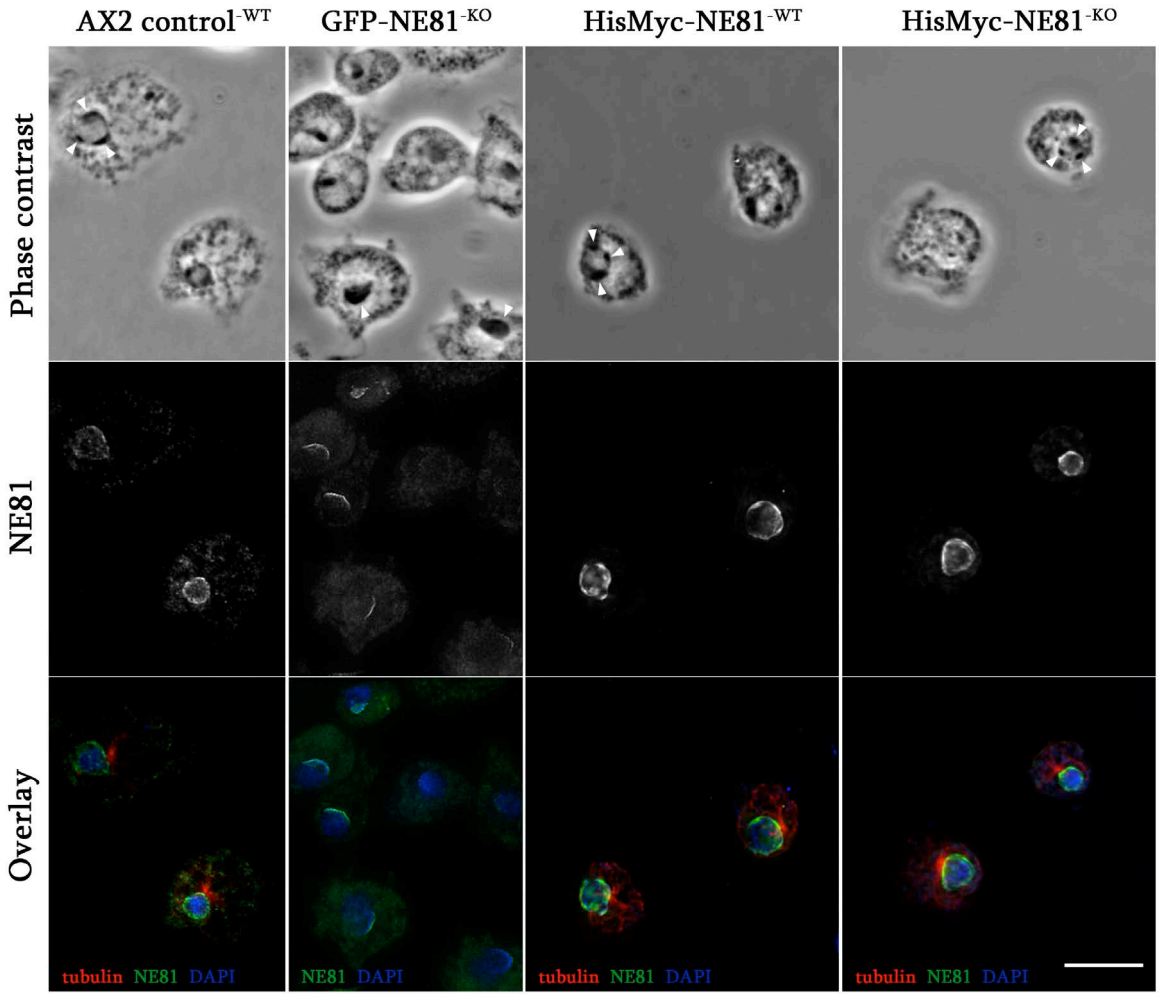

Figure 7 Expression of tagged NE81 in *Dictyostelium* wild type cells (WT) or NE81 knockout cells (KO). Fluorescence deconvolution microscopy using a PlanApo 1.4/100× objective. Cells were fixed on cover slip with glutaraldehyde and stained with DAPI. Additional staining: wild type AX2 cells (anti-NE81/anti-rabbit-Alexa Fluor 488), HisMyc-NE81^{KO}, HisMyc-NE81^{WT} (anti-Myc/anti-mouse-Alexa Fluor 488) and anti-tubulin/anti-rat-Alexa Fluor 568. Arrowheads indicate nucleoli in phase contrast images. Merged images show NE81 in green, DAPI in blue and if outlined tubulin in red. Scale bar = 5 µm.

GFP-tagged full length NE81 expressed in the endogenous NE81 background in *Dictyostelium* had the same localization as endogenous NE81 (Krüger et al., 2012). When the endogenous *NE81* gene was disrupted and the GFP-NE81^{KO} cells were forced to live with GFP-fusion protein only, GFP-NE81 showed a pericentrosomal, crescent-like distribution at the

nuclear envelope indicating an interference of the GFP-tag with NE81 assembly (Figure 7). Furthermore, nucleoli visible as perinuclear dark zones in phase-contrast images were clustered into one nucleolus (arrowheads), located at the pericentrosomal GFP-NE81 region, instead of the usual two to three nucleoli in wild type cells (first column AX2). In contrast, NE81 knockout cells expressing the N-terminal HisMyc-tagged NE81 variant (HisMyc-NE81^{KO}) showed an even distribution of HisMyc-NE81 at the nuclear envelope and a normal number of nucleoli, which was also observed in cells still expressing endogenous NE81 (wild type AX2 and HisMyc-NE81^{WT}).

The abnormal distribution of GFP-NE81 in NE81 knockout cells indicates that GFP-NE81 is not completely functional and is not able to assemble accurately. Therefore, instead of using GFP-NE81 variants for further structural analysis of NE81, the shorter N-terminal 8×HisMyc construct was the tag of choice to investigate formation and structure.

2.2 Analysis of NE81ΔNLS assemblies at the outer nuclear membrane

In most experimental systems a microscopic analysis of lamin assemblies *in situ* is hampered by their close association with chromatin. Ultrastructural analysis of membrane-associated lamin assemblies was for a long time only successful in the *Xenopus* system. Due to the large size of *Xenopus* egg nuclei and their rapid cell cycles switching only between S and M-phase, their nuclear envelope can manually be dissected and the inner nuclear membrane can be exposed without the usually bound chromatin. Preliminary experiments had shown that NE81 without a functional NLS (GFP-NE81ΔNLS) localizes at the outer nuclear envelope (Dr. Petros Batsios, unpublished data). Since there is no disturbing association with chromatin, the *Dictyostelium* nuclei isolated from this cell line were expected to provide a promising specimen for the analysis of NE81 assemblies at the nuclear surface with various techniques.

Two cell lines with ectopic integration of the HisMyc-construct were generated; one with a G418 selection marker controlled by a V18-promotor and one with a blasticidin resistance controlled by an act15-promotor. The G418 resistance construct leads to chromosomal

tandem insertions (up to 200-times), whereas plasmids with the blasticidin cassette usually generate single insertions, hence the fusion protein is less expressed compared to the first one (Pang et al., 1999). Screening for expression of the fusion protein was done by fluorescence microscopy and Western blot analysis. In positive mutants the protein bands were densitometrically evaluated to estimate the NE81ΔNLS protein expression levels (Figure 8).

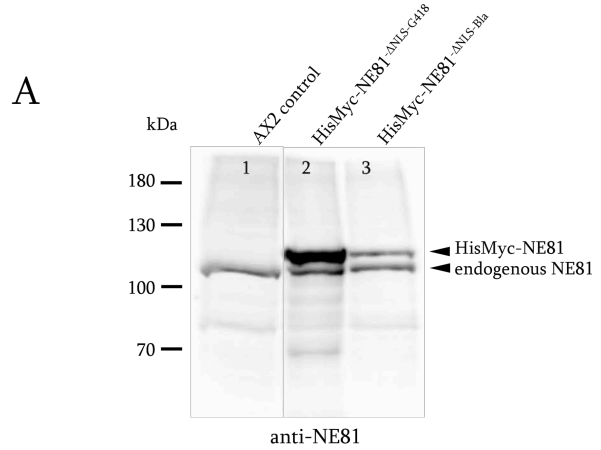

B

Expression levels

	2	3
HisMyc-NE81	3,59	0,72
endogenous NE81	1	1

Figure 8 Expression of endogenous and tagged NE81 in AX2 control cells and NE81ΔNLS mutant strains. **A**: Immunoblot showing relative expression levels of endogenous NE81 compared to the tagged HisMyc-NE81ΔNLS variants. Whole-cell extracts of $4{\cdot}10^5$ cells lysed in 10 µl urea buffer were loaded. Immunoblot was stained with anti-NE81/anti-rabbit-horseradish peroxidase and visualized with ECL. Loading per lane was proved by Ponceau S protein staining. Lane 2 showed overloading and lane 3 was underload. Therefore, expression levels cannot be compared with the control but the relative expression levels of endogenous NE81 compared to the overexpressed NE81 with one another. **B**: Expression levels of NE81, densitometrical measurements of immunoblot bands were done with ImageJ. Value of endogenous protein was set to 1 and fusion protein values were normalized.

Both mutant strains showed a band shift of the tagged protein compared to endogenous NE81, that runs below the fusion proteins (A). The moderate fusion protein expression of the blasticidin mutant NE81ΔNLS$^{\text{-Bla}}$ was confirmed by the Western blot analysis (B): the NE81ΔNLS protein expression level was slightly reduced compared to the endogenous NE81 protein (0.72 times). In contrast the G418 mutant NE81ΔNLS$^{\text{-G418}}$ showed a 3.6 times overexpression of the fusion protein.

For a better understanding, how the fusion protein behaves in cells, they were examined with expansion fluorescence microscopy (ExM) adapted from the protocols of the Boyden and Vaughan groups (Tillberg et al., 2016, Chozinski et al., 2016). Expansion microscopy is based on a physical enlargement of the specimen after its fixation in a swellable matrix and

expansion in water with a scale factor up to four times of the initial size. The cells were fixed on coverslips and the fusion proteins were labeled with α-Myc/anti-mouse-Alexa Fluor 488. The specimen was cross-linked with glutaraldehyde to a swellable polyacrylamide matrix and proteins were digested with Proteinase K to ensure isotropic swelling of the specimen. Afterwards the gel was expanded for two hours in water and the DNA was post-stained with Hoechst 33342 (Figure 9).

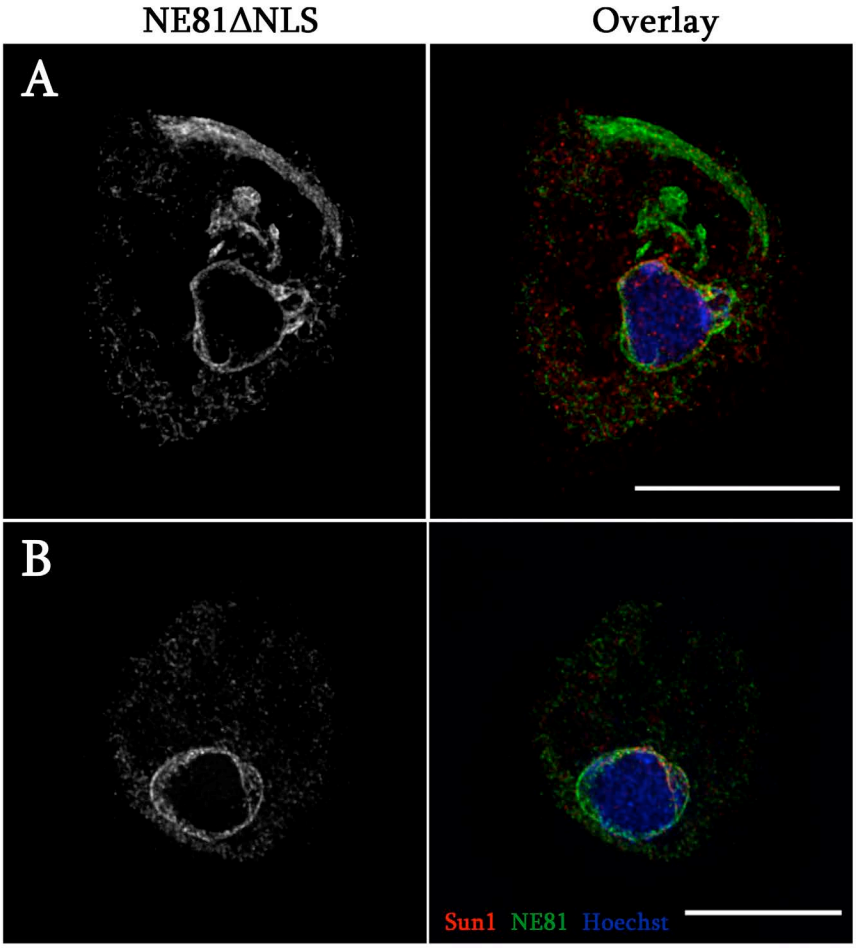

Figure 9 NE81ΔNLS localizes at the outer nuclear membrane in *Dictyostelium* cells. Expansion microscopy employing an LCI PlanNeo 1.3/63× objective and theoretical deconvolution. Cells were fixed with glutaraldehyde and stained with Hoechst 33342, anti-Myc/anti-mouse-Alexa Fluor 488, and anti-sun1/anti-rabbit-Alexa Fluor 568. Specimen were expanded as described and post-stained with Hoechst 33342. Merged images show Sun1 in red, NE81 in green and chromatin in blue. **A**: HisMyc-NE81ΔNLS (G418), **B**: HisMyc-NE81ΔNLS (blasticidin). Expansion factors are 3.8 in A and 3.7 in B; scale bars = 5 µm (referring to the original size).

HisMyc-NE81ΔNLS was located at the nuclear surface. Upon very strong overexpression with G418, the fusion protein localized at the nuclear envelope and at the endoplasmic reticulum (A), whereas the localization remained limited to the nuclear envelope during the more moderate expression with blasticidin selection (B). For that reason, the NE81ΔNLS

strain with moderate protein expression was used for ultrastructural surface analysis of NE81 lamin assemblies with field-emission scanning electron microscopy (feSEM).

The nuclei were isolated by density gradient centrifugation and prepared for feSEM according to Goldberg and Allen, 1992.

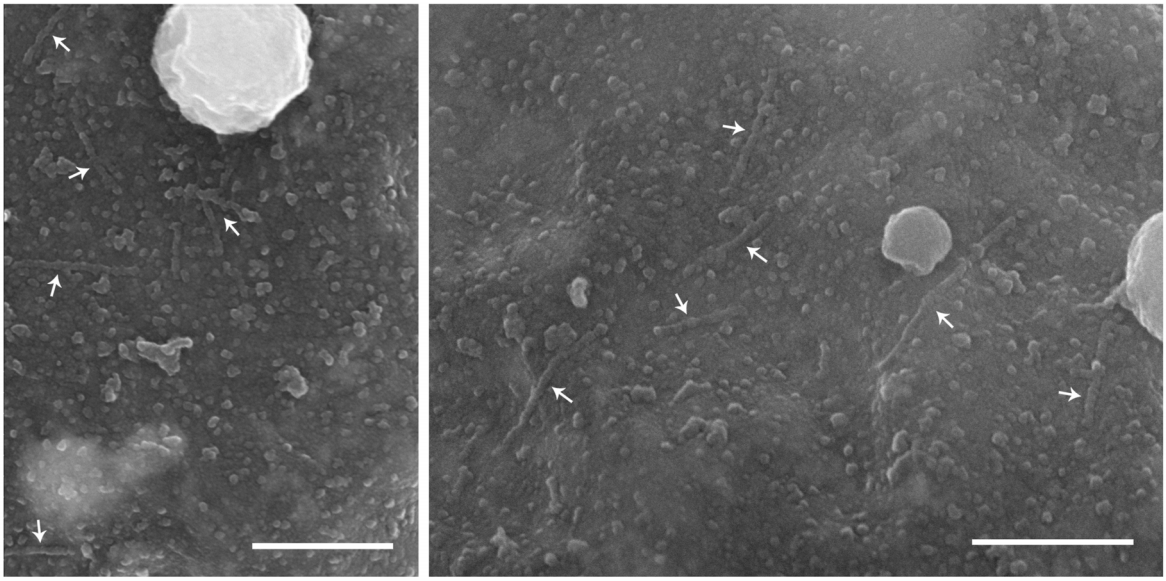

Figure 10 Structures at the outer nuclear membrane of *Dictyostelium* cells expressing HisMyc-NE81ΔNLS. feSEM image. Arrows indicate filamentous structures of the expected thickness of lamin structures according to the published diameter of NE81 filaments (Grafe et al., 2019). Scale bars = 200 nm.

The nuclei of NE81ΔNLS cells showed a lot background and just a few filaments in the expected size but no repetitive filamentous structures on the surface (Figure 10). NE81 filaments exhibited a diameter of 10.4 ± 1.3 nm (mean ± SD; n = 80). In less magnified pictures nuclear pore complexes (NPCs) were detectable on the surface (Figure 11). However, most of the nuclear surface appeared to be covered with other cytosolic material, probably endoplasmic reticulum and associated proteins.

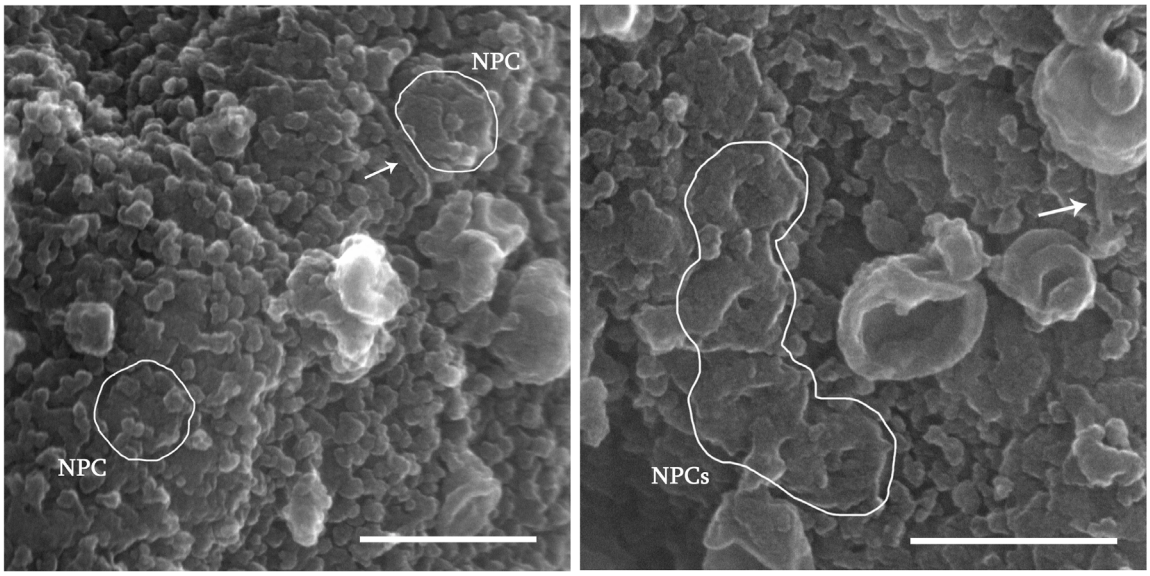

Figure 11 Structures at the outer nuclear membrane of *Dictyostelium* cells expressing HisMyc-NE81ΔNLS. feSEM image. Nuclear pore complexes (NPCs) are encircled. Arrows indicate filamentous structures of the expected thickness of lamin structures. Scale bars = 200 nm.

2.3 Analysis of metazoan lamin assemblies at the outer nuclear membrane

The strategy for structural analysis of the nuclear lamina at the outer surface of nuclei should also be tested for metazoan lamins. Two distinct lamins were chosen to generate a ΔNLS-construct and express it in *Dictyostelium* cells. As a proof of principle *Xenopus* lamin LIII was used, since its structure of membrane-associated lamin filaments have been investigated in detail and secondly, *C. elegans* lamin that can easily be expressed in bacteria and therefore many *in vitro* assembly data are available (Aebi et al., 1986, Foeger et al., 2006).

2.3.1 Heterologous expression of Xenopus lamin LIII

NE81 has already been successfully expressed in HeLa cells and in *Xenopus* oocytes (Krüger et al., 2012, Grafe et al., 2019). Yet, the question remained whether vertebrate lamin can be expressed in *Dictyostelium* cells as well. In first experiments of a project related Master thesis, *Xenopus* lamin LIII was tagged with FLAG and GFP (Suckau, 2016). As above, the NLS was mutated to enforce an assembly at the outer nuclear surface. However, the corresponding fusion proteins could not be expressed in *Dictyostelium*. The translation apparatus of *Dictyostelium* is adapted to AT-rich sequences. Consequently, the different codon usage of

the *Xenopus* sequence could have caused the failure. Hence, for further expression experiments a codon-optimized variant of the coding sequence was produced by gene synthesis. Instead of GFP or FLAG the engineered 8xHisMyc-tag was used as its suitability for this purpose has already been proven in earlier experiments.

The HisMyc-LIIIΔNLS construct was transformed in *Dictyostelium* and expression of the fusion protein was determined by fluorescence microscopy. Cells were fixed with glutaraldehyde and stained as described before (Figure 12).

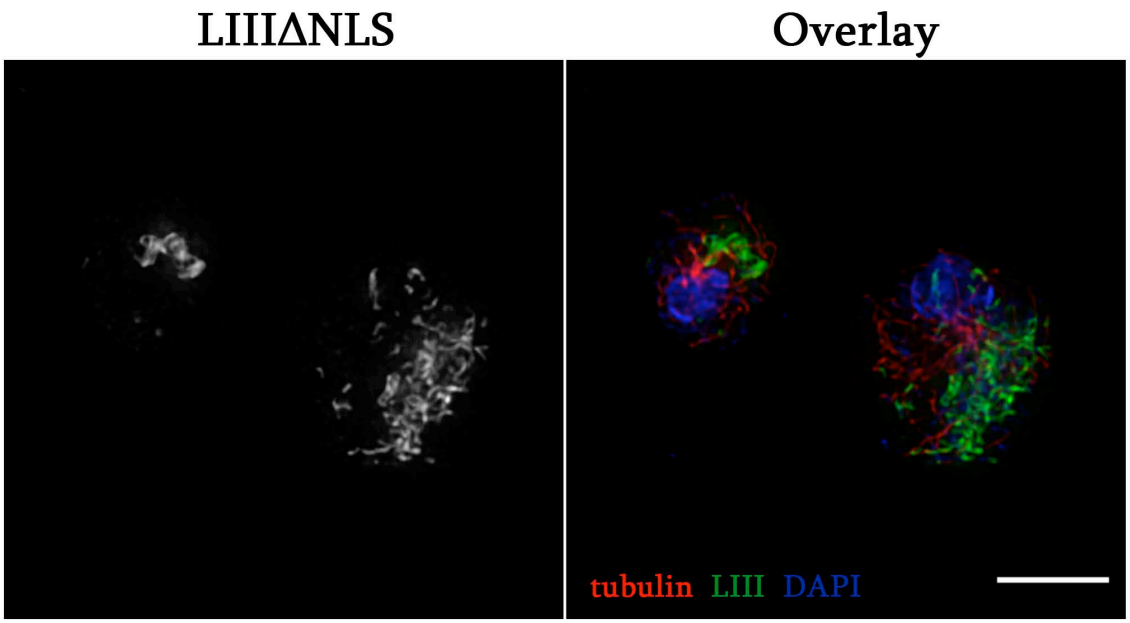

Figure 12 HisMyc-LIIIΔNLS shows no localization at the nuclei of *Dictyostelium* cells. Fluorescence deconvolution microscopy using a PlanApo 1.4/100× objective. Cells were fixed with glutaraldehyde and stained with anti-Myc/anti-mouse-Alexa Fluor 488, anti-tubulin/anti-rat-Alexa Fluor 568 and DAPI. Merged image shows tubulin in red, LIII in green and chromatin in blue. Scale bar = 5 µm.

HisMyc-LIIIΔNLS showed no localization at the nuclei of *Dictyostelium* cells. Some cells contained protein aggregates in the cytoplasm with peripherally located nuclei, but the fusion protein was not expressed in most cells.

The lamin CaaX box (C: cysteine, a: aliphatic amino acid, X: any amino acid) undergoes post-translational modifications for prenylation at the C-terminal end ensuring attachment to cell membranes. It is unknown how significant the amino acids following cysteine are for the organism specific farnesyltransferase. Therefore, the CaaX box of Xenopus LIII (CSIM) was replaced by the functioning CLIM sequence of NE81 to ensure proper prenylation of the

protein and to investigate an influence of the CaaX box sequence on anchoring to the *Dictyostelium* nuclear envelope. Expression of the fusion protein was determined by fluorescence microscopy (Figure 13).

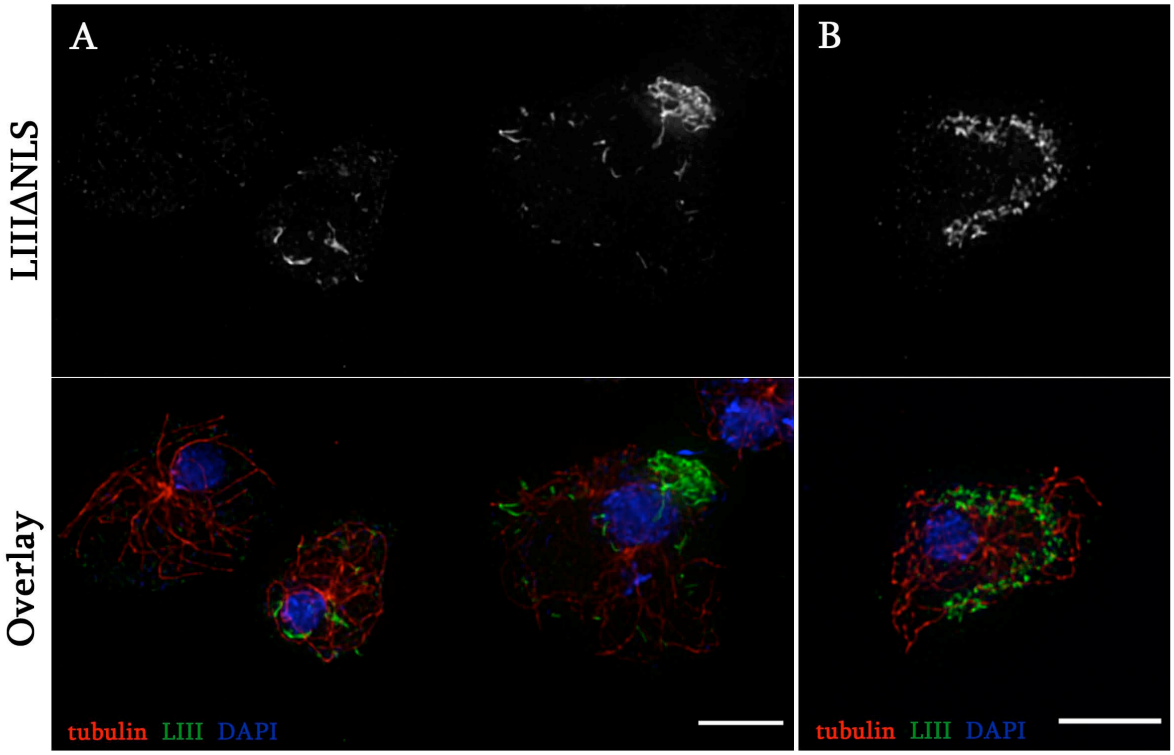

Figure 13 HisMyc-LIIIΔNLS^{-CLIM} shows no uniform localization at the nuclei of *Dictyostelium* cells. Fluorescence deconvolution microscopy using a PlanApo 1.4/100× objective. Cells were fixed with glutaraldehyde and stained with anti-tubulin/anti-rat-Alexa Fluor 568, DAPI and **A**: anti-Myc/anti-mouse-Alexa Fluor 488; **B**: anti-LIII/ anti-mouse-Alexa Fluor 488. Merged images show tubulin in red, LIII in green and chromatin in blue. Scale bars = 5 µm.

Replacement of the CaaX box did not yield to a significant change in distribution of the fusion protein. HisMyc-LIIIΔNLS^{-CLIM} cells also showed no uniform localization of the fusion protein around the nuclei. Instead some cells exhibited large protein aggregates in the cytoplasm and short fibers near to the nucleus. Again, most of the cells did not express the fusion protein.

A Western blot analysis (Figure 14) confirmed that both HisMyc-mutant strains expressed LIII fusion protein, which has a size about 70.4 kDa. They showed a band around 70 kDa detected with anti-Myc and with anti-LIII. Thus, the cytosolic aggregates present heterologously expressed LIII protein.

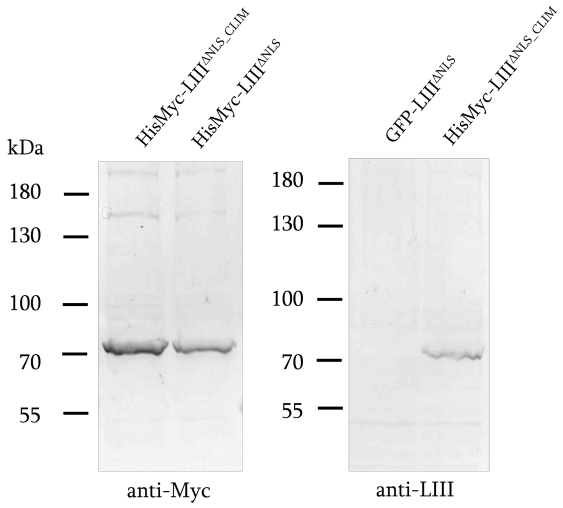

Figure 14 Expression of heterologous LIIIΔNLS in *Dictyostelium* cells. Whole-cell extracts of $4 \cdot 10^5$ cells lysed in 10 µl urea buffer were loaded. The immunoblot was stained with anti-Myc/anti-mouse-AP (left) or anti-LIII/anti-mouse-AP (right) and detected with NBT/BCIP. HisMyc-LIIIΔNLS has a size of 70.4 kDa. Protein samples of both HisMyc-strains showed the right relative mobility. In contrast the GFP-strain showed no specific LIII expression.

In a corresponding Bachelor thesis supervised by myself (Meyfarth, 2017) the mutated NLS in LIII was replaced by the functional NE81-NLS in order to test whether heterologous expression of the *Xenopus* lamin combined with correct assembly at the nuclear envelope in *Dictyostelium* is possible at all. Importin-α should bind to the signal peptide of the LIII fusion protein, initialize import into the nucleus and prevent an aggregation in the cytoplasm (Adam et al., 2008). The LIII fusion protein was indeed imported into the nucleus and localized at the nuclear envelope, but the nuclei showed no uniform distribution of the fusion protein. The nuclear envelope localization of HisMyc-LIII was observed with both CaaX boxes suggesting that both variants are functional in *Dictyostelium*. Therefore, the absence of HisMyc-LIIIΔNLS at the outer nuclear envelope cannot be caused by a dysfunctional *Xenopus* CaaX box.

Additionally, just a minor population of cells expressed the LIII fusion protein at all. To exclude that the endogenous NE81 suppresses the LIII fusion protein and to prove, if *Dictyostelium* cells can survive with a vertebrate lamin only, a NE81 knockout strain should be generated. These attempts failed indicating that *Dictyostelium* cannot live with the *Xenopus* lamin LIII only.

2.3.2 Heterologous expression of C. elegans lamin

One of the best *in vitro* studied lamin proteins is the invertebrate *C. elegans* lamin Ce-lamin. It is classified as a B-type lamin and differs a bit from vertebrate lamins. The tripartite domain structure displays a longer head domain lacking the SPTR sequence representing the CDK1 phosphorylation site, and a shorter tail domain. Moreover, Ce-lamin is the only lamin that can be assembled into regular and stable 10-nm IF-like filaments *in vitro* (Ben-Harush et al., 2009). Lamin assembly studies from other organisms showed that these lamins indeed form 10-nm filaments but they are not stable and keep on growing laterally ending up in paracrystalline fibers or arrays.

The *lmn-1* sequence encoding the Ce-lamin protein was amplified by PCR and fused into the N-terminal HisMyc construct. In a second step the NLS was mutated using SLiCE cloning. The overexpression plasmids were transformed into *Dictyostelium* cells and screened for expression by immunofluorescence microscopy (Figure 15).

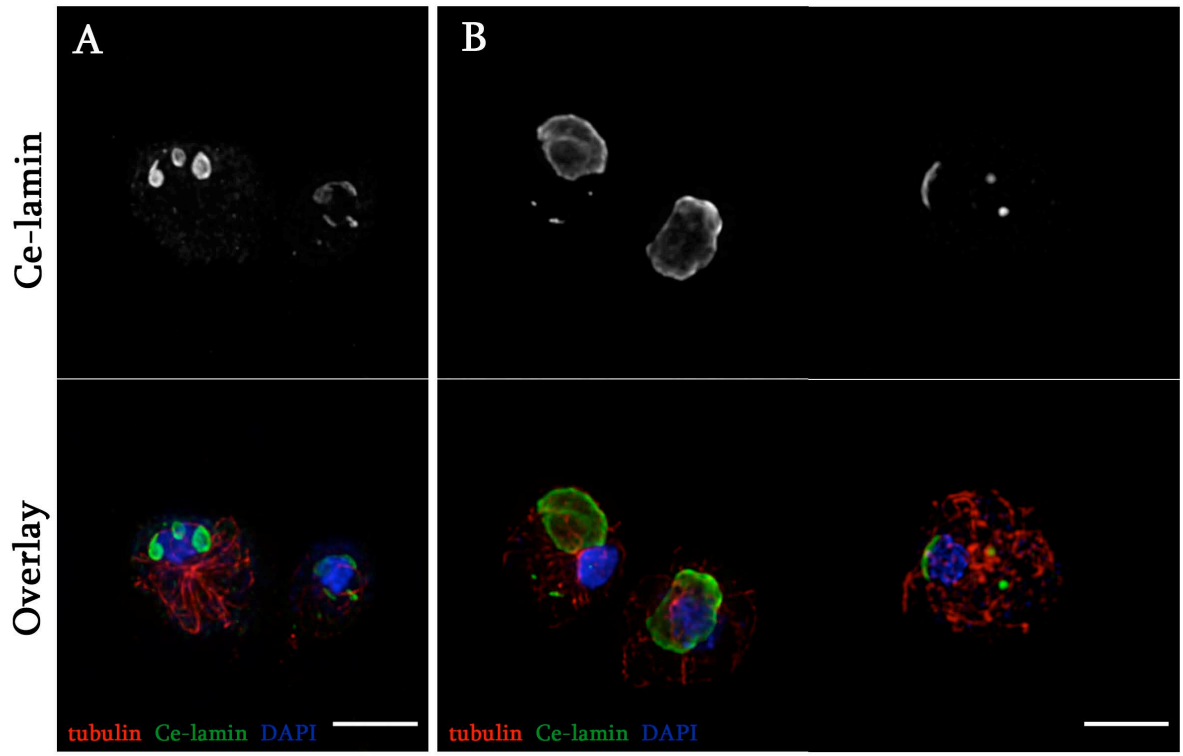

Figure 15 HisMyc-Ce-lamin expressed in *Dictyostelium* cells. Fluorescence deconvolution microscopy using a PlanApo 1.4/100× objective. Cells were fixed with glutaraldehyde and stained with anti-Myc/anti-mouse-Alexa Fluor 488, anti-tubulin/anti-rat-Alexa Fluor 568 and DAPI. **A**: HisMyc-Ce-lamin; **B**: HisMyc-Ce-laminΔNLS. Merged images show tubulin in red, Ce-lamin in green and chromatin in blue. Scale bars = 5 µm.

Expression of the heterologously expressed Ce-lamin in *Dictyostelium* had a similar outcome as the LIII fusion proteins. Both the mutant with functional NLS (HisMyc-Ce-lamin) and the mutant with altered NLS (HisMyc-Ce-laminΔNLS) showed no correct assembly at the nuclear envelope in *Dictyostelium*. In contrast, the appearance of the fusion proteins was different. The HisMyc-Ce-laminΔNLS strain had diverse phenotypes. The fusion protein localized near the nucleus, but showed no uniform distribution all around it or it exhibited cytosolic spheres of different sizes (Figure 15 B). The HisMyc-Ce-lamin protein with functional NLS localized partially at the nuclear envelope, forming small rings usually three to four per nucleus (A). *Dictyostelium* nuclei contain two to three nucleoli, but there was no co-localization of the Ce-lamin rings and nucleoli.

A Western blot analysis with anti-Myc and anti-His antibodies revealed bands around 70 kDa representing the HisMyc-Ce-lamin fusion proteins, i.e. well in the range of their calculated size of 68.3 kDa (Figure 16).

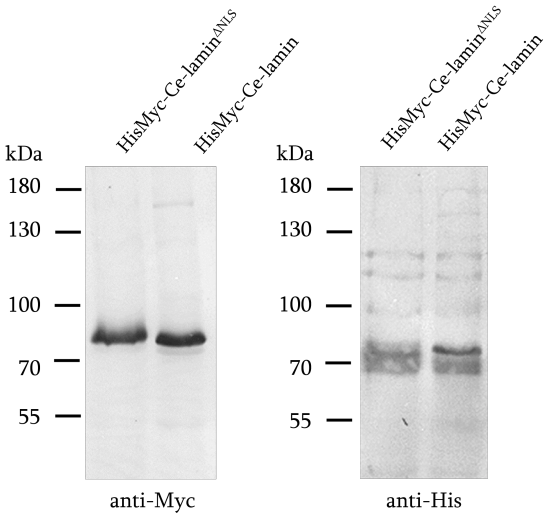

Figure 16 Expression of heterologous Ce-lamin in *Dictyostelium* cells. Immunoblot showing expression of heterologous Ce-lamin with mutated NLS (HisMyc-Ce-laminΔNLS) and functional NLS (HisMyc-Ce-lamin). Whole-cell extracts of $4 \cdot 10^5$ cells lysed in 10 µl urea buffer were loaded. The immunoblot was stained with anti-Myc/anti-mouse-AP (left) or anti-His/anti-mouse-AP (right) and detected with NBT/BCIP. HisMyc- Ce-lamin has a size of 68.3 kDa. Protein samples of both HisMyc-strains showed the right relative mobility.

To prove whether the fusion proteins are expressed inside or outside of the nucleus, the nuclei of both mutants were isolated and fixed with or without detergent. The nuclei were stained with anti-Myc directed against the respective fusion protein and anti-NE81 directed against the nuclear lamina at the inner nuclear membrane. Without detergent there should

be no staining with anti-NE81 and in case of HisMyc-Ce-lamin no staining of Ce-lamin, if it is expressed inside the nucleus. The fusion protein HisMyc-Ce-laminΔNLS should be visible with or without detergent, as it should interact with the outer nuclear membrane and not be transported into the nucleus.

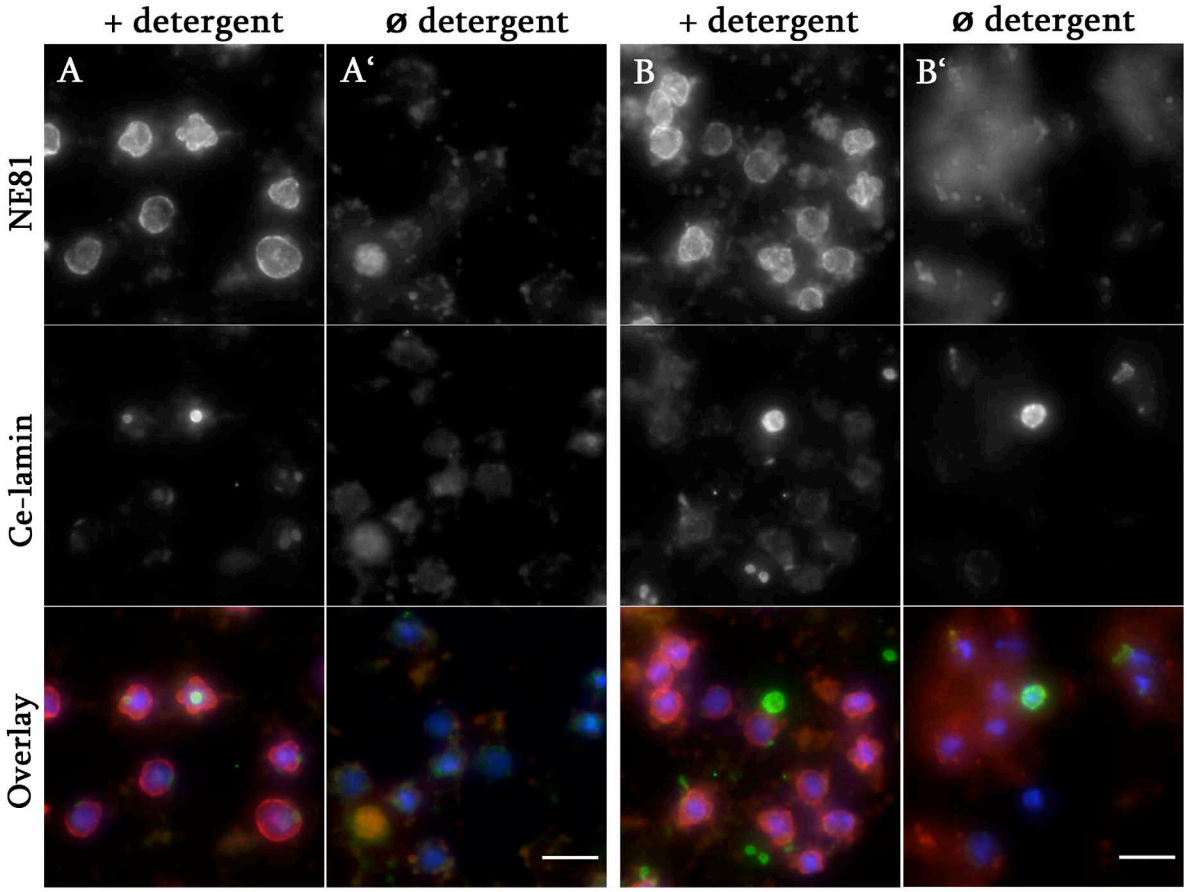

Figure 17 Nuclei isolated from HisMyc-Ce-lamin expressing *Dictyostelium* cells. Fluorescence microscopy using a PlanApo 1.4/100× objective. Nuclei were isolated and fixed with detergent (+) or without detergent (ø) with glutaraldehyde and stained with anti-Myc/anti-mouse-Alexa Fluor 488, anti-NE81/anti-rabbit-Alexa Fluor 568 and DAPI. **A**: HisMyc-Ce-lamin; **B**: HisMyc-Ce-laminΔNLS. Merged images show NE81 in red, Ce-lamin in green and chromatin in blue. Scale bars = 5 µm.

Both Ce-lamin mutants showed a distinct NE81 signal associated with the isolated nuclei, when fixed with detergent (Figure 17 A, B first row). HisMyc-Ce-lamin could be detected as small rings at the NE (A) and HisMyc-Ce-laminΔNLS had an anti-Myc signal near the nuclear envelope and in the background (B). In the experiment without detergent, antibodies were unable to penetrate the intact nuclear envelope and did not label NE81 associated with the inner nuclear membrane. There is only a weak background signal. The nuclei from the HisMyc-Ce-lamin mutant showed also no Ce-lamin signal (A’), indicating the protein is

located inside the nuclei. In contrast, the nuclei from HisMyc-Ce-laminΔNLS showed again a Ce-lamin signal detected with anti-Myc (B'), indicating that some fusion protein is associated with the outer nuclear membrane in *Dictyostelium*.

Since the heterologous expressed *Xenopus* and *C. elegans* lamins showed no uniform localization at the outer nuclear envelope, none ultrastructural feSEM analysis was undertaken.

2.4 Analysis of soluble NE81 by *in vitro* protein assembly

Preliminary experiments with bacterially expressed NE81 have shown that the protein cannot be functionally expressed in *E. coli*. Thus, *Dictyostelium* was chosen as an autologous expression system for isolation of assembly-competent NE81 protein. Previous results (with GFP as protein tag) indicated that clusters of CaaX box-deficient NE81 variants lacking the lipid anchor form three-dimensional protein assemblies. These clusters are cell cycle regulated and disappear at mitotic onset and reappear in late telophase (Krüger et al., 2012). In ultrathin sections of cells with additional NLS-mutated NE81, the cytosolic clusters appeared spongy and homogeneous with an intermediate electron density (Batsios et al., 2016). These features notably for the clusters of the cytosolic ΔNLSΔCLIM variant seemed useful as a source to isolate assembly-competent NE81 for *in vitro* experiments. In pre-experiments an enrichment of GFP-NE81ΔNLSΔCLIM clusters by density gradient centrifugation of the cytosolic extract was already successful (Dr. Petros Batsios, unpublished data), indicating that cytosolic NE81 assemblies were easier to isolate than nuclear envelope-associated assemblies bound to chromatin and other lamin-binding proteins.

2.4.1 Purification of soluble NE81 from Dictyostelium extract

The normal distribution of HisMyc-NE81 in NE81 knockout cells points out that the fusion protein HisMyc-NE81 is able to assemble accurately (Figure 7). Therefore, the N-terminal 8×HisMyc-tag construct was used for the purification experiments.

A strain was generated expressing an N-terminal tagged HisMyc-NE81 with a non-functional NLS through replacement of basic NLS-residues by alanine, and a deleted CaaX box lacking

the prenylation site (HisMyc-NE81ΔNLSΔCLIM). Screening for expression of the fusion protein was done by fluorescence microscopy. All mitotic stages were shown in normal deconvolution fluorescence images in a project related Bachelor thesis (Lisin, 2017). In order to gain a better resolution of the cytosolic fusion protein, expansion microscopy was carried out as previously described (Figure 18).

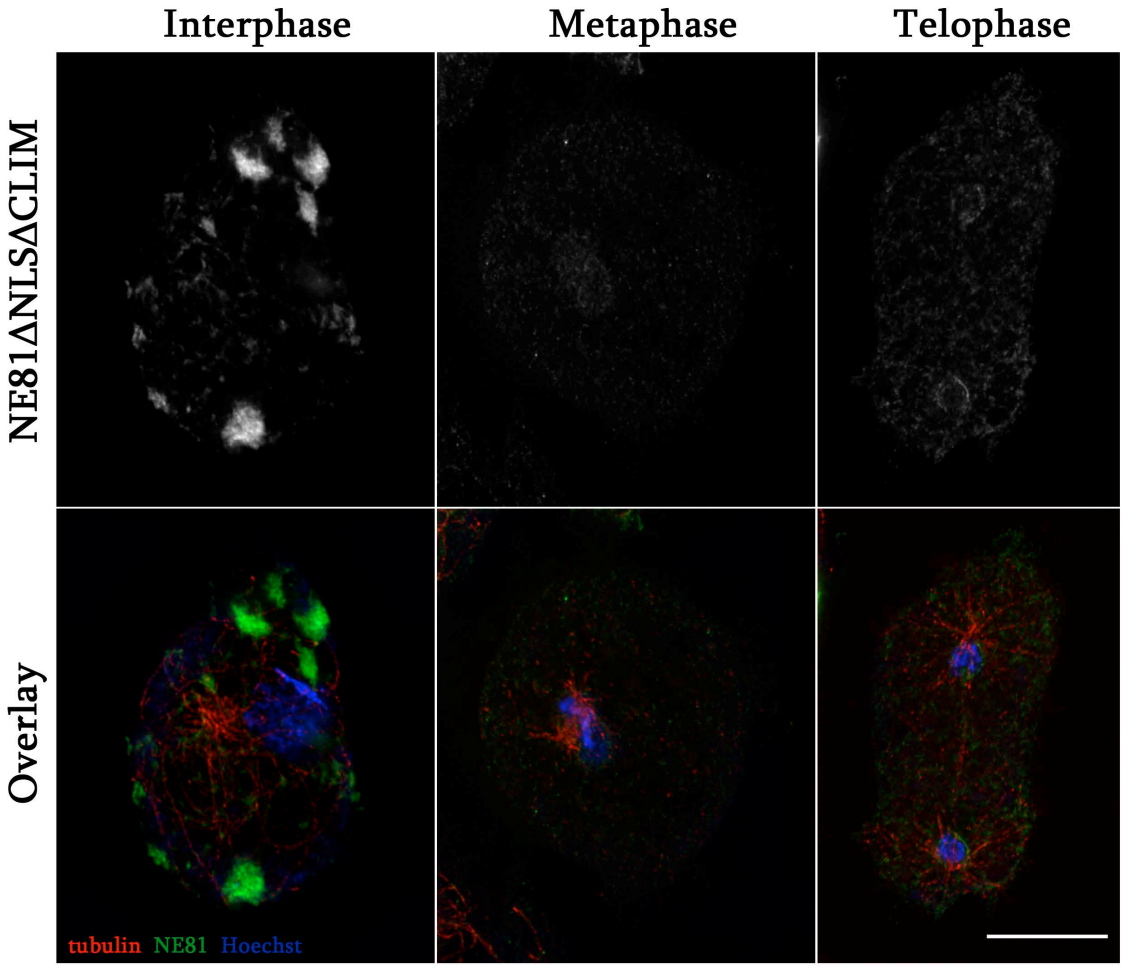

Figure 18 *Dictyostelium* cells expressing HisMyc-NE81ΔNLSΔCLIM. Representative interphase, metaphase and telophase. Expansion microscopy using a LCI PlanNeo 1.3/63× objective and theoretical deconvolution. Cells were fixed with glutaraldehyde and stained with anti-Myc/anti-mouse-Alexa Fluor 488, and anti-tubulin/anti-rat-Alexa Fluor 568, expanded as indicated and post-stained with Hoechst33342. Merged images show tubulin in red, NE81 in green and chromatin in blue. Cytosolic HisMyc-NE81ΔNLSΔCLIM clusters are present in interphase cells and disappear at the onset of mitosis; assemblies are gone in metaphase and come back during telophase. Expansion factor 3.2; scale bar = 5 µm (referring to the original size).

As expected from previous experiments with GFP (Batsios et al., 2016), the fusion protein occurred as cytosolic clusters during interphase. Clusters varied in size and among cells also in quantity. They were usually round-oval and sometimes club-shaped occupying up to one quarter of the cytoplasm. At higher resolution due to expansion the appearance of clusters

was suggestive of an organized meshwork of filaments. Furthermore, assembly of the mislocalized protein is still cell cycle regulated. During interphase, assemblies were present and disappeared at onset of mitosis. In metaphase, assemblies were gone and a weak background signal was visible. At the end of telophase, the signal came back indicating reassembly of the protein. During telophase a minor population was located near the nuclear envelope (refer to the supplemental material for high quality images).

The vector used for transformation of DNA coding for the fusion protein is an overexpression construct containing a G418 resistance cassette leading to multiple chromosomal tandem insertions and strong overexpression (Barth et al., 1998). Whole-cell extracts were examined by immunoblotting and the protein bands were densitometrically evaluated to quantify the expression levels of endogenous and fusion proteins, respectively (Figure 19).

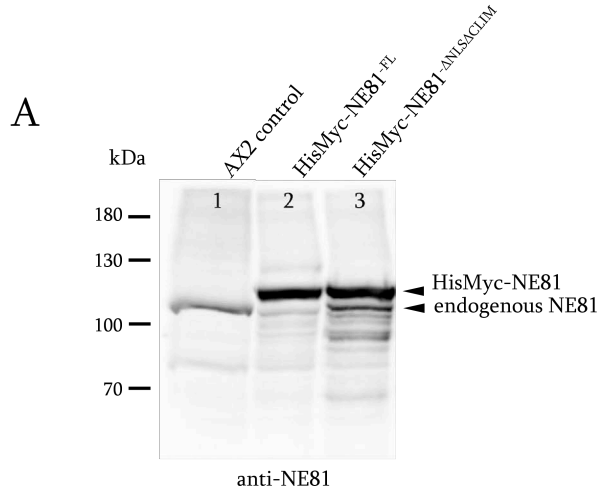

B

Expression levels	1	2	3
HisMyc-NE81	0	2,10	2,53
endogenous NE81	1	0,19	0,72

Figure 19 Expression of endogenous and tagged NE81 in AX2 control cells and HisMyc-mutant strains (FL = full length). **A**: Immunoblot showing relative expression levels of endogenous NE81 compared to the tagged variants. Whole-cell extracts of $4 \cdot 10^5$ cells lysed in 10 µl urea buffer were loaded. The immunoblot was stained with anti-NE81/anti-rabbit horseradish peroxidase and visualized with ECL. Equal loading per lane was proved by Ponceau S protein staining for comparing of expression levels with the control. **B**: Expression levels of NE81, densitometrical measurements of immunoblot bands were done with ImageJ. Value of endogenous protein in control was set to 1 and all values were normalized.

As expected for overexpression constructs, the protein levels of tagged fusion proteins in both mutant strains were higher than the level of endogenous NE81 in control cells (2.1 times and 2.5 times). However, the HisMyc-NE81 full length (FL) mutant showed a highly reduced endogenous protein level (0.2 times) compared to control cells and the HisMyc-NE81ΔNLSΔCLIM mutant, whose expression of endogenous NE81 was just slightly

suppressed (0.7 times). Suppression of endogenous proteins upon high expression levels of the equivalent fusion protein is a common phenomenon in altered *Dictyostelium* overexpression strains (Batsios et al., 2016, Meyer et al., 2017).

Successful purification and assembly experiments in the *C. elegans* system revealed that high salt molarity and high pH favor the solubility of lamin proteins (Foeger et al., 2006). In analogy to these experiments, parameters like pH-value, salt-content and protein concentration were optimized and will be outlined in the following experiments. As shown above, the generated HisMyc-NE81ΔNLSΔCLIM mutant is expressing the NE81 fusion protein in the cytoplasm and moreover, the overexpression construct ensures high protein levels. The cells were grown in shaking culture up to a content of 1-2·10^9 cells. The cells were washed and resuspended in a Tris-HCl buffer with high salt molarity, were the clusters are solubilized to maximize the yield of NE81 protein. After mechanical cell lysis, the cytosolic extract was separated from nuclei and cell debris by centrifugation. Further purification employed Ni-NTA beads that interact with the His-tag and allows affinity purification. The fractions were eluted with 250 mM imidazole and evaluated on polyacrylamide gel stained with Coomassie blue.

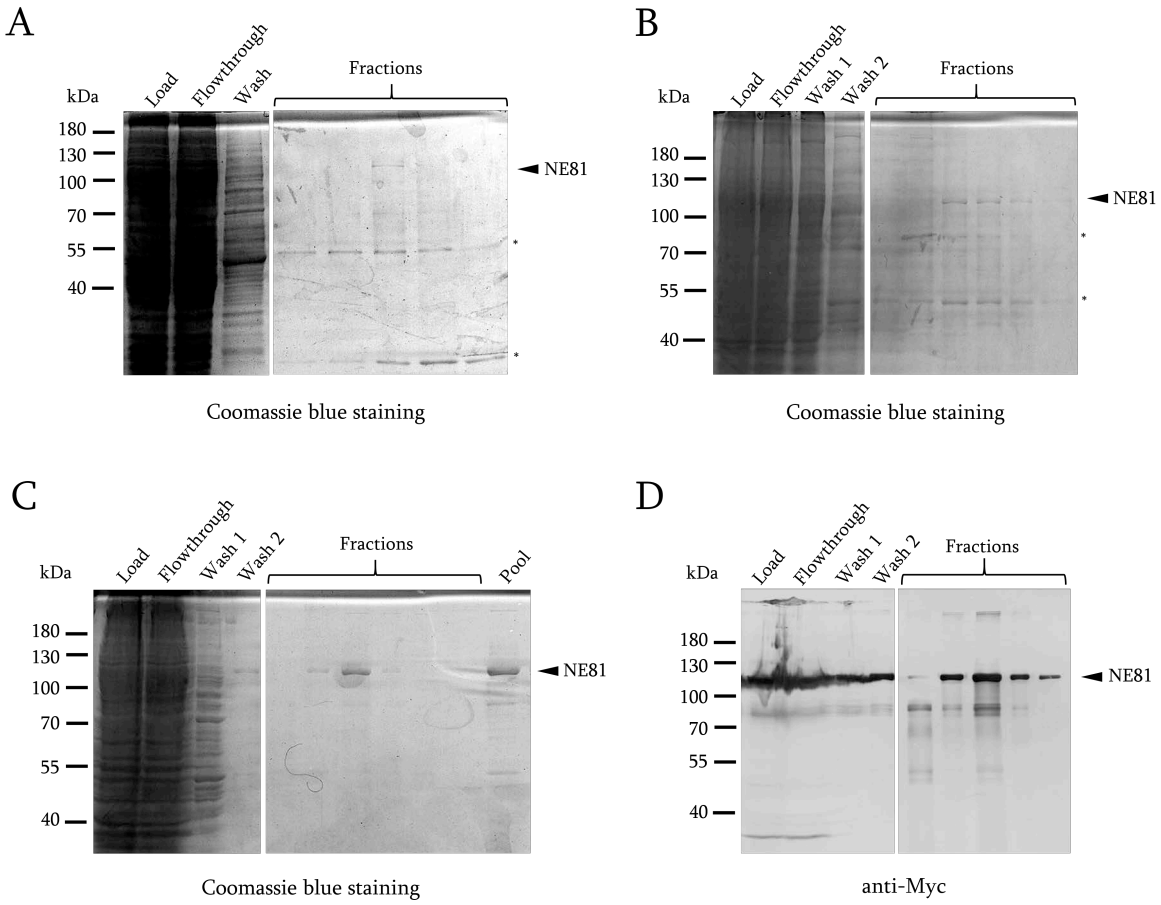

Figure 20 HisMyc-NE81ΔNLSΔCLIM expressed in *Dictyostelium* followed by affinity purification with Ni-NTA beads in **A**: 25 mM Tris-HCl, pH 8.0, 0.3 M NaCl; **B**: 50 mM Tris-HCl, pH 8.0, 0.3 M NaCl; and **C/D**: 25 mM Tris-HCl, pH 8.0, 0.5 M NaCl. **A-C**: 10% SDS gel Coomassie blue stained; **D**: immunoblot stained with anti-Myc/anti-mouse-AP visualized with NBT/BCIP. Asterisks indicate bands above and under NE81 peak fraction.

First approaches starting with 25 mM or 50 mM Tris-HCl, pH 8.0 and 0.3 M NaCl did not lead to a satisfying protein purification. Coomassie stained gels showed bands above and under the NE81 peak fraction (Figure 20 A + B, asterisks). Therefore, a buffer with 25 mM Tris-HCl, pH 8.0 and high salt molarity of 0.5 M NaCl was used for all purifications. Elution with 250 mM imidazole resulted in a clear peak fraction containing the HisMyc-NE81ΔNLSΔCLIM protein (C). Coomassie stained protein gels and anti-Myc Western blot analysis indicated that NE81 protein fractions contained no relevant amounts of contaminating proteins (C, D). The high protein fractions were pooled and dialyzed to remove the imidazole for further assembly studies. Protein yields were up to 1.5 mg per 400 ml cell culture batch. The concentration was quantified by absorption measurement at 280 nm or by Amido black staining.

2.4.2 Sedimentation behavior of NE81 at low ionic strength

To study the solubility of NE81, the sedimentation behavior of the fusion protein at varying pH and NaCl concentrations was tested. Samples were dialyzed at different starting protein concentrations into the corresponding buffer and after centrifugation at 17,000× *g* the amount of protein in pellets and supernatants were determined by Western blot analysis.

A

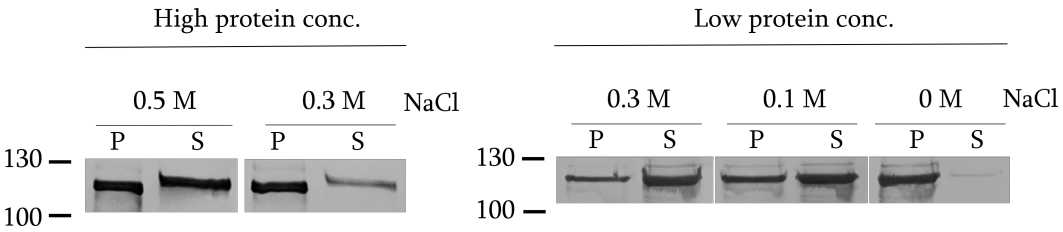

B

NaCl	0.3 M pH 8.0	0.1 M pH 8.0	0 M pH 8.0	0 M pH 9.0
P %	27	41	86	43
S %	73	59	14	57
Solubility	++	+	--	+

Figure 21 Salt-dependent solubility and assembly of *in vitro* HisMyc-NE81ΔNLSΔCLIM. **A**: Dialysis of purified HisMyc-NE81ΔNLSΔCLIM at two starting concentrations (low concentration = 0.2 mg/ml; high concentration = 0.4 mg/ml) against 25 mM Tris-HCl, pH 8.0, and indicated NaCl concentration (0 – 0.5 M) followed by centrifugation at 17,000x *g*; equal amounts of pellet (P) and supernatant (S) were loaded on SDS gels, blotted and stained with anti-Myc/anti-mouse-AP and detected with NBT/BCIP. **B**: Table showing densitometric percentages of a representative immunoblot of HisMyc-NE81ΔNLSΔCLIM in supernatants and pellets obtained at the indicated salt and pH conditions (low protein concentration = 0.2 mg/mL). Key: ++ most protein in supernatant, + around half of protein in supernatant, - - most of protein in pellet.

Western blot results (Figure 21 A) showed a decreasing protein amount in the supernatant with decreasing salt concentration. When comparing the sedimentation of low and high protein concentration at 0.3 M NaCl, the higher protein concentration yielded to a bigger pellet. This indicated that high protein concentration favored unspecific aggregation and/or has a higher tendency of assembled protein to remain in the assembled state. However, the solubility increased considerably at high ionic strength - the amount of protein in supernatant

increased at 0.5 M NaCl compared to the lower NaCl concentration in dialysis buffer. Consequently, at high protein concentrations, which also occur in the peak fractions during purification, the purified protein requires higher salt concentrations to solubilize. A closer look at the experiments with low protein concentration makes clear that protein amounts in pellets increased with decreasing salt concentration (A right and B), indicating that NE81 polymerizes into filament assemblies at low-ionic strength. With 0.3 M NaCl only 27% of the protein was found in the pellet whereas more than 80% of HisMyc-NE81ΔNLSΔCLIM could be pelleted when the buffer contained no NaCl. Additionally, a higher pH of 9.0 instead of pH 8.0 led to more soluble protein also in the absence of salt. These results confirm that for NE81, high ionic strength and a high pH promote solubility, as seen for other lamins before (Aebi et al., 1986, Foeger et al., 2006).

To prove that the *in vitro* cluster formation of NE81 results from a specific assembly reaction of filaments and not due to nonspecific aggregation of the HisMyc-NE81ΔNLSΔCLIM protein, protein solutions dialyzed at low ionic strength (both at high and low protein starting concentration) were again dialyzed against high salt buffer. In case of a specific assembly reaction the protein should get soluble again. All solutions were centrifuged and examined by Western blot analysis followed by densitometric evaluation as described before. The values are displayed in a bar chart (Figure 22).

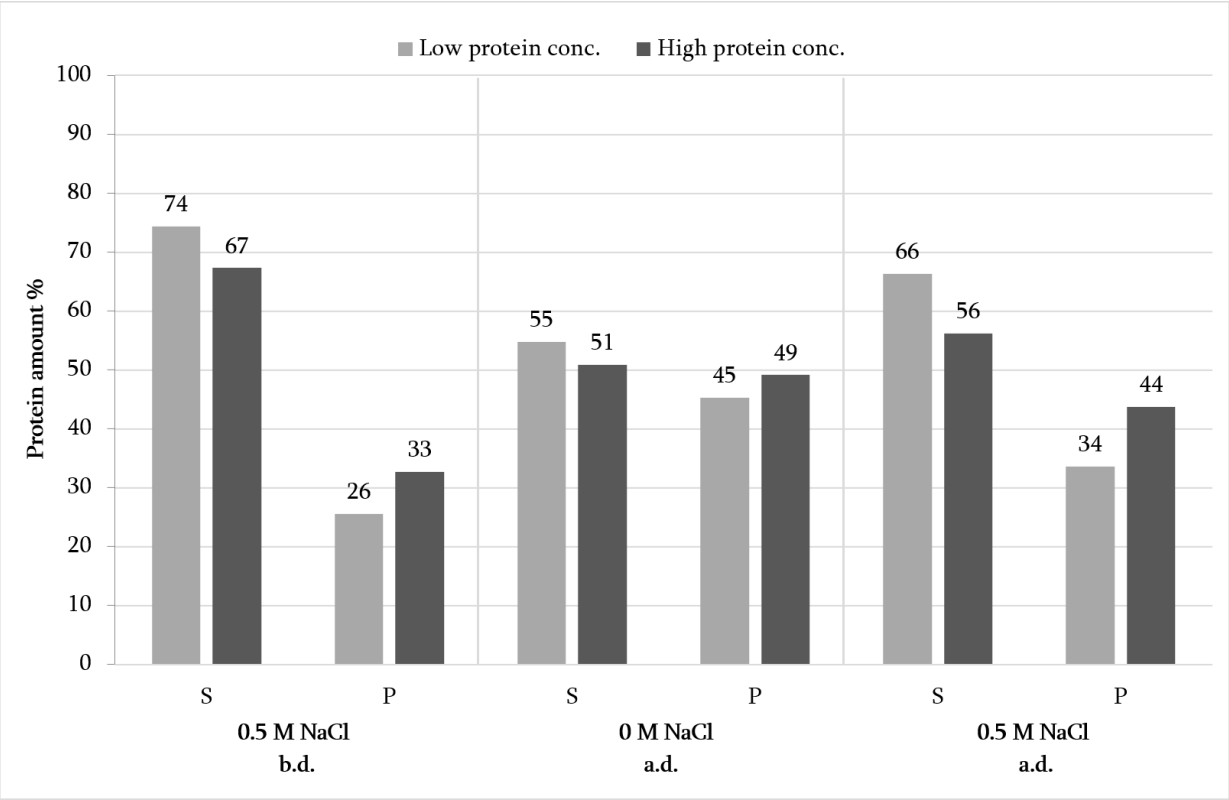

Figure 22 Proof of the specific assembly/disassembly reaction of HisMyc-NE81ΔNLSΔCLIM protein. Protein solution of 0.25 mg/ml (low protein concentration) and 0.5 mg/ml (high protein concentration) were prepared in triplicate. One sample of each concentration was centrifuged for 1h 17,000x *g* without dialysis (0.5 M NaCl before dialysis b.d.). The other copies were dialyzed for 3 h against 25 mM Tris-HCl, pH 8.0. One sample of the duplicate was centrifuged for 1h 17,000x *g* (0 M NaCl after dialysis a.d.) the other was again dialyzed for 4.5 h against 25 mM Tris-HCl, pH 8.0, 0.5 M NaCl and centrifuged for 1h 17,000x *g* (0.5 M NaCl a.d.). Equivalent amounts of pellet (P) and supernatant (S) were loaded on SDS gels, blotted, stained with anti-Myc/anti-mouse-AP and detected with NBT/BCIP.

As described above, the HisMyc-NE81ΔNLSΔCLIM protein amount found in the supernatant under high ionic strength (0.5 M NaCl b.d.) was higher at lower protein concentration compared to the high protein concentration. After dialysis in the absence of salt (0 M NaCl a.d.) the outcome at both protein concentrations was similar: the protein amount in the pellets increased in both cases, but slightly more at the high protein concentration. Next, the protein solutions were dialyzed again against 0.5 M NaCl Tris-buffer (0.5 M NaCl a.d.) to prove a specific assembly/disassembly reaction. The protein amount in both supernatants increased once again and reached 88% (low protein concentration) and 84% (high protein concentration) of the initial starting value, indicating the polymerization under low ionic strength was not due to nonspecific aggregation but specific assembly of HisMyc-NE81ΔNLSΔCLIM protein.

2.4.3 In vitro assembly of NE81 at low ionic strength

The next step was the structural analysis of *in vitro* formed HisMyc-NE81ΔNLSΔCLIM assemblies. In accordance to other publications that investigated lamin morphologies, a protein concentration of 0.1 mg/ml was used for dialysis against filament forming buffer. For a first overview the assembled protein was centrifuged on cover slips, fixed with formaldehyde, then stained with anti-Myc/anti-mouse-Alexa Fluor 488 and analyzed in a fluorescence microscope (Figure 23).

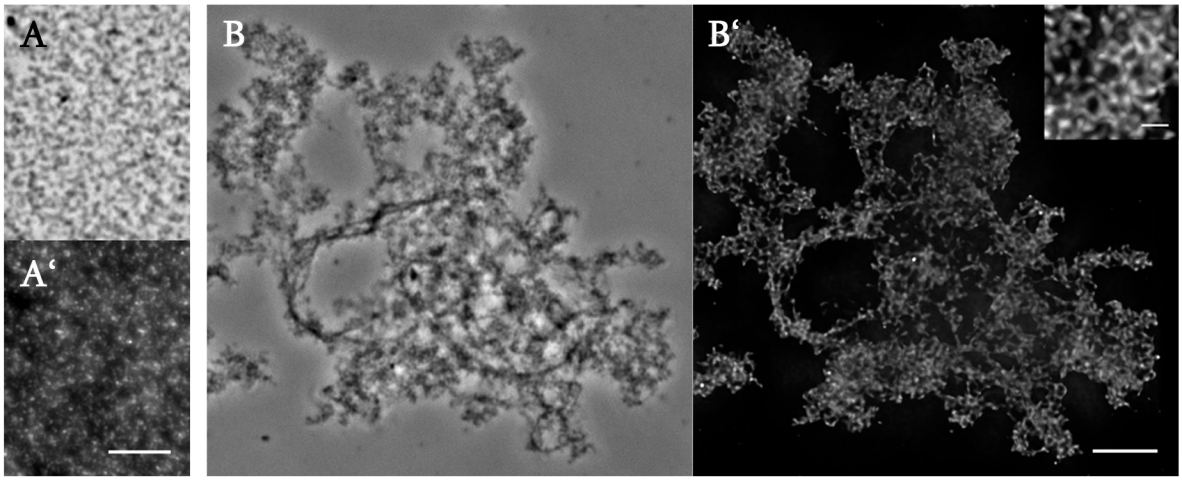

Figure 23 Widefield deconvolution microscopy of purified HisMyc-NE81ΔNLSΔCLIM (c=0.1 mg/ml). Protein was fixed with formaldehyde and stained with anti-Myc/anti-mouse-Alexa Fluor 488. Phase contrast (A, B) and deconvolution-fluorescence images (A', B') are shown. **A**: Control protein solution in high salt buffer shows no filament assembly. **B**: Protein under low-ionic strength forms a meshwork of filaments. Scale bars = 5 µm (inset 1 µm).

HisMyc-NE81ΔNLSΔCLIM protein solution of 0.1 mg/ml was dialyzed against no-salt buffer to favor filament assembly. As control the solution was also analyzed under high salt condition (= disassembled). The control (A, A') showed a background signal finely dispersed all over the cover slip, indicating that most of the protein was disassembled. In contrast, after dialysis HisMyc-NE81ΔNLSΔCLIM formed large reticular structures showing filament-like structures inside the meshwork. The enlarged inset of the fluorescence image displayed structures reminiscent of a lamin meshwork at the nuclear envelope detected in mammalian cells by super-resolution microscopy (Shimi et al., 2015) (Figure 3 B).

Former publications disclosed that most purified intermediate filaments as well as lamins show different assembly behavior and that various experimental conditions can lead to filament assembly *in vitro* (Foeger et al., 2006). In case of HisMyc-NE81ΔNLSΔCLIM the proposed buffer compositions did not result in single-filament assembly visible in light-microscopy. As a consequence, the starting protein concentration was reduced to 5 - 10 µg/ml. Under these conditions HisMyc-NE81ΔNLSΔCLIM formed long thin filament assemblies (Figure 24).

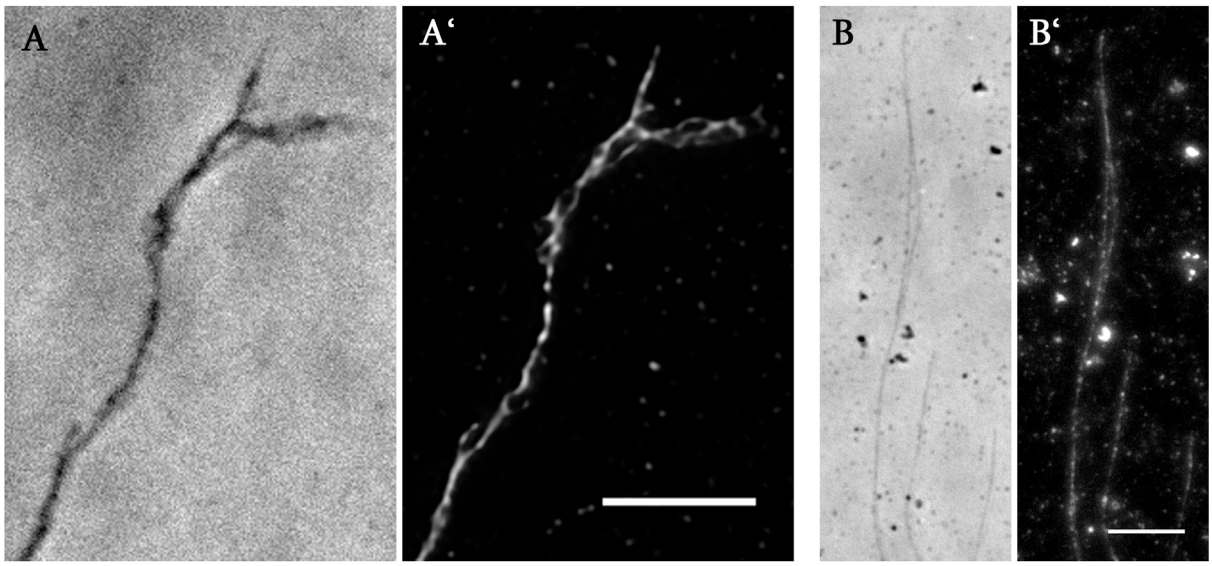

Figure 24 Widefield deconvolution microscopy of low concentrated HisMyc-NE81ΔNLSΔCLIM shows thin filament assembly. Filaments were fixed with formaldehyde and stained with anti-Myc/anti-mouse-Alexa Fluor 488. Phase contrast (A,B) and deconvolution-fluorescence images (A',B') are shown. **A**: 5 µg/mL; **B**: 10 µg/ml. Scale bars = 5 µm.

The applied widefield deconvolution microscopy achieves an optical resolution of ~170 nm (Pitzen et al., 2018). To reach a higher resolution two different super-resolution methods were used.

For expansion microscopy the filaments were fixed and stained as described before.

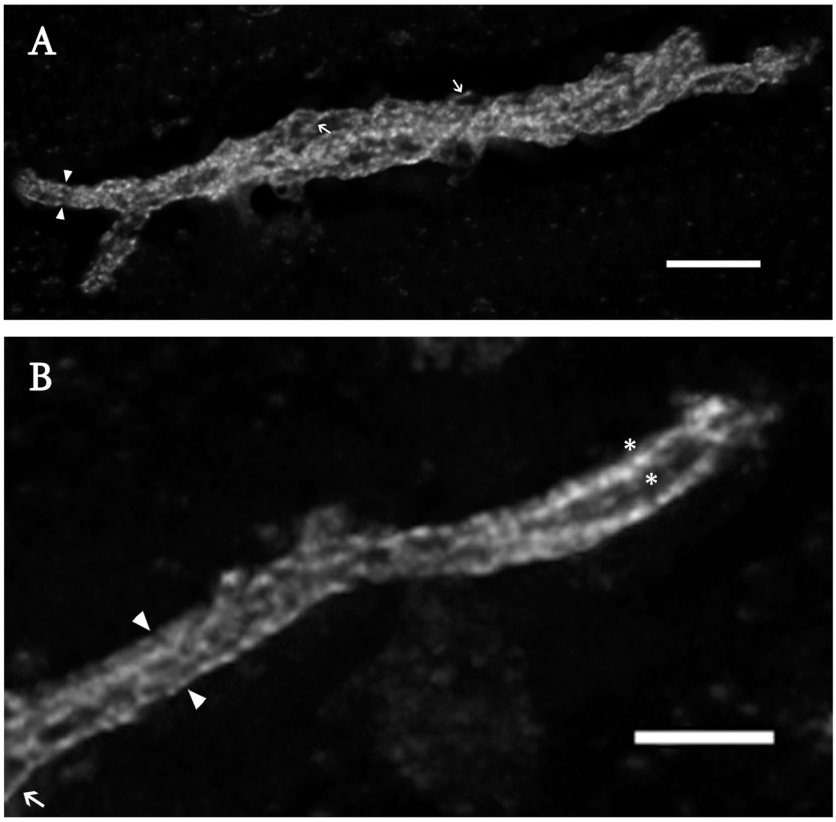

Figure 25 Expansion microscopy of HisMyc-NE81ΔNLSΔCLIM filaments formed at 5 µg/ml. Filaments were fixed with paraformaldehyde and stained with anti-NE81 antibody overnight and afterwards at least two hours with anti-rabbit-Alexa Fluor 488. Post-fixation was done with 0.1% glutaraldehyde followed by digestion with proteinase K and two hours swelling in water. Long filaments are formed that differ in diameter. Arrows display thinnest filaments and arrowheads the thickest filaments. A potential helix-like structure is shown between the asterisks. Maximum intensity projections are presented. Scale bars 2 µm (**A**) and 1 µm (**B**) refers to the original size of the specimen.

HisMyc-NE81ΔNLSΔCLIM assemblies formed at low protein concentration of 5 µg/ml showed long filaments that differed in diameter (Figure 25). The thickest assemblies between the arrowheads are about 10 times the size of the thinnest filaments (arrows). A closer look on B reveals that these could be two filaments twining around each other building a helix (between asterisks). In general, the ExM images indicated that these twisted filaments were closely aligned in parallel arrangements (arrowheads). The supplemental material contains a three-dimensional movie of a HisMyc-NE81ΔNLSΔCLIM filament assembly (Scale bar = 2 µm, refers to the original size).

The second super-resolution method used to visualize filaments was stimulated emission depletion (STED) microscopy (Hell and Wichmann, 1994). In this method the diffraction rings of the fluorescence emitting spot are physically reduced by a depletion laser allowing just the

signal from the inner airy disc to reach the detector, which increases the optical resolution up to 25 nm (xy) at optimal conditions. Specific fluorophores are required that have excitation and emission spectra at the STED wavelength and show low photobleaching. The filaments were fixed as described before and stained with anti-NE81/anti-rabbit-Atto 647N (Figure 26).

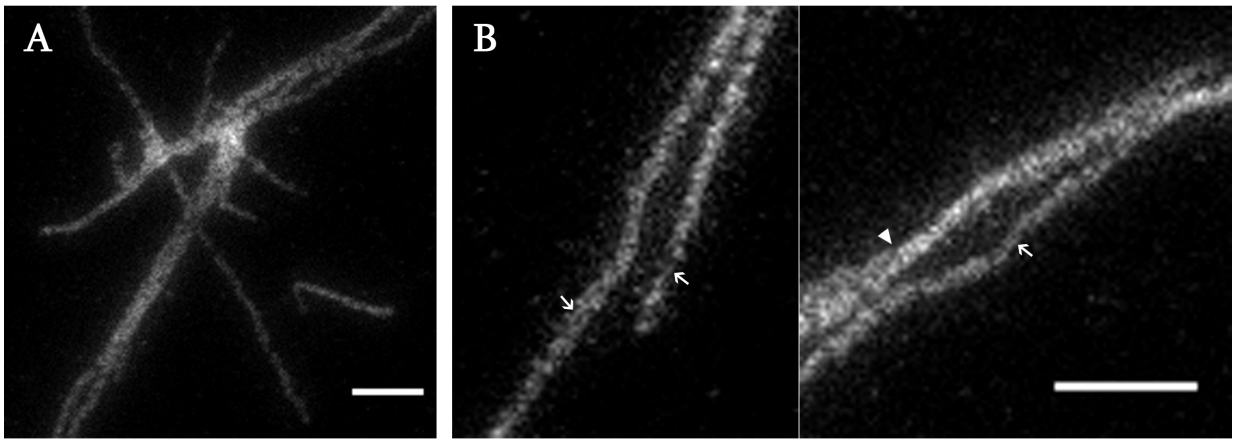

Figure 26 Stimulated emission depletion (STED) microscopy of HisMyc-NE81ΔNLSΔCLIM filaments formed at 5 µg/ml. Filaments were fixed with paraformaldehyde and stained with anti-NE81/anti-rabbit-Atto 647N. **A**: Overview of filament assembly. **B**: Magnification of filaments. Small filaments (arrow) in a greater filament arrangement can be detected and a filament showing a helix-like assembly (arrowhead). Scale bars = 1 µm.

STED images of HisMyc-NE81ΔNLSΔCLIM filament assemblies showed once more long filaments sometimes closely aligned. The overview (A) revealed crossing and to some extent overlapping filaments. A higher magnification detected small filaments (B, arrows) within the greater filament arrangement that had the same diameter as the thin filaments observed with expansion microscopy. A thicker strand parallel to it looked like filaments bundled into a helix (arrowhead). Overall structure and shape of the protein filaments are reminiscent of their appearance in expansion microscopy.

Both super-resolution methods have an optical resolution too low to resolve the filament size expected from diameters of intermediate filaments or lamin filaments seen before in feSEM images (Goldberg et al., 2008, Grafe et al., 2019). Hence, the measurements were not evaluated in these light microscopic images, although they gave a great impression how these filaments may be constructed and how they are arranged to each other.

Consequently, HisMyc-NE81ΔNLSΔCLIM filaments were analyzed by negative-staining transmission electron microscopy (TEM) to get a further insight into the thickness of *in vitro* polymerized filaments (Figure 27).

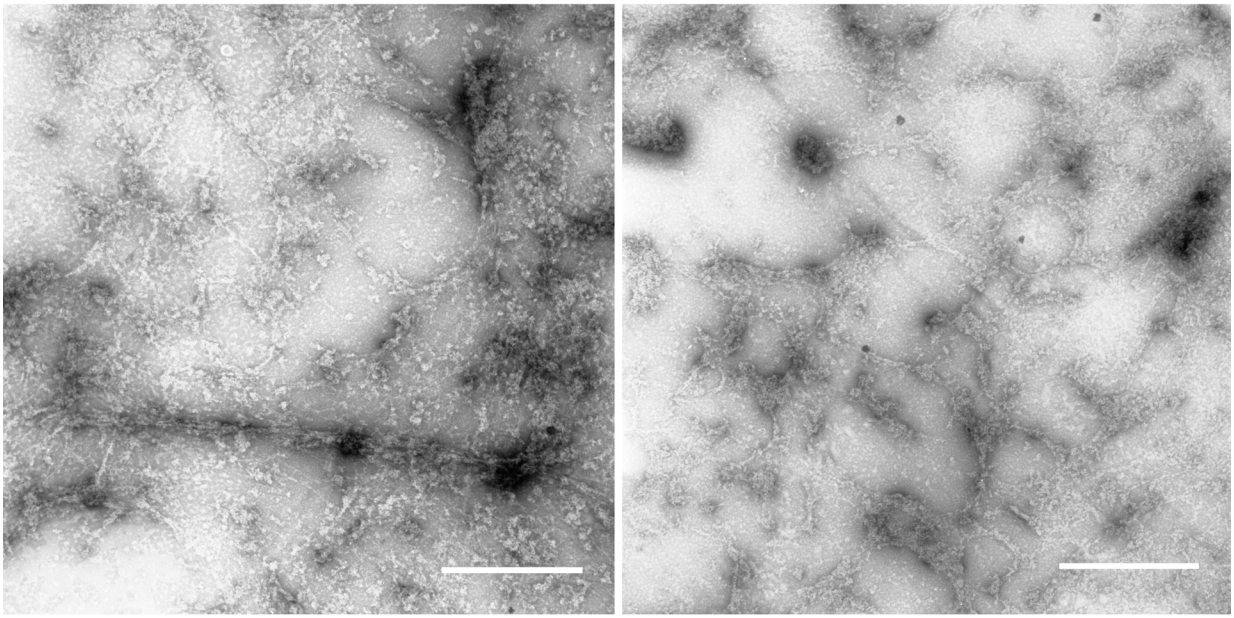

Figure 27 Reticular HisMyc-NE81ΔNLSΔCLIM filament networks visualized by negative-staining transmission electron microscopy. Two representative examples are shown. Scale bars = 1 µm.

As expected from light microscopic appearance of assemblies at higher protein concentration (Figure 23 B), the corresponding TEM images showed filamentous structures in reticular arrangements with a filament thickness varied with a mean size of 13.2 ± 4.2 nm (mean ± SD, n = 50). In addition, the higher concentrated protein sample showed a large amount of short filaments that stuck together in clusters. In general, the samples had too much contrast. From other publications it is known that all lamin types have various requirements in buffer composition and salt concentration for filament formation. For further experiments, the salt concentration in dialysis buffer was increased from zero to 50 mM NaCl and a centrifugation step was skipped (Figure 28).

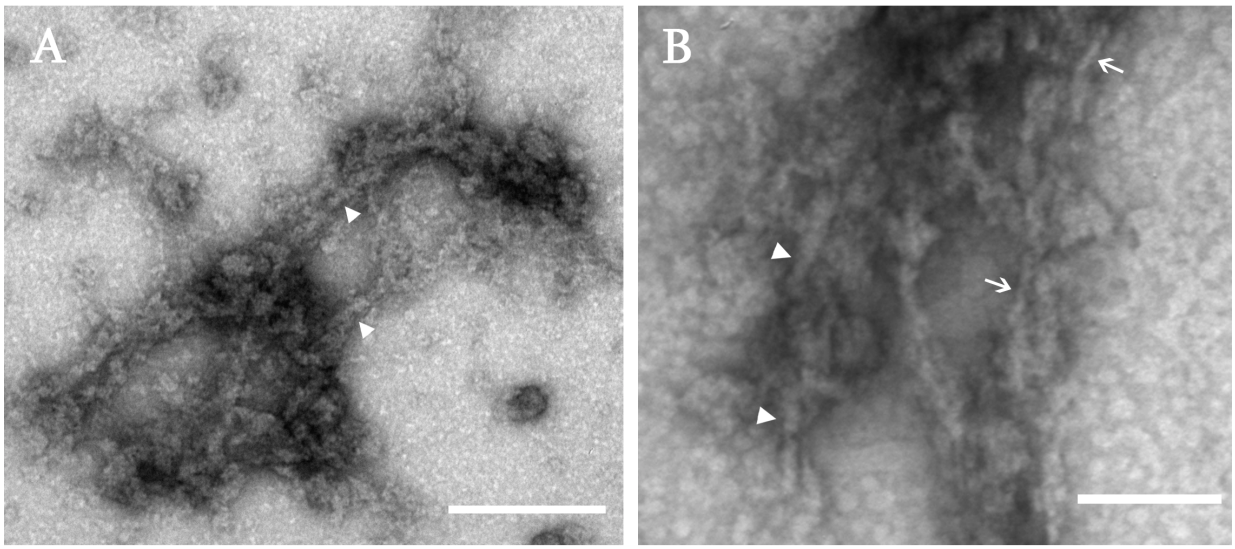

Figure 28 Reticular HisMyc-NE81ΔNLSΔCLIM filament networks formed of 0.1 mg/ml protein solution visualized by uranylacetate negative-staining transmission electron microscopy. Two representative examples are shown. Arrowheads indicate filaments with a diameter of 9.4 ± 1.1 nm (mean ± SD, *n* = 50). Arrows show thinner filaments. Scale bar **A** = 200 nm and **B** = 100 nm.

These TEM images showed longer fibers or filaments that were sometimes clustered. However, they had a better contrast and clearly distinguishable details. The filaments (arrowheads) had a diameter of 9.4 ± 1.1 nm (mean ± SD, *n* = 50) and varied in length. A higher magnification in B revealed a very few fine filaments (arrows) with an average diameter of 5.6 nm.

An attempt of a TEM analysis of filaments assembled at lower protein concentration turned out to be difficult due to the small amount of protein per grid. Thus, the sample was spun down after the assembly process for concentration, which however, could cause cluster formation. The detected protein filaments had a mean thickness of 10.1 ± 0.9 nm (mean ± SD, *n* = 10). They appeared to be twisted around each other reminiscent of a coiled-coil structure (Figure 29).

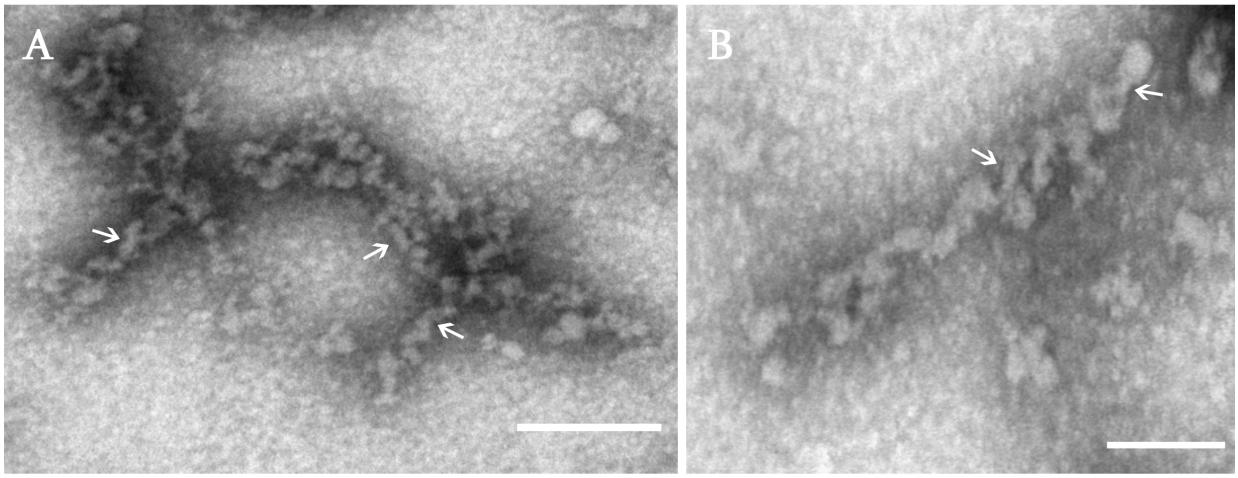

Figure 29 HisMyc-NE81ΔNLSΔCLIM filaments formed of 10 µg/ml protein solution visualized by negative-staining transmission electron microscopy. Two representative examples are shown. Arrows indicate examples of measured filaments with a diameter of 10.1 ± 0.9 nm (mean ± SD, *n*=10). Scale bars **A** = 200 nm, **B** = 100 nm.

All microscopic methods yielded comparable results and clearly showed that HisMyc-NE81ΔNLSΔCLIM is capable of forming protein assemblies made of filamentous structures.

2.5 NE81 mutants of the CDK1 phosphorylation site

Lamins are phosphorylated by CDK1 at mitotic onset, which finally triggers nuclear envelope breakdown (NEBD). Although *Dictyostelium* has a semi-closed mitosis with no NEBD, it was shown before that NE81 is also regulated by CDK1 and that serine 122 within the lamin head-domain is the main phosphorylation site. In cells with an open mitosis the lamin meshwork disassembles after lamin phosphorylation by CDK1 and the signal around the nucleus is gone. In *Dictyostelium* the nuclear membrane stays intact, but FRAP experiments indicate that phosphorylation at the onset of mitosis causes disassembly of NE81, which remains bound to the inner nuclear membrane through its lipid anchor. In contrast, a mutant expressing a S122A mutation, which mimics the unphosphorylated state shows a CDK1 independent behavior (Krüger et al., 2012). The clusters of a GFP-S122AΔNLS mutant were not able to disassemble during mitosis due to the lack of phosphorylation and persisted throughout mitosis. To have a better insight into the NE81 assembly properties, a phosphomimetic NE81-S122E mutant that mimics a permanent phosphorylation was generated

lacking the CaaX box and the NLS, which should express a disassembled protein in the cytosol. Cells were fixed, stained and prepared for ExM as described before (Figure 30).

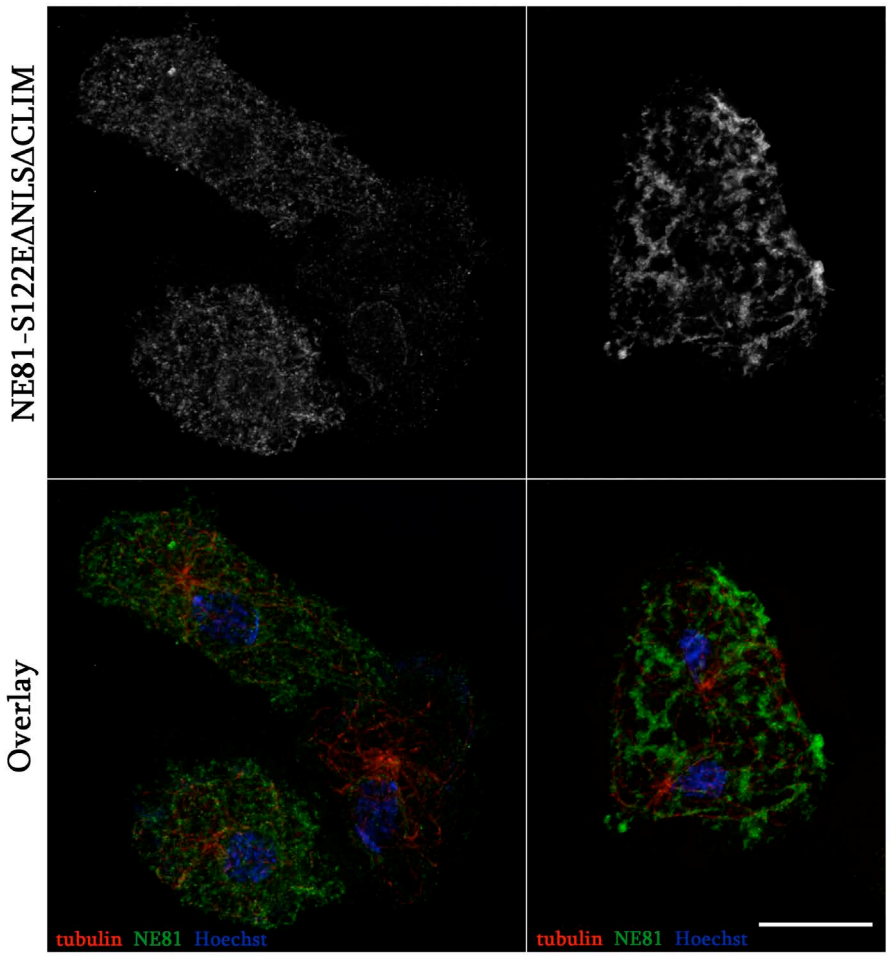

Figure 30 *Dictyostelium* cells expressing HisMyc-NE81-S122EΔNLSΔCLIM. Expansion microscopy employing an LCI PlanNeo 1.3/63× objective. Cells were fixed with glutaraldehyde and stained with anti-Myc/anti-mouse-Alexa Fluor 488, anti-tubulin/anti-rat-Alexa Fluor 568 and post-stained with Hoechst 33342. Merged images show tubulin in red, NE81-S122EΔNLSΔCLIM in green and chromatin in blue. Recombinant HisMyc-NE81-S122EΔNLSΔCLIM protein is mainly disassembled in the cytosol; no prominent cytosolic clusters are present in cells carrying the phosphomimetic S122E mutation. Expansion factor 3.8; scale bar = 5 µm (referring to the original size).

All cells of the HisMyc-NE81-S122EΔNLSΔCLIM mutant had a cytoplasmic NE81 signal. Most cells showed a thinly spread HisMyc-NE81-S122EΔNLSΔCLIM protein distribution throughout the whole cytoplasm. Some of it was reminiscent of a spider webs-like finely woven meshwork and some cells contained small clusters but not as prominent and big as in the HisMyc-NE81ΔNLSΔCLIM mutant. The existence of the point mutation was confirmed by sequencing genomic DNA containing a part of the NE81 gene amplified by PCR.

2.5.1 Light-induced NE81-S122E assembly formation

Surprisingly a GFP variant for live cell imaging showed a reversible light-sensitive assembly of NE81-S122EΔNLSΔCLIM protein in the cytoplasm. When illuminated with blue light, the disassembled protein began to assemble into small clusters, which disassembled again in the darkness (Figure 31).

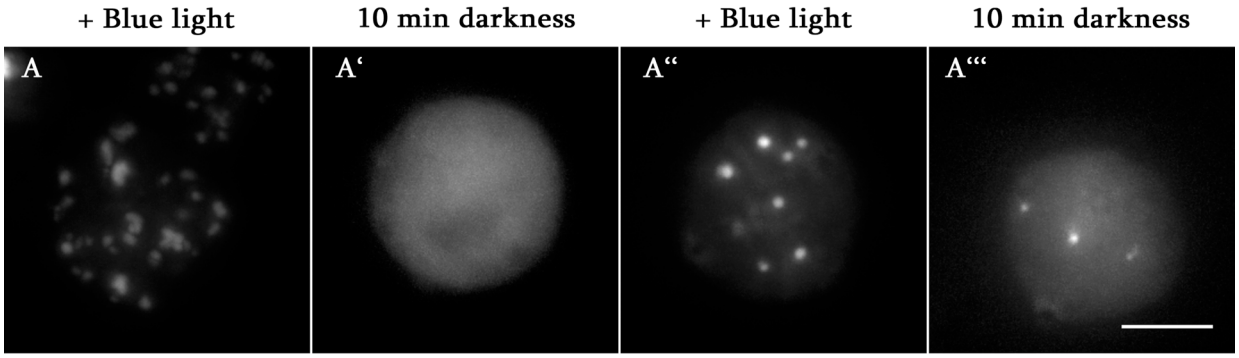

Figure 31 GFP-NE81-S122EΔNLSΔCLIM is blue light-sensitive and forms reversible cytosolic protein clusters. Selected time points of a live cell imaging series using a PlanApo 1.4/100× objective excitation with 488 nm. **A**: GFP-NE81-S122EΔNLSΔCLIM cell after 1:30 min excitation with 488 nm; **A'**: same cell after 10 min in the dark without excitation. **A''**: same cell after 1 min excitation with 488 nm. **A'''**: same cell after 10 min in the dark without excitation. Scale bar = 5 µm.

A GFP-NE81ΔNLSΔCLIM mutant without the phosphomimetic mutation shows the same assembly behavior in early telophase, where reassembly of the interphase GFP-NE81ΔNLSΔCLIM cluster takes place (Batsios et al., 2016). The size of the NE81 clusters increased along telophase and during cytokinesis (displayed in Figure 32, taken from the former publication).

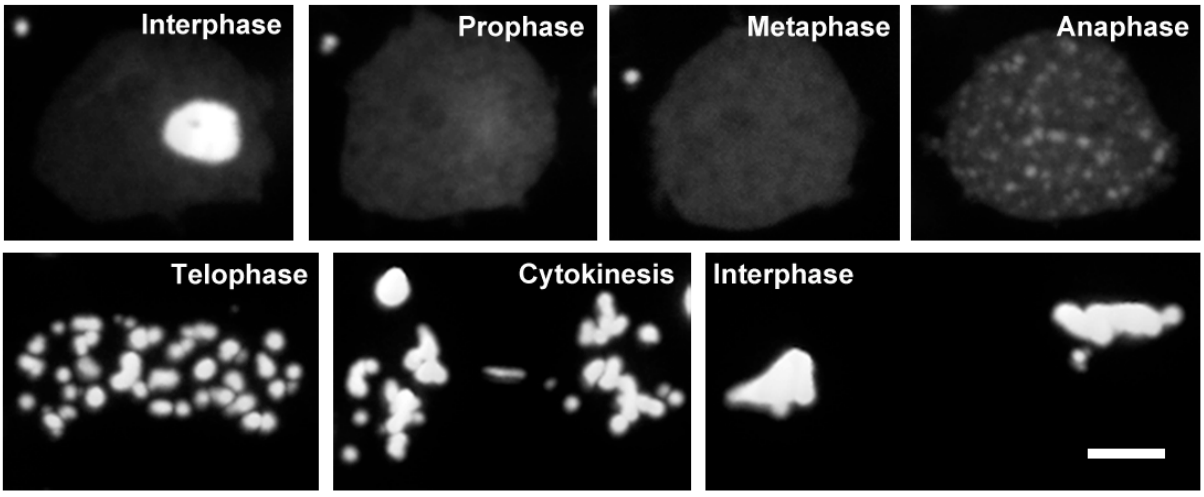

Figure 32 taken from Batsios et al. (2016). Dynamic behavior of GFP-NE81ΔNLSΔCLIM clusters during mitosis. Scale bar = 5 µm.

In a project-related Bachelor thesis supervised by myself this phenomenon was examined in more detail (Hofmann, 2019). It was found that the light-induced polymerization of NE81-S122EΔNLSΔCLIM was independent from the used fluorescence proteins. A mutant tagged with the red fluorescence protein mRuby showed the same behavior. Furthermore, assembly of the NE81-S122EΔNLSΔCLIM protein occurred only upon blue light illumination (488 nm) but not with violet (405 nm) or green light (561 nm). Mechanical stress by an agar-overlay triggered the formation of clusters as well, whereas mechanical stress from a shaking culture had no influence. Adding Vitamin C to prevent oxidative stress had no influence on cluster formation under blue light indicating that the reaction is not caused by oxidative stress. Also, a hypo- and hyperosmotic stress stimulation did not trigger cluster formation.

Although the mutant had a mutated NLS, some of the GFP-NE81-S122EΔNLSΔCLIM protein was incorporated into the nucleus (Figure 33 A, arrowhead).

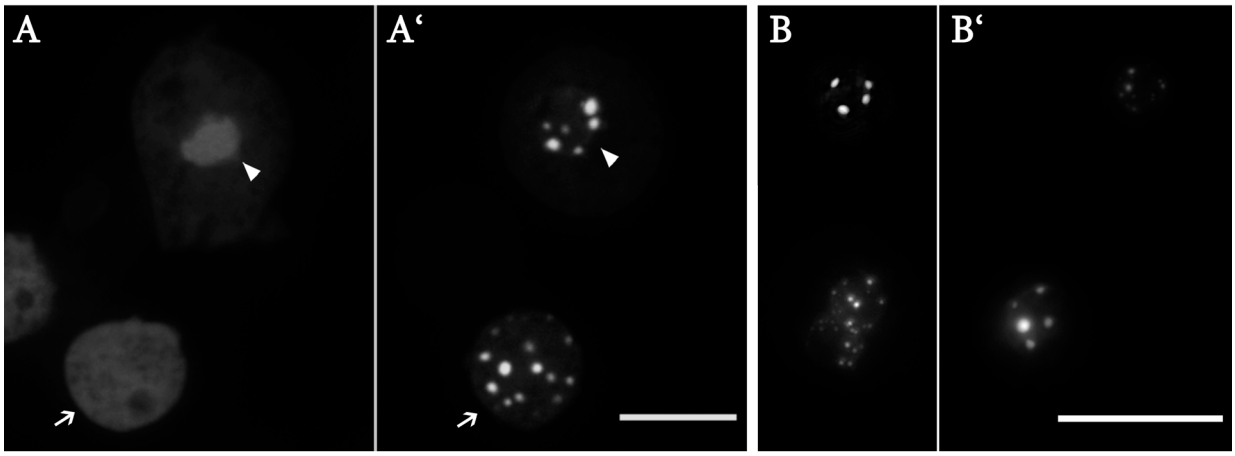

Figure 33 GFP-NE81-S122E mutants under distinct light exposure (A,B: no light ; A'B': blue light). Fluorescence light microscopy using a PlanApo 1.4/100× objective and excitation with 488 nm. **A,A'**: GFP-NE81-S122EΔNLSΔCLIM. Fusion protein expressed in whole cell (arrow) and in nucleus (arrowhead) is disassembled without light exposure and assembles into small clusters upon blue light illumination; **B,B'**: GFP-NE81-S122EΔCLIM. Fusion protein is located in the nucleus and forms small clusters independent from light-exposure. Scale bars = 10 µm.

Blue light illumination revealed that this fusion protein was still light-sensitive (A'). In contrast, a CaaX box deficient mutant with functional NLS (GFP-NE81-S122EΔCLIM), where the whole fusion protein was imported into the nucleus, showed a light-independent cluster formation throughout interphase instead of expected disassembled proteins (B, B'). The clusters inside the nucleus only disassembled during mitosis, as it is true for cells without S122 mutation.

The cytosolic cluster formation is also independent from a fluorescent protein tag. The mutant with the smaller HisMyc-tag showed the same blue light-sensitive formation of NE81-S122EΔNLSΔCLIM clusters in the cytoplasm (Figure 34 A). When cells were kept permanent in dark they consistently showed a disassembled NE81-S122EΔNLSΔCLIM protein in the whole cytoplasm (B).

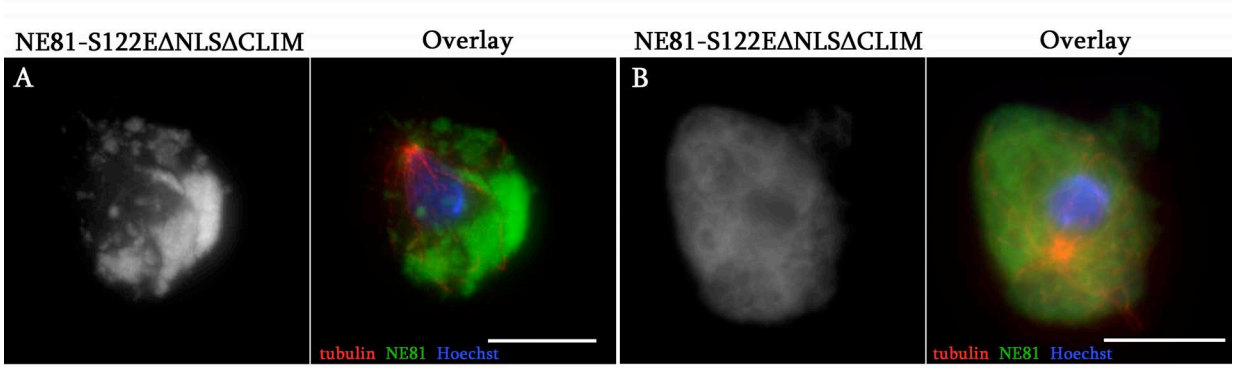

Figure 34 HisMyc-NE81-S122EΔNLSΔCLIM is blue light-sensitive and forms reversible cytosolic protein clusters. Expansion microscopy employing an LCI PlanNeo 1.3/63× objective. Cells were fixed with glutaraldehyde and stained with anti-Myc/anti-mouse-Alexa Fluor 488, anti-tubulin/anti-rat-Alexa Fluor 568 and post-stained with Hoechst 33342. Merged images show tubulin in red, NE81-S122EΔNLSΔCLIM in green and chromatin in blue. **A**: blue light stimulation, **B**: without light. NE81-S122EΔNLSΔCLIM is assembled in cytosolic clusters under blue light exposure (A) but disassembled when kept in dark (B). Expansion factors are 3.3 in A and 3.7 in B; scale bars = 5 µm (referring to the original size).

The comparison of the clusters with the HisMyc-NE81ΔNLSΔCLIM mutant without the S122 mutation shows a high similarity of the polymerized assemblies (Figure 35).

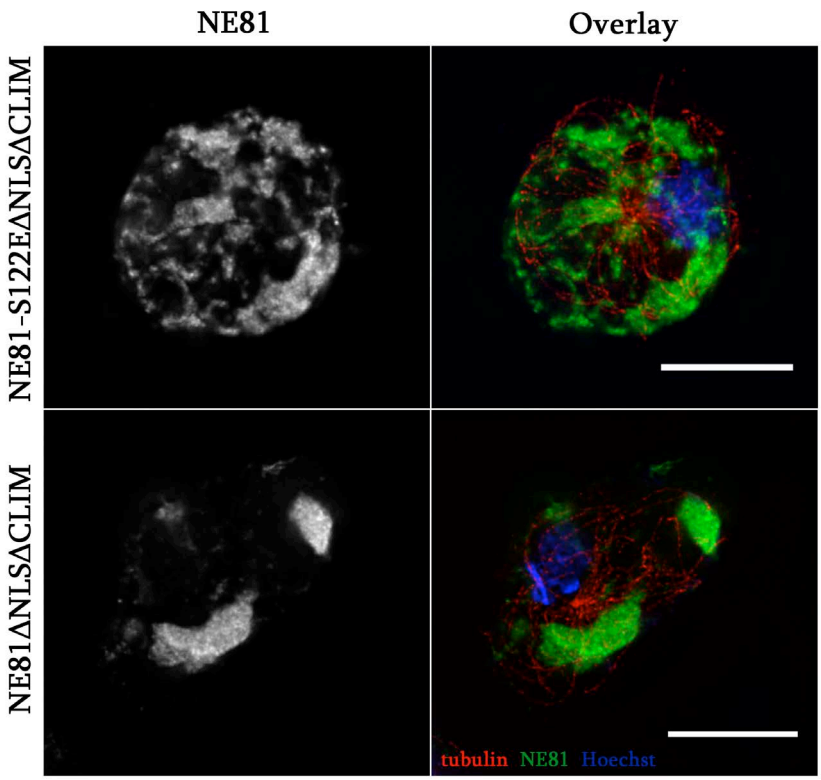

Figure 35 Similarity of NE81-S122EΔNLSΔCLIM and NE81ΔNLSΔCLIM cytosolic clusters. Expansion microscopy employing an LCI PlanNeo 1.3/63× objective and theoretical deconvolution. Cells were fixed with glutaraldehyde and stained with anti-Myc/anti-mouse-Alexa Fluor 488, anti-tubulin/anti-rat-Alexa Fluor 568 and post-stained with Hoechst 33342. Merged images show tubulin in red, fusion protein in green and chromatin in blue Top: HisMyc-NE81-S122EΔNLSΔCLIM mutant after blue light excitation. Bottom: HisMyc-NE81ΔNLSΔCLIM mutant. Expansion factors are 3.3 in A and 3.2 in B; scale bars = 5 µm (referring to the original size).

A better insight how these clusters are built-up should give a TEM analysis of these cells.

2.5.2 Purification and assembly properties of soluble NE81-S122E protein

To get an overview of solubility and assembly properties of the phosphomimetic mutant, HisMyc-NE81-S122EΔNLSΔCLIM protein was purified using the same protocol and buffer conditions as for HisMyc-NE81ΔNLSΔCLIM cells except from the growth conditions used. One cell batch was grown under normal light conditions in the cell culture laboratory and one batch in the dark. After affinity purification the fractions were compared on polyacrylamide gel stained with Coomassie blue (Figure 36).

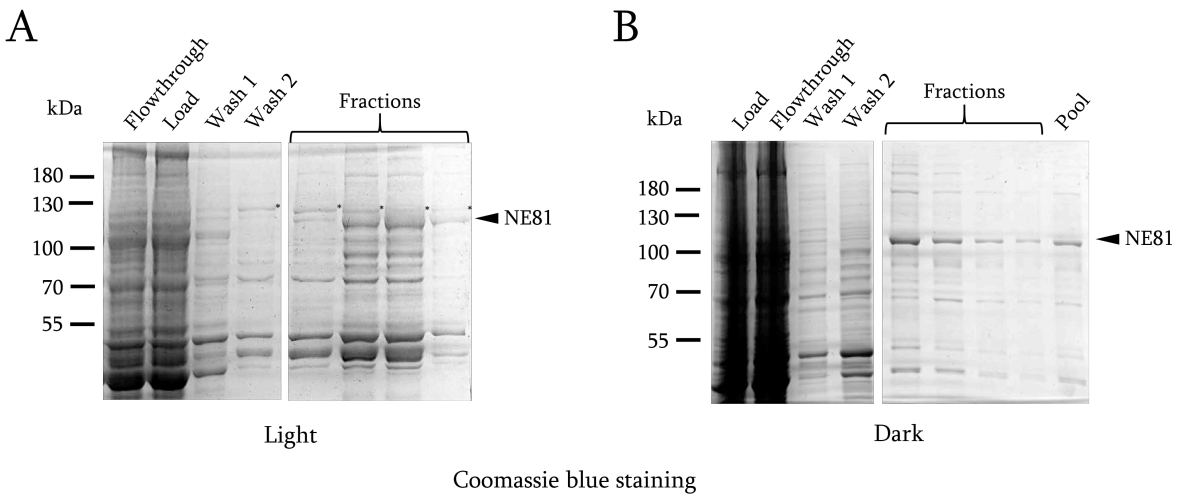

Figure 36 HisMyc-NE81-S122EΔNLSΔCLIM expressed in *D. discoideum* followed by affinity purification with Ni-NTA beads in 25 mM Tris-HCl, pH 8.0, 0.5 M NaCl. 8% SDS-gel Coomassie blue stained. **A**: Cells were grown under normal light conditions. Asterisks indicate additional prominent bands; **B**: Cells were grown in the dark.

In both batches the peak fractions contained more bands beside the NE81 band after affinity purification. Interestingly, cells grown with light had additional prominent bands e.g. above the NE81 protein (A, asterisks), which were missing when cells were grown in the dark (B). Western blot analysis with anti-NE81 confirmed that these bands did not contain NE81 protein. For further analysis, only protein purified from dark-grown cells was used.

Pooled and imidazole-free peak fractions were measured and a concentration of 0.2 mg/ml was used for assembly/disassembly experiments at low ionic strength. The NE81-S122EΔNLSΔCLIM protein was dialyzed against low salt buffer and then again against high salt buffer. All solutions were centrifuged and examined by immunoblotting followed by densitometric evaluation as described before. The values are displayed in a bar chart (Figure 37).

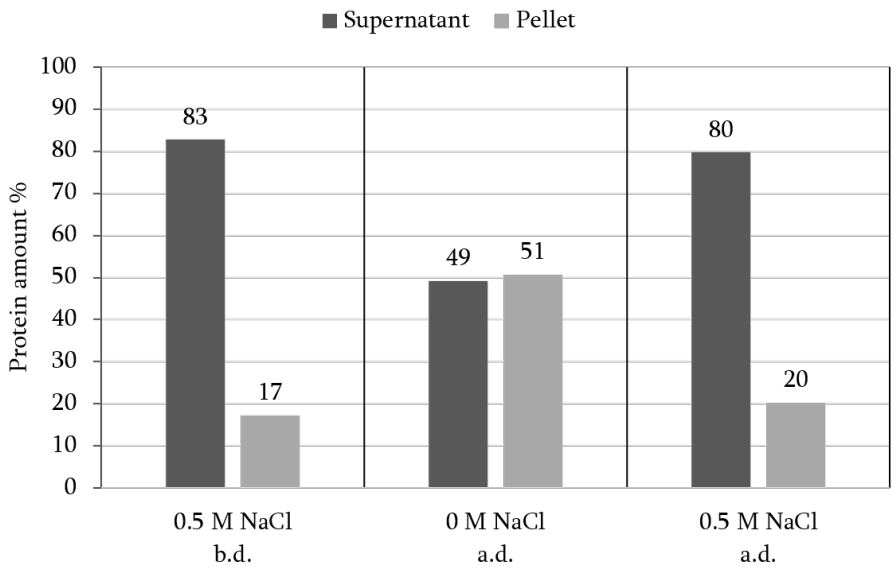

Figure 37 Proof of the specific assembly/disassembly reaction of NE81-S122EΔNLSΔCLIM protein. Protein solutions of 0.2 mg/ml were prepared in triplicate. One sample was centrifuged for 1 h 17,000x g without dialysis (0.5 M NaCl before dialysis b.d.). The other copies were dialyzed for 3 h against 25 mM Tris-HCl, pH 8.0. One sample of the duplicate was centrifuged for 1h 17.000x *g* (0 M NaCl after dialysis a.d.), the other was again dialyzed for 4.5 h against 25 mM Tris-HCl, pH 8.0, 0.5 M NaCl and centrifuged for 1h 17.000x *g* (0.5 M NaCl a.d.). Equivalent amounts of pellet (P) and supernatant (S) were loaded on SDS gels, blotted, stained with anti-Myc/anti-mouse-AP and detected with NBT/BCIP. Each value presents the average of triplicate determination.

HisMyc-NE81-S122EΔNLSΔCLIM is also soluble at high ionic strength. Before dialysis (0.5 M NaCl b.d.) the protein amount found in the supernatant was higher compared to the protein amount in the pellet. After dialysis in the absence of salt (0 M NaCl a.d.) the protein polymerized and the amount in the pellet increased. However, no macroscopic precipitate indicating filament assembly was visible in the dialysis tube as it was observed for HisMyc-NE81ΔNLSΔCLIM. The assembly behavior after three hours dialysis was just slightly different with 51% protein in pellet and 49% protein in supernatant comparable with the high protein concentration of HisMyc-NE81ΔNLSΔCLIM (Figure 22, 0.5 mg/ml). 80% of the protein got soluble again after dialysis against 0.5 M NaCl Tris-buffer (0.5 M NaCl a.d.) indicating that the polymerization at low ionic strength results from a specific assembly reaction of filaments and was not due to nonspecific aggregation. However, the phosphomutated protein showed a more efficient depolymerization with a level of 96% compared to HisMyc-NE81ΔNLSΔCLIM that just reached up to 88% of the starting value (Figure 22).

Taken together the *in vitro* assembly properties of HisMyc-NE81-S122EΔNLSΔCLIM were just slightly different from HisMyc-NE81ΔNLSΔCLIM without the phosphomimetic mutation.

3 Discussion

3.1 The suitability of the small 8xHisMyc-tag

A fluorescence protein tag is a sizeable addition to a protein and hence may interfere with protein folding, assembly or function (Andresen et al., 2004). GFP-variants and other fluorescence proteins have a size around 27 kDa, which is in case of NE81 one third of the protein of interest. It was shown before for intermediate filaments (vimentin), that a fused fluorescence protein has steric effects on the assembly and protein function (Kreplak et al., 2008). Therefore, the influence on structure and function of tagged NE81 was tested in NE81 knockout cells with fluorescence microscopy.

Dictyostelium cells that were forced to live with GFP-fusion protein only were viable but the GFP-tag clearly interfered with NE81 localization (Figure 7). Instead of a continuous distribution at the nuclear envelope, the fusion protein showed a pericentrosomal, crescent-like distribution at the nuclear membrane and the nucleus contained just one big nucleolus. In contrast, cells that only expressed the NE81 fusion protein with a small HisMyc-tag, showed an even distribution of HisMyc-NE81 at the nuclear envelope. The NE81 knockout strain HisMyc-NE81^{-KO} still displayed normal cell and nucleus shape and the common two to three nucleoli. Obviously, the cell is able to substitute the endogenous NE81 with the highly similar ectopically expressed tagged NE81-variant, which exhibits the same localization and behavior as the endogenous expressed protein. Moreover, the reduced endogenous expression level in the full length HisMyc-NE81^{-FL} mutant led to the conclusion that the increased protein level through expression of HisMyc-NE81 becomes compensated by suppression of expression of endogenous NE81 (Figure 4).

Since GFP-NE81 in NE81 knockout cells exhibited an abnormal distribution indicating that GFP-NE81 is not completely functional and is not able to assemble accurately, the shorter N-terminal 8×HisMyc construct was the tag of choice to investigate formation and structure of NE81.

3.2 Analysis of NE81ΔNLS assemblies at the outer nuclear membrane

Preliminary experiments have shown that NE81 without a functional NLS forms assemblies at the outer face of the nucleus. However, the GFP-NE81ΔNLS protein formed small cytosolic clusters in addition to its distribution at the nuclear envelope. HisMyc-NE81ΔNLS^{-G418} likewise showed a cytosolic signal in addition to its localization at the nuclear envelope although the smaller HisMyc-tag was used (Figure 9). In contrast, the HisMyc-NE81ΔNLS^{Bla} mutant containing another transformation cassette showed a uniform distribution around the nuclear envelope and had no cytosolic signal. Both plasmids are ectopically integrated into the genome, but the use of the blasticidin cassette typically leads to single insertions instead of multiple chromosomal tandem repeats, that are usually encountered when using the G418 cassette (Pang et al., 1999). Therefore, the cytoplasmic signal could well be an overexpression artifact and should not be caused by the fluorescence tag. The HisMyc-NE81ΔNLS^{-Bla} mutant was used for ultrastructural surface analysis with feSEM, as it was expected to allow a better view on the nuclear surface and the nuclear lamina that has assembled on it.

Although the feSEM picture of NE81ΔNLS nuclei (Figure 10) clearly showed a few filaments in the expected size, there were no repetitive filamentous structures on the surface and a large amount of other cytosolic material. The mean size (10.4 nm) of the filaments is comparable to that of lamins in a related assay (Goldberg et al., 2008, Grossman et al., 2012). Here the protein was overexpressed in *Xenopus* oocytes, which causes assembly at intranuclear membrane stacks. In this assay the invertebrate *C. elegans* lamin exhibited a diameter of 4 - 6 nm whereas somatic lamin B measured 7.3 nm and lamin A was thicker and formed 15.7 nm filaments. NE81 examined in the same assay showed a filament thickness around 8.5 nm (Grafe et al., 2019). This underscores the high similarity of NE81 to B-type lamins besides the shared domain organization.

3.3 Analysis of metazoan lamin assemblies at the outer nuclear membrane

Heterologous expression of *Xenopus* lamin LIII in *Dictyostelium* cells was only possible with a codon-optimized variant of the coding sequence. Nevertheless, the HisMyc-LIIIΔNLS fusion protein was not expressed in most cells and the ones that did, displayed irregular protein aggregates in the cytoplasm (Figure 12). Since the CaaX box differs between NE81 and lamin LIII and the importance of the individual amino acids within the CaaX box is not known completely, a mutant with the NE81-CaaX box was generated. In this mutant the expression of the fusion protein did not differ from that of the LIII-CaaX box mutant (Figure 13). No HisMyc-LIIIΔNLS CaaX box variant led to a continuous expression around the nuclear envelope indicating that the *Xenopus* CaaX box did not cause the absence of HisMyc-LIIIΔNLS at the outer nuclear envelope. Although the LIII fusion protein with functional NLS was imported into the nucleus, it showed no uniform assembly around the nuclear envelope. However its irregular distribution was somewhat reminiscent of overexpressed LIII in *Xenopus* oocytes (Ralle et al., 2004). Overexpressed *Xenopus* lamin B2 leads to intranuclear membrane assemblies in *Xenopus* A6 cells and *Drosophila* Lamin C-CaaX showed formation of paracrystals in the same assay, which was observed before in Sf9 cells upon high overexpression (Prüfert et al., 2004, Krohne et al., 1998). All transformation constructs used for LIII mutants in this study should lead to single genomic insertion of the construct encoding the fusion protein and hence, the irregular aggregation in the cytoplasm might not be caused by overexpression artifacts.

In contrast, the distribution of Ce-lamin expressed in *Dictyostelium* cells was not reminiscent of irregularly spread aggregates and was quite polymorphic (Figure 15). The Ce-laminΔNLS fusion protein appeared as small dots and curves very close to the nuclear envelope or exhibited cytosolic spheres. The Ce-lamin protein with functional NLS was expressed and imported into the nucleus but showed a discontinuous distribution in the form of small rings associated with the nuclear envelope (Figure 17). The mislocalization makes it very likely that the protein will not behave like a functional lamin in *Dictyostelium*. For this purpose, it could be tested whether the expressed Ce-lamin fusion protein could rescue the NE81 function in NE81 knockout cells.

Likewise, both mutants expressing *Xenopus* or *C. elegans* lamin with a functional NLS showed a different distribution compared to NE81. The fusion proteins were just partly associated with the inner nuclear membrane and showed an irregular and uneven assembly at the nuclear envelope. Since NE81 localizes to the nuclear envelope in mammalian cells (Krüger et al., 2012), it is possible that higher-order organisms may have evolutionary conserved proteins necessary for assembly and localization of lamins from low-ranking organisms. Vice versa some of the proteins necessary for localization of metazoan lamins could be absent in evolutionary older organisms.

Since both metazoan lamins could not be expressed properly at the outer nuclear membrane of *Dictyostelium* nuclei, the strategy to express heterologous ΔNLS-variants at the outer nuclear surface seemed not suitable to study the structure of lamin assemblies from other organisms. A possible reason for the binding of NE81 to the outer nuclear membrane could be its special composition in *Dictyostelium.* The NE81 interactor Sun1 is present in the inner nuclear membrane as well as at the outer nuclear membrane (Schulz et al., 2009a). Besides that, the nuclear surface of NE81ΔNLS cells appeared to be covered with other cytosolic material, probably endoplasmic reticulum and associated proteins (Figure 11), which makes this assay not ideal to study lamin assemblies at the outer nuclear surface in general. Therefore, this experimental strategy was refuted.

3.4 Analysis of soluble NE81 by *in vitro* protein assembly

Since NE81 could not be functionally expressed in bacteria, *Dictyostelium* was chosen as autologous expression system. An overexpression strain was generated, expressing a NE81 variant lacking a functional NLS and the CaaX box to facilitate protein isolation from the cytosol without chromatin or other nuclear envelope protein contamination. A small N-terminal 8×HisMyc-tag was used for purification and detection that exhibited no interference with NE81 assembly or function in previous experiments.

3.4.1 Same protein localization leads to suppression of endogenous protein

HisMyc-NE81ΔNLSΔCLIM clusters were expressed in the cytoplasm during interphase and showed a cell cycle regulated assembly/disassembly of the protein as expected (Figure 18). The overexpression construct ensured high expression levels of the fusion protein that were upregulated 2.5 times compared to endogenous NE81, which was slightly down-regulated (Figure 19). In contrast, a mutant expressing the full length fusion protein (HisMyc-NE81) also showed an upregulation of the fusion protein but associated with a strong down regulation of the endogenous NE81. The full length fusion protein is capable of replacing the endogenous NE81 at the inner nuclear membrane, whereas the truncated HisMyc-NE81ΔNLSΔCLIM protein mislocalizes in the cytoplasm and thus, cannot replace NE81 at the inner nuclear membrane. Hence, the suppression of endogenous protein only takes place if the endogenous and the mutant protein share the same localization. For further insights, this phenomenon should be examined with different proteins to develop more specific constructs for dominant negative effect studies.

3.4.2 Purification of soluble NE81 from Dictyostelium extract

The HisMyc-NE81ΔNLSΔCLIM cells were used as source to isolate high amounts of soluble NE81 protein. In analogy to purification and assembly experiments in the *C. elegans* system, parameters like pH-value, salt-content and protein concentration were optimized. Affinity purification with Ni-NTA beads in a buffer with high salt molarity of 0.5 M NaCl led to a strong and clear NE81 protein fraction without relevant amounts of contaminating proteins or protein degradation (Figure 20). Protein amounts up to 1.5 mg per 400 ml cell batch displayed an adequate protein yield.

3.4.3 Sedimentation behavior of NE81 at low ionic strength

The solubility of NE81 was further investigated by its sedimentation behavior under various buffer conditions with varying pH and NaCl concentration. Pellet and supernatant of the dialyzed samples were determined before and after centrifugation. The results confirmed

that high pH as well as high ionic strength favor the solubility of NE81 (Figure 21), as observed for other lamins before (Aebi et al., 1986, Foeger et al., 2006). A decreasing salt concentration yielded in a bigger pellet indicating formation of supramolecular complexes. Since it was possible to solubilize these complexes again by dialyzing against high salt buffer (Figure 22), it was not far-fetched to assume that these supramolecular complexes represented assemblies of NE81 resulted from a specific assembly reaction of filaments and are not from nonspecific aggregation of the HisMyc-NE81ΔNLSΔCLIM protein, even without microscopic analysis. Secondly, an influence of the starting protein concentration on the solubility could be shown. The lower the starting protein concentration, the higher was the solubility of the fusion protein. This could indicate a nonspecific interaction that leads to partial aggregation at high protein concentration. Lamins are elongated intermediate filament proteins and readily polymerize in concentrated solutions.

3.4.4 In vitro assembly of NE81 at low ionic strength

A dependence of the assembly behavior on the starting protein concentration was once more supported by the structural analyses of HisMyc-NE81ΔNLSΔCLIM assemblies formed at low ionic strength *in vitro*. Filament assemblies formed at protein concentrations of 0.1 mg/ml showed filament-like structures inside a meshwork detected by widefield microscopy (Figure 23). The appearance of these reticular NE81 networks was reminiscent of lamin meshworks detected in mammalian cells by super-resolution microscopy from Shimi and co-workers (Shimi et al., 2015). No single filament assembly was achieved by varying the buffer conditions as it was shown for Ce-lamin (Foeger et al., 2006). However, when the protein was dialyzed at a lower starting concentration, it assembled into long thin filaments (Figure 24). Hence, the HisMyc-NE81ΔNLSΔCLIM assemblies formed at low protein concentration were used for super-resolution microscopy analysis.

In addition to the well established STED method for super-resolution microscopy (Hell and Wichmann, 1994), I also explored the capabilities of the novel method of expansion microscopy as this method imposes less restrictions in the use of fluorophores and requires no

specialized technical equipment (Chozinski et al., 2016, Tillberg et al., 2016). In ExM, the specimen gets physically expanded in an isotropic fashion resulting in an up to four times increased resolution. The *in vitro* formed HisMyc-NE81ΔNLSΔCLIM assemblies displayed long filaments that differed in diameter and were often bundled into a helix-like structure (Figure 25). The intertwined arrangement of the filaments was reminiscent of paracrystalline arrays formed by the tunicate *Ciona* lamin (Karabinos et al., 2003). The latter differs from other metazoan lamins, as they are lacking the central 105-residue region of the lamin tail domain (LTD). This highly conserved domain usually forms an immunoglobulin-like fold (Ig-fold), which is a β-sandwich of nine β–strands. Although the LTD is present in NE81, it is not highly conserved and unlikely to build an Ig-fold (Stick and Peter, 2017), which could explain the structural similarity to paracrystalline arrangements of *Ciona* lamin. The evaluation of the NE81 filament thickness is not meaningful, since the resolution limit of expansion deconvolution microscopy is inadequate. According to the Rayleigh criterion (J. W. Strutt, 1989), the theoretical resolution limit is about 200 nm. In ExM with a four times increased species and applied theoretical deconvolution it would be 40 – 50 nm and hence, insufficient for the expected size of the filaments. The diameter of the smallest filaments was about 40 nm, which is in the range of the resolution limit for this microscopy method.

The second employed super-resolution method was STED (stimulation emission depletion) microscopy. Here the PSF is physically reduced leading to an increase in optical resolution up to 25 nm (xy) at optimal conditions. The latter are besides an accurately aligned STED laser setup, a close distance from fluorophores to the antigen and a minimal optic aberration. In case of HisMyc-NE81ΔNLSΔCLIM assemblies, the filaments were labeled with a primary anti-NE81 antibody and a secondary anti-rabbit antibody coupled with the Atto 647N fluorophore. The distance from antigen binding site to the fluorophore in an antibody-antibody labeling is greater than 10 nm, whereas in a more directly labeling with nanobodies the organic dye has a distance of just 2.5 nm to the target molecule (Mikhaylova et al., 2015). As a result, the measured diameter of anti-tubulin labeled microtubules is about 45 nm compared to ~ 26 nm with nanobody labeling (Gao et al., 2018). Thus, the optical resolution in the displayed STED experiment was lower than the optimal resolution of 25 nm. This is

underlined by the finding that the thinnest filaments detected with STED microscopy and ExM had approximately the same diameter. The STED images revealed long single filaments, whereby smaller filaments were bundled into a helix-like structure (Figure 26).

Although widefield deconvolution microscopy with an optical resolution of 170 nm (Pitzen et al., 2018) as well as super-resolution methods have a resolution limit beyond the expected size of NE81 filaments, these methods gave a great impression how these filaments could be constructed and how they are arranged with respect to each other.

A better insight into the thickness of *in vitro* polymerized HisMyc-NE81ΔNLSΔCLIM filaments was achieved by negative-staining TEM. First approaches displayed an irregular meshwork of filaments with a diameter around 13.2 nm (Figure 27) similar to light microscopic appearance of assemblies at higher protein concentration (Figure 23 B). Often the filaments stuck together in clusters and showed no satisfying contrast for size analysis of filaments. From previous studies it is known that lamins show different modes of assemblies under various experimental conditions (Foeger et al., 2006). Thus, further experiments were performed at various buffer conditions. An approach, in which the protein was dialyzed into 25 mM Tris-HCl, pH 8.0, 50 mM NaCl, resulted in longer and better distinguishable filaments (Figure 28). These filaments varied in length and displayed an average diameter of 9.4 nm. The images showed very few thinner filaments. A difficulty was the discovered dependency of the assembly behavior on the NE81 starting protein concentration. Although lower protein concentrations exhibited more single filament assemblies, it was difficult to detect the consequential few protein filament assemblies per grid. A concentration step by centrifugation turned out to be not useful, since most filaments clustered together and were twisted around each other (Figure 29). Nevertheless, the detected filament assemblies had a similar mean thickness of 10.1 nm. The difference in thickness could solely based on different methodology or inaccuracies in scale calibration, since another TEM instrument was used for the latter experiments. During the project the in-house TEM has been irreparably broken, which is why the electron microscopic images are unfortunately reduced to a minimum, as the analyses on another device were limited. It was not possible to calculate the number of protofilaments assembling into native NE81 filaments from the obtained data. The

results indicate that NE81 do not assemble into stable 10-nm filaments, as observed for other lamins before. *In vitro* experiments with other lamin proteins clearly showed that in most organisms the 10-nm filaments do not represent a stable species and are only temporary observed during lamin assembly (Aebi et al., 1986, Heitlinger et al., 1992, Sasse et al., 1997). The exact structural organization of lamin filaments was studied for decades and is still a controversial matter. Most *in vitro* experiments were done in the *C. elegans* system, as this was the only lamin building stable 10-nm intermediate filaments starting from purified, bacterially expressed recombinant protein (Karabinos et al., 2003). The filaments derived from lamin dimers assembled into head-to-tail polymers called protofilaments and are composed of three to four protofilaments (Ben-Harush et al., 2009). Data from Ce-lamin expressed in *Xenopus* oocyte nuclei revealed that the tetrameric protofilaments are just 4-6 nm thick (Grossman et al., 2012). The absence of transmembrane proteins and/or post-translational modifications in the *in vitro* assembly system could be a reason for different assembly of *in vivo* and *in vitro* filaments. In cells, lamins get post-translational processed allowing B-type lamins anchor to lipid membranes by an attached prenyl group and build 2D assemblies at the nuclear envelope. Missing of these binding may allow lamins *in vitro* to arrange in multiple self-interactions up to paracrystalline arrays. Recently the ultrastructural lamin network could be dissected in mouse embryonic fibroblasts (MEFs) carrying a knockout of the cytosolic IF vimentin. Here, cryo-EM images revealed that lamins assemble into tetrameric filaments of only 3.5 nm, i.e., about the size of a typical IF protofilament. In contrast to early experiments with lamin LIII structures in *Xenopus* oocyte nuclei by Aebi and co-workers (1986), who discovered highly ordered, orthogonally arranged 10 nm filaments at the inner nuclear membrane, the filaments in vimentin-null MEFs were not only much thinner, their arrangement beneath the inner nuclear membrane was also quite irregular (Turgay et al., 2017). In case of the *Xenopus* oocyte nuclei the meshwork consists almost completely of the embryonic B-type lamin LIII (= B3), which is absent in most differentiated cells. One interpretation of these obvious differences is that lamin filaments in more differentiated cells consist of just one protofilament arranged in an irregular criss-cross pattern. Another (less likely) possibility is that knockout of vimentin influences lamin assembly.

3.5 NE81 mutants of the CDK1 phosphorylation site

Entry into mitosis and the nuclear envelope breakdown are regulated by the CDK1 kinase that phosphorylates lamins at defined phosphorylation sites initiating the disassembly of the nuclear lamina (Simon and Wilson, 2013). *In vitro* studies on lamin assembly have indicated that phosphorylation of CDK1 sites in human lamin A or chicken lamin B2 are involved in regulating the head-to-tail polymerization of lamin dimers (Haas and Jost, 1993, Heitlinger et al., 1991). Although *Dictyostelium* has a semi-closed mitosis with no NEBD it is known that NE81 is regulated by CDK1. FRAP experiments showed that phosphorylation at the onset of mitosis causes disassembly of NE81 and serine 122 within the lamin head-domain is the main phosphorylation site (Krüger et al., 2012).

3.5.1 Light-induced NE81-S122E assembly formation

Studies on a phosphorylation mutant of cytosolic NE81 variants accidentally revealed a rather unexpected assembly behavior. In these mutants serine 122 of the CDK1 phosphorylation motif within NE81 was mutated to glutamic acid (S122E), which mimics a permanent phosphorylation (= phosphomimetic). Cells expressing tagged NE81-S122EΔNLSΔCLIM protein lacking the NLS and the CaaX box usually showed a disassembled protein in the cytosol as expected, but some cells contained small assemblies (Figure 30). Live cell imaging with a GFP variant revealed that the protein behaves light-sensitive (Figure 31). When cells were illuminated with blue light, the disassembled protein reversibly assembled into small clusters. Cell culture usually occurred under normal daylight-dependent conditions, which is an explanation of the small cluster formation in HisMyc-NE81-S122EΔNLSΔCLIM cells. When kept in dark permanently, GFP and HisMyc-tag mutant cells exhibited no assembly of fusion protein clusters, however when illuminated with blue light cluster formation was quite prominent indicating that NE81-S122EΔNLSΔCLIM is affected by a light-sensitive regulatory mechanism (Figure 34).

Until today no dedicated photoreceptor proteins were discovered in *Dictyostelium* such as LOV (Light-Oxygen-Voltage), BLUF (Sensors of Blue Light Using Flavin Adenine Dinucleo-

tide) or cryptochromes. The latter are flavin-type photoreceptors found in plants and animals and are sensitive to blue light (Chaves et al., 2011). BLAST searches for sequence and domain similarities to these proteins generated no hit for Dictyostelids. The amoeba carries a blue light photoreducible cytochrome b (cytB) protein evolutionary conserved in the mitochondrial genome. Although no evidence was found that the transmembrane protein controls any physiological responses in *Dictyostelium*, a cytB null mutant showed an impairment of phototaxis (Manabe and Poff, 1978, Francione and Fisher, 2011).

Interestingly a NE81 mutant still expressing a functional NLS is imported into the nucleus and showed light-independent clusters throughout interphase (Figure 33 B), which only disassembled during mitosis. In contrast, fusion proteins of the NE81-S122EΔNLSΔCLIM mutant that were unexpectedly imported into the nucleus were disassembled. It is very likely that the cytoplasmic fusion protein with mutated NLS binds co-translationally to endogenous NE81 and is imported into the nucleus as a dimer. Since the amount of the overexpressed NE81-S122EΔCLIM protein in the nucleus is much higher compared to the co-translationally imported NE81-S122EΔNLSΔCLIM protein, an assembly triggered by the high pressure inside the nucleus is possible. It is congruent with the fact that the NE81-S122EΔCLIM protein disassembles at the onset of mitosis, when the nucleus expands and get permeable to some point during cell division. Moreover, agar-overlay experiments with the NE81-S122EΔNLSΔCLIM mutant showed that the cytosolic protein is mechanosensitive to pressure.

Besides building the structure of the nuclear lamina, lamins are important for gene regulation and nuclear mechanotransduction processes (Lochs et al., 2019, Maurer and Lammerding, 2019). Hence, the mechanosensitive and light-dependent NE81 assembly could be a rescue mechanism ensuring protection of the *Dictyostelium* genome.

3.5.2 Purification and assembly properties of soluble NE81-S122E protein

As for NE81ΔNLSΔCLIM the *in vitro* assembly properties of the phosphomimetic variant were studied. The protein was purified using the same buffer and protocol except for the growth conditions. Since the mutant showed a light-sensitive behavior, cells were grown either at light or darkness. Interestingly, the protein band pattern of the peak fractions differed in both purification batches. The one grown at light, where the cells displayed partly assembled protein in the cytoplasm, showed various protein bands above and under the main peak fraction, which was not the case of the cell batch grown in the dark (Figure 36).

The solubility of NE81-S122EΔNLSΔCLIM was just slightly different compared to the NE81ΔNLSΔCLIM protein (Figure 37), i.e. the protein was soluble at high ionic strength and polymerized into fast sedimenting clusters at low ionic strength. An assembly/disassembly experiment showed that the polymerization resulted from a specific assembly reaction of filaments and was not due to nonspecific aggregation. However, NE81-S122EΔNLSΔCLIM showed no macroscopic precipitates and its depolymerization behavior was more efficient. A higher protein percentage was soluble again compared to the depolymerization of NE81ΔNLSΔCLIM. TEM analysis of *in vitro* NE81-S122EΔNLSΔCLIM protein should give a better insight, whether the phosphomimetic mutant behaves differently in filament assembly. An altered supramolecular structure of *in vitro* assembled filaments was previously shown for *C. elegans* lamin that carried a mutation in an evolutionarily conserved residue that causes the Hutchison-Gilford progeria syndrome in humans (Ben-Harush et al., 2009).

3.6 Conclusion

The major goal in this work was to test whether NE81 is capable of forming filamentous structures at all. Although the filaments observed in the diverse microscopic analyses showed rather complex patterns and variable lengths, the formed arrays appeared similar and exhibited a consistent diameter. Since it was originally claimed that non-metazoans possess no intermediate filaments, the research on the *Dictyostelium* protein NE81 clearly revealed that non-metazoan organisms do contain *bona fide* lamins that are able to form filamentous assemblies as evidenced by ultrastructural data. *Dictyostelium* is the only non-metazoan model organism so far with a well-characterized nuclear envelope expressing all relevant protein components known from higher cells. The speed and low cost of cell culture, the simplicity of genetic manipulation, and good applicability for microscopic analysis makes *Dictyostelium* an excellent non-metazoan experimental model to study nuclear envelope organization dynamics and potential related diseases such as laminopathies.

3.7 Outlook

In an alternative approach membrane-associated lamin protein assemblies can be obtained expressing NE81 at the surface of giant unilamellar vesicles (GUVs) using Sf21 insect cell extracts (Sachse et al., 2014). A basic requirement for the assembly of NE81 on the surface of GUVs is the ability of the translated protein to bind to lipid membranes. In preliminary experiments the expression of soluble NE81 was successful in such extracts, however with relatively low yields. Furthermore, NE81 translated *in vitro* was not associated with the microsome fraction (Suckau, 2016). Since the expressed control protein eYFP-CaaX did not bind the microsomes either, it is likely that the activity of the ER-bound enzymes required for lamin processing in the insect cell extract was too low; without a functional Farnesyltransferase it is not possible to isoprenylate a CaaX box protein. Since NE81 was properly associated with nuclear envelopes in Hela cells (Krüger et al., 2012), the attachment of a farnesyl group should be unproblematic in a mammalian cell system. Since processing should principally work, this experimental approach should be repeated with another, verified insect cell

lysate batch. The association of expressed NE81 with the surface of GUVs offers two advantages. First, it allows separation of the expressed protein from other proteins in the extract by sedimentation of GUVs. Second, at the correct experimental conditions NE81 should form supramolecular assemblies similar to those at the inner nuclear envelope in intact cells. The NE81 assemblies will be at the outer face of the membrane compartment and hence, well accessible for ultrastructural analyses.

Additionally, further TEM analyses could be implemented with *in vitro* NE81 assembled under various buffer conditions. These examinations may find conditions that make it possible to evaluate the length and number of protofilaments assembling into native NE81 filaments.

The interesting NE81-S122EΔNLSΔCLIM mutant should be further investigated to possibly find the trigger of the light-sensitive assembly behavior. NE81 could be the light-sensor itself or more likely another protein in the cell that rescues the NE81 filament assembly. This could be tested by *in vitro* polymerization of the purified NE81-S122EΔNLSΔCLIM protein under different light conditions (blue light vs. no light). If the purified protein shows no light-sensitive behavior *in vitro*, it is very likely that light-sensitive assembly *in vivo* depends on the cellular environment. A candidate for the light-sensor *in vivo* would be cytochrome b. NE81-S122EΔNLSΔCLIM could be expressed in cytB null mutants in order to prove whether blue light illumination still leads to a cluster formation of the S122E mutant or if cytB has an effect on the NE81 assembly.

4 Materials and Methods

4.1 Materials

4.1.1 Chemicals

Unless otherwise stated, chemicals and reagents were purchased from Carl Roth (Karlsruhe), Sigma-Aldrich (St. Louis, MO, USA), Thermo Fisher Scientific (Waltham, MA, USA), and AppliChem GmbH (Darmstadt) and had *pro analysis* grade. Solutions were prepared with deionized ultra-pure water (ddH_2O).

4.1.2 Buffers, Solutions, Media

Phosphate-buffered saline

- 70 mM Na_2HPO_4; 30 mM KH_2PO_4; 137 mM NaCl; 2.6 mM KCl; pH 7.4

Soerensen-phosphate buffer

- 14.6 mM KH_2PO_4; 2 mM Na_2PO_4; pH 6.0

Phosphate agar

- Soerensen-phosphate buffer with 15 g/l bacto agar

Electroporation buffer

- 50 mM Saccharose, 10 mM KH_2PO_4, pH 6.1

SDS-PAGE buffers

- Resolving gel buffer: 1.5 M Tris-HCl, pH 8.7, 0.4% SDS, pH 8.7
- Stacking gel buffer: 500 mM Tris-HCl, pH6.8, 0.4% SDS
- Running buffer: 100 mM Tris-HCl, pH 8.3; 0.1% SDS; 100 mM glycin

6x Laemmli sample buffer

- 300 mM Tris-HCl, pH 6.8; 30% glycerol; 20% SDS; 0.025% bromphenol blue; 15% 2-mercaptoethanol

Urea sample buffer

- 10% SDS, 9 M urea, 5% 2-mercaptoethanol

Coomassie blue staining solutions

- Staining solution: 0.1% Coomassie R250, 25% isopropyl alcohol; 10% acetic acid
- Destaining solution: 25% isopropyl alcohol; 10% acetic acid

Western blot buffers

- Blotting buffer I: 300 mM Tris, 10 % methanol
- Blotting buffer II: 30 mM Tris, 10 % methanol
- Blotting buffer III: 30 mM Tris, 10 % methanol, 40 mM ε-aminocaproic acid

Ponceau S staining solution

- 0.1% Ponceau S, 5% acetic acid

TBS

- 20 mM Tris-HCl, 150 mM NaCl, pH 7.4

TBST

- 20 mM Tris-HCl, 150 mM NaCl, 0.05% Tween-20, pH 7.4

Alkaline phosphatase reaction buffer

- 100 mM Tris-HCl, 100 mM NaCl, 50 mM $MgCl_2$, pH 9.5

Buffers for plasmid DNA Mini-preparation

- DNA buffer I: 50 mM Glucose, 25 mM Tris, 10 mM EDTA, RNaseA (10 μg/ml)
- DNA buffer II: 0.2 N NaOH, 1% (w/v) SDS
- DNA buffer III: 3 M KaOAc, pH 5.2

TE buffer

- 10 mM Tris, 1 mM EDTA, pH 8.0

TAE running buffer

- 40 mM Tris, 0.1% acetic acid, 1 mM EDTA, pH 8.3

50x protease inhibitor cocktail (PC)

- 50 mM Pefabloc SC, 100 mM benzamidine, 1.25 mg/ml leupepti, 0.5 mg/ml soybean trypsin inhibitor, 0.5 mg/ml tosyl-arginine-methylester, 50 µg/ml pepstatin, 50 µg/ml aprotinin

Affinity purification buffers

- Affinity lysis buffer: 50 mM Tris-HCl, pH 8.0, 1 M NaCl, 20 mM imidiazol
- Equilibration buffer: 25 mM Tris-HCl, pH 8.0, 0.5 M NaCl, 10 mM imidiazol
- Washing buffer: 25 mM Tris-HCl, pH 8.0, 0.5 M NaCl, 25 mM imidiazole
- Elution buffer: 25 mM Tris-HCl, pH 8.0, 0.5 M NaCl, 250 mM imidiazole
  > All buffers contained freshly added imidiazole
- Dialysis buffer: 25 mM Tris-HCl, pH 8.0, 0.5 M NaCl

Assembly buffers

- High salt buffer: 25 mM Tris-HCl, pH 8.0, 0.5 M NaCl, 1 mM DTT
- Low salt buffer: 25 mM Tris-HCl, pH 8.0, 1 mM DTT

Amido black staining solutions

- Wash solution: acetic acid/methanol 1:10
- Staining solution: 2.6 mg/ml amido black in wash solution

Buffer for nuclei isolation

- Nuclei lysis buffer: 100 mM Na-PIPES, pH 6.9, 2 mM $MgCl_2$, 10% (w/v) sucrose; 1 x PC, 2 µM cytochalasin, 1 mM DTT
- Gradient buffer: 100 mM Na-PIPES, pH 6.9, 2 mM MgCl2; 2 mM DTT, 1x PC
- Sucrose solutions: 30% or 50% (w/v) sucrose, 100 mM Na-PIPES, pH 6.9, 2 mM $MgCl_2$, 2 mM DTT, 1x PC

PHEM

- 60 mM PIPES, 25 mM HEPES, 10 mM EGTA, 2 mM $MgCl_2$, pH 6.9

SEM buffer

- 2% glutaraldehyde, 0.2% tannic acid, 0.1 M Hepes, pH 7.4

Expansion microscopy solutions

- Monomer solution: 1xPBS, 2 M NaCl, 2.5% (wt/wt) acrylamide, 0.15% (wt/wt) N,N′-methylenebisacrylamide, 8.625% (wt/wt) sodium acrylate
- Accelerator solution: 10% TEMED (AppliChem)
- Initiator solution: 10% APS (AppliChem)
- Digestion buffer: 50 mM Tris-HCl, pH 8.0, 1 mM EDTA, 0.5% Triton X-100, 0.8 M guanidine HCl

Mounting medium

- 120 mg/ml polyvinyl alcohol 4-88, 30% glycerol, 0.2 M Tris-HCl, pH 8.8

HL5c medium Formedium™, Hunsanton, UK

HL5c medium without glucose Formedium™, Hunsanton, UK

- 10 g/l sterile filtered glucose added after autoclaving

LoFlo-Medium Formedium™, Hunstanton, UK

LB medium

- 10 g/l tryptone; 5 g/l yeast extract; 10 g/l NaCl; pH 7.0

LB agar plates

- LB-Medium with 1.5 % bacto agar

SM-agar plates

- 10 g/l peptone (Oxoid); 1 g/l yeast extract (Oxoid); 10 g/l glucose; 20 g/l bacto agar; 1.6 g/l K_2HPO_4; 2.2 g/l KH_2PO_4; 1 g/l $MgSO_4$; pH 6.5

4.1.3 Antibiotics

Ampicillin	100 µg/ml	Carl Roth
Blasticidin S	4 µg/ml	Carl Roth
Geneticin (G418)	10 µg/ml	Carl Roth
Kanamycin	50 µg/ml	Carl Roth
Penicillin/Streptomycin	100 µg/ml	PAA GmbH (Pasching, Austria)

4.1.4 Antibodies

Primary antibodies

Anti-NE81	Krüger et al. (2012)
Anti-Myc (9E10)	Evan et al. (1985)
Anti-tubulin (YL 1/2)	Wehland et al. (1983)
Anti-Sun1	Schulz et al. (2009a)
Anti-LIII	Benavente et al. (1985)
Anti-His	Thermo Fisher

Secondary antibodies

Anti-mouse Alexa Fluor 488	Thermo Fisher
Anti-rabbit Alexa Fluor 488	Thermo Fisher
Anti-rabbit Alexa Fluor 568	Thermo Fisher
Anti-rat Alexa Fluor 568	Thermo Fisher
Anti-rabbit Atto 647N	Sigma-Aldrich
Anti-rabbit AP IgG	Sigma-Aldrich
Anti-mouse AP IgG	Sigma-Aldrich
Anti-rabbit POD	Dianova (Hamburg)

4.1.5 Enzymes

Phusion polymerase	Thermo Fisher
Taq polymerase	Roboklon (Berlin)
HotStart polymerase	Qiagen (Hilden)
HybridX polymerase	Roboklon (Berlin)
Restriction enzymes	Thermo Fisher
T4-DNA-Ligase	Thermo Fisher
FastAP phosphatase	Thermo Fisher
T4 PNK	New England Biolabs (Ipswich, MA, USA)
Proteinase K	Macherey-Nagel (Düren)

4.1.6 Kits

NucleoSpin® Gel and PCR Clean Up	Macherey-Nagel (Düren)
NucleoBond® Xtra Midi	Macherey-Nagel
NucleoSpin® Tissue	Macherey-Nagel
CloneAmp™ HiFi PCR Premix	Takara Bio Europe (Saint-Germain-en-Laye, France)
In-Fusion® HD Cloning Plus	Takara Bio Europe

4.1.7 Oligonucleotides

	8xHisMyc_F	CTAGCCATCATCATCATCATCATCATCATGCTGAAGAAC AAAAATTAATTTCAGAAGAAGATTTAtG
	8xHisMyc_R	TCGACaTAAATCTTCTTCTGAAATTAATTTTTGTTCTTC -AGCATGATGATGATGATGATGATGATGG
B24	VP3-1Sal_F	TAAATTGTCGACTAATGGATATGTCAAAAAAGAAAAGTAAAC
B25	VP3-2Bam_R	TTTGGATCCTTACATAATCAAACAATTTGATTTACC
B55	NE81_Ala_NLS_F	GCTGCGGCAGCGGCAGCAGCACTTCAACATGAATTCAATGCTGCTG
B56	NE81_Ala_NLS_R	TGCTGCTGCCGCTGCCGCAGCATCATCAACGGTCTTTTCAAAACCT
B77	NE81Bam-CLIM	gcgcggatccttaATTTGATTTACCAGCTGAAGAAGG
B89	NE81-S122E_F	CACAAATAGGTACACCATTAgaACCAAATAG
B91	NE81-S122E_R	GTTGAGCTGCTCTATTTGGTtcTAATGGTG
B117	NE81-test_R	gttttatttatttaattaagcattttggg
B119	NE81-KO_R	CATATGCCGCATGGTTAATTCCT
B121	NE81-test_F	TCGATCCAGAAATTCCACTTGAT
M4	LIII_Sal_F	gtggaaGTCGACtaATGGCTAC
M5	LIII_Bam_R	gcatggatccTTACATAATTGAACA
M6	LIII_Bam_CLIM_R	attggatccTTACATAATCAAACATGAACGATCA
M13	CeLamin_Slice_F	CAGAAGAAGATTTAtGTCGAatgtcatctcgtaaaggtactcgt
M14	CeLamin_Slice_R	TTCGAGCTCTAGTCGAttacatgatggaacaacgatcgg
M15	CeL_dNLS_F	gcaagcgctcaggctgcggcagcggcagcagcagttgtcgatgtaaatg
M16	CeL_dNLS_R	catttacatcgacaactgctgctgccgctgccgcagcctgagcgcttgc

4.1.8 Plasmids

pIS76	GFP-Blasticidin resistance cassette	Schulz et al. (2009b)
pIS77	GFP-G418 resistance cassette	Schulz et al. (2009b)
pIS419	NE81 knockout cassette	Krüger et al. (2012)
pIS922	pIS76 w/o GFP + 8xHisMyc	this work
pIS966	pIS77 w/o GFP + 8xHisMyc + NE81 FL	this work
pIS956	pIS922 + NE81ΔNLS	this work
pIS977	pIS966 + NE81ΔNLS	Lisin (2017)
pIS928	pIS922 + LIII^{CSIM} ΔNLS	this work
pIS1084	pIS922 + LIII^{CLIM} ΔNLS	this work
pIS1219	pIS922 + Ce-Lamin	this work
pIS1220	pIS922 + Ce-Lamin ΔNLS	this work
pIS976	pIS966 + NE81ΔNLSΔCLIM	Lisin (2017)
pIS1026	pIS77 + NE81-S122EΔNLSΔCLIM	this work
pIS1015	pIS966 + NE81-S122EΔNLSΔCLIM	Lisin (2017)
pIS1031	His-Ce-lamin pET24d #429 (TEV)	Foeger et al. (2006)

4.1.9 Biological Strains

Escherichia coli strains: TOP10 and DH5a (Thermo Fisher), Stellar™ (Takara Bio Europe)

Klebsiella aerogenes (Williams and Newell, 1976)

Dictyostelium discoideum strains

AX2^{-214}	Axenic wild type	Guenther Gerisch lab
IS301	GFP-NE81^{FL}-G418 *NE81* knockout-blasticidin	RG45 + pIS419
MG7	HisMyc-NE81^{FL}-G418	AX2 + pIS966
MG28	HisMyc-NE81^{FL}-G418 *NE81* knockout-blasticidin	MG7 + pIS419
MG27	HisMyc- NE81ΔNLS-blasticidin	AX2 + pIS956
MG11	HisMyc- NE81ΔNLS-G418	AX2 + pIS977
MG4	HisMyc-LIII^{CSIM} ΔNLS-blasticidin	AX2 + pIS928
MG14	HisMyc-LIII^{CLIM} ΔNLS-blasticidin	AX2 + pIS1084
MG19	HisMyc-Ce-Lamin-blasticidin	AX2 + pIS1219
MG20	HisMyc-Ce-LaminΔNLS-blasticidin	AX2 + pIS1220
MG10	HisMyc-NE81ΔNLSΔCLIM-G418	AX2 + pIS976
MG26	GFP-NE81-S122EΔNLSΔCLIM-G418	AX2 + pIS1026
MG15	HisMyc-NE81-S122EΔNLSΔCLIM-G418	AX2 + pIS1015
PB13	GFP-NE81-S122EΔCLIM-G418	Petros Batsios (unpublished)

4.1.10 Software

Adobe Photoshop CS5 extended V.12	(Adobe Inc., San José, CA, USA)
ApE – A plasmid Editor v2.0.49	(M. Wayne Davis)
AxioVs40x64 V 4.9.1.0	(Carl Zeiss Microscopy GmbH, Jena)
Azure c300 imaging software	(Azure Biosystems, Dublin, CA, USA)
EndNote X9.2	(Clarivate Analytics, Philadelphia, PA, USA)
ImageJ 1.51j8/1.52i	(Wayne Rasband, NIH, USA)
Intas-Capture-Software	(Intas Science Imaging Instruments GmbH, Göttingen)
Microsoft Office 2013	(Redmond, WA, USA)
Zen 2 blue edition	(Carl Zeiss Microscopy GmbH, Jena)

4.1.11 Data Bases

BLAST	https://blast.ncbi.nlm.nih.gov/Blast.cgi
Coiled coil- pred	http://www.ch.embnet.org/
Dictybase	http://www.dictybase.org/
ELM motif search	http://elm.eu.org/search/
HMMER biosequence analysis	http://hmmer.org/
NCBI Pubmed	http://www.ncbi.nlm.nih.gov/pubmed
Uniprot	https://www.uniprot.org/

4.2 Molecular Biological Methods

4.2.1 Polymerase Chain Reaction

All PCR reactions took place in a thermo cycler (peqSTAR 96 Universal Gradient) according to the following PCR protocols.

- *Phusion PCR*

The required DNA fragment was amplified by PCR using the thermostable Phusion™ High Fidelity DNA Polymerase (Thermo Fisher). The template was either genomic DNA (5 – 125 ng) or plasmid DNA (0.5 pg – 5 ng) in a 25 µl reaction mixture. The general protocol was used with distinct annealing temperatures calculated for every primer pair with the NEB Tm calculator (http://tmcalculator.neb.com/). Extension temperature was set to 68°C with 40 s/kb.

Program:			50 µl attempt
2min 98°C		32.5	µL ddH_2O
5-10 s 98°C	} 30 – 35 x	10	µl 5x HF buffer
15-30 s Tm°C		2	µL d'NTP Mix 5mM
40 s/kb 68°C		2	µL Primer 1/2 10 µM
5 min 68°C		0.5	µl Phusion polymerase
		1	template

Product	Primer pair
NE81	B24/B25
LIII	M4/M5
LIII	M4/M6

- *Overlap-Extension PCR*

For the overlap-extension PCR according to Nelson and Fitch (2011) the particular DNA fragments were amplified using the Phusion PCR protocol (Step1). As second step, the two purified PCR products (fragment 1 and fragment 2) with equimolar ratios of 0.1 pmol in total, served each other as primers and templates at the same time. During annealing, the complementary partial sequences overlap and the entire sequence is then completed during extension, resulting in a hybrid PCR product of the two fragments. The PCR was done with HotStart polymerase (Qiagen) with an extension temperature of 68°C and 1 min/kb. The hybrid PCR product was purified and eluted in 30 µl. 10 µl served as template and was amplified again using the forward primer of fragment 1 and the reverse primer of fragment 2 applying the Phusion PCR protocol in a 50 µl reaction mix (Step3).

Program Step2:			50 µl attempt
5min 98°C		10	µl HotStart buffer with dNTPs
15 s 94°C	13 x	X	µL Fragment I
1 min 60°C		X	µL Fragment II
4 min 68°C		1.5	µl HotStart polymerase
10 min 72°C		ad 50	µL ddH_2O

Program Step3:			50 µl attempt
30 s 98°C		17.5	µL ddH_2O
10 s 98°C	31 x	10	µl 5x HF buffer
30 s Tm°C		2	µL d'NTP Mix 5mM
40 s/kb 68°C		5	µL Primer 1/2 10 µM
5 min 68°C		0.5	µl Phusion polymerase
		10	µl DNA purified from Step2

Product	Primer Step 1	Primer Step3
NE81ΔNLS	B24/B56 (f1) and B55/B25 (f2)	B24/B25
NE81ΔNLSΔCLIM	B24/B56 (f1) and B55/B77 (f2)	B24/B77
NE81-S122EΔNLSΔCLIM	B24/B91 (f1) and B89/B77 (f2)	B24/B77

- *Knockout PCR*

Successful insertion of the knockout construct pIS419 in *Dictyostelium* strains MG28 and IS301 was tested with genomic DNA by PCR. Primer pairs B121 and B117 were used as positive control for intact genomic DNA (product 824 bp) and B119 with B117 to prove the right insertion of the knockout cassette (product 845 bp). B121 binds to the coding sequence of NE81, which is in the endogenous gene and the knockout plasmid and the reverse primer B117 binds in the 3'UTR region right behind the stop codon as well as in the inserted knockout plasmid. Control strains and mutant strains should be positive if the genomic DNA is intact. The forward primer B119 binds elusively in the knockout plasmid and just results in a product when the cassette knocked out the endogenous *NE81* gene. Since normal extension temperatures were not working, a two-step protocol using the HybridX polymerase (Roboklon, Berlin) was used and the annealing/extension temperature was set to 60°C, which favors amplification of AT-rich DNA sequences.

Program:			25 µl attempt
2:30 min 98°C		17.25	µL ddH_2O
20 s 98°C	}	2.5	µl 10x Hybrid buffer II
1:30 min 60°C	} 35 x	1	µL d'NTP Mix 5mM
5 min 68°C		1.5	µL Primer 1/2 10 µM
		0.25	µl Hybrid X
		1	µl template

- *PCR for Verification of Transformants*

The existence of ectopic insertion of the plasmid DNA was confirmed by amplifying a part of the transformed gene construct in the genomic DNA followed by sequencing. The general PCR protocol for Taq polymerase was used and annealing temperature was calculated for

every primer pair with the NEB Tm calculator. Extension temperature was set to 68°C with 1 min/kb.

Program:			25 µl attempt
2 min 95°C		17.25	µL ddH_2O
20 s 95°C		2.5	µl 10x Hybrid buffer II
30 s Tm°C	35 x	1	µL d'NTP Mix 5mM
1 min/kb 68°C		1.5	µL Primer 1/2 10 µM
5 min 68°C		0.25	µl Hybrid X
		1	µl template

Product	Primer pair
NE81	B24/B25

- *CloneAmp™ HiFi PCR*

Primers were designed according to the protocol of the In-Fusion® HD Cloning Kit (Takara Bio Europe) with at least 15 bp homologies to the vector for one insert and 20 bp homologies for two insert fragments. The CloneAmp HiFi PCR 2X master mix already contains a polymerase, a deoxynucleotide mix and reaction buffer. The CloneAmp HiFi Polymerase is sensitive and highly efficient in DNA amplification. Required template DNA amount is < 1 ng for plasmid DNA and < 100 ng for genomic DNA.

Program:			25 µl attempt
30 s 98°C		11	µL ddH_2O
10 s 98°C		12.5	µl CloneAmp HiFi PCR Premix
15 s Tm°C	35 x	0.5	µL Primer 1/2 10 µM
10 s/kb 68°C		0.5	µL template
5 min 68°C			

Product	Primer pair
Ce-laminΔNLS	M12/M13

4.2.2 Agarose Gel Electrophoresis

For visualization and purification of the PCR products, the DNA fragments were separated according to their size in an agarose gel electrophoresis. Gels were made with TAE buffer and 1% agarose. The corresponding volume of 6X loading buffer (Thermo Fisher) was added to the DNA solution before loading on the gel. The marker for estimation of the DNA size was either GeneRuler 1 kb DNA Ladder or GeneRuler 100 bp DNA Ladder (Thermo Fisher). Separation was performed at 100 V for one hour. Afterwards the gel was stained with 1 µg/ml ethidium bromide in TAE buffer for 20 min. Visualization and cutting out of bands was performed with the LED-Transilluminator (Blue Light, SERVA). Documentation was done with the Gel Doc System (Inventas, Göttingen) using UV illumination. Purification of DNA fragments in gel was done with the NucleoSpin® Gel and PCR Clean Up Kit.

4.2.3 Vector Constructions

The coding sequences for NE81, LIII and Ce-lamin were cloned into overexpression vectors based on the N-terminal GFP-fusion vector pIS76 and pIS77 (blasticidin and G418 resistance, respectively) as described previously (Schulz et al., 2009b). The coding sequences were amplified by PCR using suitable linker primers containing the restriction enzyme binding site (see 4.2.1). For 8xHisMyc-vectors the GFP-cassette was replaced with restriction enzymes NheI and SalI.

- Restriction Enzyme Digestion and Ligation

Before cloning, the plasmids as well as the purified PCR products (=inserts) were digested with fast digest restriction enzymes (SalI/BamHI for gene insertion and NheI/SalI for tag insertion) according to the manufacturers datasheet with 1 µl enzyme per DNA for two hours at 37°C. The DNA Fragments were purified by agarose gel preparation and the NucleoSpin® Gel and PCR Clean Up Kit. The DNA content was determined by measurement of OD_{260} with a spectrometer (Nanodrop, Thermo Scientific). For ligation with T4 ligase, the required DNA amount of insert and backbone was calculated using a ligation calculator (http://www.insilico.uni-duesseldorf.de/Lig_Input.html). Additionally, a 15 µl reaction con-

tained 1 µl T4 ligase and 1,5 µl 10x ligation buffer. The ligation batch was incubated for 16 h at 16°C.

Construction of the 8xHisMyc-tag plasmid was done by oligonucleotide annealing. The primers (complementary sequences) were mixed in equimolar DNA amounts and incubated for one hour in a water bath (100°C water in a beaker at room temperature were the water cools down within the hour). The 50 µl batch contained 5 µl oligonucleotide (100 µM) each and 5 µl 10x TBS in ddH2O. The annealed oligonucleotides were phosphorylated for 30min at 37°C and inactivated at 65°C for 20 min. A 50 µl phosphorylation batch contained 5 µL 10x ligase buffer (Thermo Fisher), 1 µL T4 PNK (Thermo Fisher) and 300 pmol annealed oligonucleotide solution in ddH_2O. The corresponding backbone plasmid (pIS76 without GFP) was dephosphorylated for 10 min at 37°C and inactivated at 65°C for 15 min. A 20 µl batch contained 100 ng/µl plasmid DNA, 2 µl 10xFastAP-buffer (Thermo Fisher) and FastAP Thermosensitive Alkaline Phosphatase (Thermo Fisher) in ddH_2O. The DNA fragments were purified and ligation took place as described previously.

In SliCe cloning (Seamless Ligation Cloning Extract) short end homologies (>15 bp) with flanking heterologous sequences are recombined in an *in vitro* recombination reaction based on a bacterial extract derived from RecA- *E,coli* strains (Zhang et al., 2012). The RecA independent recombination leads to single-strand annealing relying on exonuclease-generated single-strand DNA overhangs. With this method even multiple DNA fragments can be easily assembled into a recombinant DNA construct. The cloning method was used to generate the Ce-lamin plasmids, one containing a mutation of the NLS in the Ce-lamin sequence. The PCR products were amplified using the CloneAmp HiFi PCR protocol. For linearization pIS922 was digested with SalI, purified and 80 ng was used for the In-Fusion cloning reaction using the Takara kit. The molar ratio for one insert was 1:2, one mole vector and two moles insert (pIS1219) and 1:2:2 for two inserts (pIS1220). Besides DNA, the reaction mixture contained 2 µl 5x HD Enzyme Premix and ddH_2O to a total volume of 10 µl. The reaction was incubated 15 min at 50°C. 2,5 µl was used for transformation in Stellar™ cells.

Gene synthesis Xenopus lamin LIII: Invitrogen™, LifeTechnologies (Thermo Fisher)

4.2.4 Heat Shock Transformation of Competent E. coli Cells

The chemically competent *E. coli* strains TOP10 or DH5a (Thermo Fisher) were used for standard heat-shock transformation. 100 µl freshly thawed *E. coli* cells were incubated 10 min one ice before adding to ligation solution in a 1.5 ml reaction tube. The mix incubated on ice for 30 min. Next, cells were heat-shocked for 90 s at 42°C in a thermo block (Grant-bio, PCMT) and chilled on ice for 2 min afterwards. 400 µl LB-media was added and cells were incubated at 37°C for 30 min gently shaking at 180 rpm (rounds per minute) in a thermo shaker(Grant-bio, PCMT) followed by plating on prewarmed LB media agar with the corresponding antibiotics. Plates were incubated at 37°C overnight. The next day single colonies were picked with a toothpick and transferred in 15-ml tubes with 3 ml LB media containing the corresponding antibiotic. The tubes were incubated overnight at 37°C at 220 rpm in a shaking incubator. Plasmid DNA mini-preparation was done the next morning.

Transformation procedure according to the In-Fusion® HD Cloning Kit from Takara was done with Stellar Competent Cells. 2.5 µl of the In-Fusion reaction mixture was added to the freshly thawed competent cells in a 2-ml reaction tube. Cells were incubated 30 min on ice, heat-shocked for 60 s at 42°C and placed on ice for 2 min. Then 450 µl SOC medium (Takara Bio Europe) was added and cells were incubated at 37°C for one hour gently shaking at 180 rpm .50 µl of the cells were plated on prewarmed LB media agar with the corresponding antibiotics, incubated at 37°C overnight and treated as described above.

4.2.5 Plasmid DNA Preparation

The recombinant plasmids were isolated by alkaline lysis. For the mini-preparation, cells from 1.5 ml liquid culture were transferred in 1.5 ml reaction tubes and were pelleted by centrifugation at 11,000x g for 5 min (Microcentrifuge Micro Star 17R, VWR). The pellet was resuspended in 200 µl of DNA buffer I. Then 200 µl of DNA buffer II was added. Samples were mixed by inverting 5 times and incubated for 5 min at room temperature. Next, 200 µl of buffer III was added and mixed by inverting 10-times. Tubes were centrifuged for 30 min at 17,000x *g* at 4°C. The supernatant was carefully transferred into a new reaction tube and

500 µl isopropanol was added. Samples were mixed by inverting the tubes 10-times and centrifuged for 45 min at 17,000x g at 4°C. Afterwards the supernatant was discarded and the pellet was washed with 500 µl 70% ethanol followed by centrifugation for 10 min. The supernatant was discarded and the pellet was dried at room temperature for 10 min and resolved in 30 µl sterile water. Samples were stored at 8°C. Correct insertion of the DNA fragment into the construct was verified by restriction enzyme digestion. For digestion 5 µl DNA with 0.1 µl of the corresponding enzymes (Thermo Fisher), 1.5 µl FD buffer (Thermo Fisher) in 15 µl ddH2O was incubated for 10 min at 37°C and visualized by agarose gel electrophoresis as described previously. Positive clones were sequenced. The corresponding bacteria culture was used to inoculate 50 ml LB media for a midi-preparation. The cell culture was incubated at 37°C overnight and the next day centrifuged 11,000x g for 30 min (Centrifuge type, Beckmann Coulter). The pellet was stored at -20°C or directly prepared with the NucleoBond PC 100 Kit (Macherey-Nagel, Düren). Separation of the cell debris was done by filtration. The DNA pellet was resolved in 100 µl ddH2O and the concentration was determined by Nanodrop measurement.

4.2.6 Dictyostelium DNA-Preparation

Mutant strains were grown in a medium cell culture flask with HL5C medium and the corresponding antibiotic. A cell concentration of $1 \cdot 10^7$ was spun down (400x *g* 2 min) and the pellet was used for DNA preparation with the NucleoSpin® Tissue Kit. The pellet was resuspended in 100 µl lysis buffer T1 and 25 µl Proteinase K and 200 µl buffer B3 was added and incubated for 10 min at 70°C. After lysation, 96% ethanol was added vortexed and the sample was applied to a column. After washing with buffer BW and B5 and removal of ethanol, the DNA was eluted with 50 µl elution buffer BE. DNA concentration was determined by Nanodrop measurement.

4.3 Cell Culture Methods

4.3.1 Transformation of Dictyostelium Cells

Transformation of the recombinant DNA was done by electroporation according to Gräf et al. (2003). *Dictyostelium* cells from -80°C stocks were inoculated in HL5c medium. The cells were grown at 21°C in a tissue culture flask to a density of $2 \cdot 10^6$ cells/ml. 25 ml were transferred in a 50 ml tube and chilled on ice for 20 min. Cells were centrifuged at 400x g for 5 min (Heraeus Multifuge 1 S-R) and washed twice with 25 ml phosphate buffer. The third washing step was done with 10 ml electroporation buffer. Cells were resolved with 700 µl electroporation buffer and transferred in a cooled electroporation cuvette (4 mm) with 25 µg of plasmid DNA. Electroporation was performed by two pulses with an electrical capacity of 3 µF, a voltage of 1.1 kV and a resistance of 1000 Ω for overexpression plasmids and 200 Ω for knockout plasmids (BIO-RAD GenePulser® II). Afterwards the cells rested at room temperature for 10 min. Sterile-filtered MgCl2/CaCl2 was added to a final concentration of 1 mM. The suspension was gently rotated for 15 min at room temperature.

For transformations with blasticidin S resistance, the cells were solved in 25 ml HL5c-PenStrep medium and pipetted to a 24-well-plate. After 24 h the medium was replaced with blasticidin S supplemented medium (4 µg/ml). Medium was carefully changed every three days. After growth, mutants were fixed and verified with widefield immunofluorescence and by Western blot analysis.

For transformations with G418 resistance, the cells were transferred to a cell culture flask with 25 ml HL5c-PenStrep medium. After 24 h the cells were harvested by centrifugation and washed twice with phosphate buffer. *Klebsiella aerogenes* bacteria, grown on SM agar at 37°C overnight were transferred in 5 ml phosphate buffer. The suspension was supplemented with 10 µg/ml G418 and 2.5 ml were used to resuspend the transformed cells. 500 µl were plated on phosphate agar plates containing 100 µg/ml G418, respectively. After 1-2 weeks plaques were visible. Single-plaques were resuspended with 5 µl HL5c-PenStrep-G418 medi-

um and transferred to 500 µl medium in a 24-well plate. After growth, mutants were fixed and verified with widefield immunofluorescence and by Western blot analysis

4.3.2 Preparation of Dictyostelium Spores

For long-term storage *Dictyostelium* cells were grown at 21°C to a density of $2 \cdot 10^6$ cells/ml. 50 ml were harvested by centrifugation (400x *g* for 5 min). After washing twice with phosphate buffer the cells were resuspended in 500 µl phosphate buffer and plated on phosphate agar. Upon starvation *Dictyostelium* cells aggregate and form a multicellular body. The last stage is a fruiting body consisting of stalk and spore cells. After 1-2 days the cells on the plates were harvested in 1 ml phosphate buffer and the spores were kept at -80°C.

4.3.3 Preparation of Dictyostelium Cells for Purification or Nuclei Isolation

50 µl spores of the mutant or the mutant were inoculated from -80°C stocks in 10 ml HL5c-G418 medium in a cell culture flask. When cells were confluent, the cell suspension was used to inoculate 400 ml HL5c-G418 medium in an Erlenmeyer flask. Cells were grown axenically to a density of $2 \cdot 10^6$ cells/ml on a rotary shaker (140 rpm) and harvested by centrifugation (400x g 10 min, Beckmann JLA-16.250 rotor). The cell pellet was washed twice with chilled phosphate buffer and a third time with phosphate buffer containing 2 µM cytochalasin A (Sigma-Aldrich) and 1x proteinase inhibitor cocktail. Cells were stored at -20C or directly used for affinity purification procedure and nuclei isolation, respectively.

4.4 Biochemical Methods

4.4.1 Protein Affinity Purification

Dictyostelium cells were grown and washed as described (see 4.3.3). The cell pellet was resuspended with an equal volume of affinity lysis buffer, 1x protease inhibitor cocktail and 1mM DTT. After filter lysation with a 5 µm Nucleopore polycarbonate filter (Whatman, GE Healthcare, Freiburg) the cell suspension was centrifuged at 4000x *g* for 15 min 4°C. Super-

natant was loaded directly onto Ni-NTA beads (Takara Bio Europe) equilibrated with equilibration buffer. After washing with equilibration buffer and washing buffer the bound protein was eluted with elution buffer. Protein fractions were checked for protein expression by Coomassie stained SDS gel, pooled and dialyzed overnight into dialysis buffer with 0.5 M NaCl. The protein solution was briefly centrifuged at 17,000x *g* and the supernatant was used for further analysis.

In pre-experiments the purification was done with buffers containing 50 mM Tris-HCl, pH 8.0, 0.3 M NaCl or 25 mM Tris-HCl, pH 8.0, 0.3 M NaCl, but with the same imidiazole concentrations as described.

4.4.2 Determination of Protein Concentration

The protein concentration was measured with the Nanodrop by OD_{280} or Amido black staining. For the amido black assay BSA (Thermo Fisher) samples of different concentrations (4 µg, 8 µg, 12 µg and 16 µg) were prepared in triplicate and were used to generate a reference curve. All protein samples were mixed with 300 µl of staining solution and were incubated for 5 min at room temperature. The precipitate was spun down at 11,000x *g* in a Microcentrifuge (Micro Star 17R, VWR), washed twice with wash solution and was resuspended in 700 µl 0.1 M sodium hydroxide. All samples were measured at 615 nm. The standard curve and evaluation of protein concentration was done with Microsoft Excel. The mean value of the triplicate was used for calculations.

4.4.3 Assembly Studies

For electrophoretic analysis of assembly behavior, the purified protein was diluted with high salt buffer to the indicated concentration and dialyzed (SpectraPor dialysis tubing, 3.5 kDa cut-off membrane) for 4 h at 4°C into the respective low salt buffers with various NaCl concentrations followed by centrifugation (17,000x *g*, 1 h, 4°C). The pellets were resuspended in a buffer volume equal to the supernatants, and 12 µl of each sample containing 2 µl

6x Laemmli buffer were loaded on SDS-PAGE followed by Western blotting. Densitometric measurements of immunoblot bands were done with ImageJ software.

4.4.4 SDS-Polyacrylamide Gel Electrophoresis

Protein samples from cell extracts were preprared from $4 \cdot 10^5$ cells lysed in 10 µl urea buffer and incubated for 5 min at 70°C (Thermoblock, Grant-bio, PCMT). In protein samples from protein purification 1/5 volume of 6x Laemmli buffer was added and incubated for 5 min at 95°C. As molecular weight standard 4 µl of PageRuler® Prestained Protein Ladder (Thermo Fisher) was used. Proteins were separated using the Biorad mini system (Biorad, München). The gels were made of 10% polyacrylamide or 8% PDA. Samples were run in SDS running buffer at a current of 15 mA per gel until the samples reached the resolving gel. The current was set to 30 mA per gel until the samples reached the end of the gel. SDS gels were either used for immunoblotting or stained for one hour in Coomassie staining solution without methanol. After staining the gel was washed in destaining solution for one hour followed by incubation in water overnight. Gels were scanned using a HP Scanjet 4890.

4.4.5 Immunoblotting

For Western blot analysis the proteins were blotted from the gel to a nitrocellulose membrane (Pore size 0.2 µm, Carl Roth) in a semidry electroblot system according to Gräf et al. (1998). Transfer was done with 25 mV for one hour. After blotting the membrane was stained with Ponceau S solution for 15 min and scanned using a HP Scanjet 4890.

For alkaline phosphatase reaction (AP) the membrane was blocked with 3% fish gelatin (Carl Roth) in TBST for 1 h. After washing three times for 3 min with TBST the primary antibody (diluted in 1% fish gelatin in TBST) was added and incubated for 1 h. Anti-NE81 was used 1:5000 and anti-Myc 1:3. After three washing cycles with TBST the secondary antibody conjugated with alkaline phosphatase diluted 1:10000 in TBST was added and incubated for 1 h. After three washing cycles with TBST and two with TBS the membrane was incubated in alkaline reaction buffer supplemented with 4.4 µl/ml NBT and 3.5 µl/ml BCIP until the pro-

tein bands were detectable. The reaction was stopped by placing the membrane into water. Detection was carried out using a HP Scanjet 4890.

For enhanced chemiluminescence (ECL) the membrane was blocked with 1% BSA and 5% milk powder (both Carl Roth) in TBST for two hours. After three washing steps 3 min each with TBST the primary antibody (diluted in 1% BSA, 1.5% milk powder in TBST) was added and incubated for 1 h. The membrane was washed three times with TBST. The secondary antibody conjugated with horseradish peroxidase was diluted 1:5000 in TBST containing 1% BSA and incubated for 1 h. The membrane was washed three times with TBST and two times for 10 min with TBS. The blot was developed with the Rotilumin ® Kit (Carl Roth) by mixing 1 ml luminol and enhancer solution each and incubation for 1 min The ECL reaction was detected with the Azure c300 (Azure Biosystems, Dublin, CA, USA).

4.4.6 Isolation of Nuclei

Cells were grown and prepared as described (see 4.3.3) and the nuclei isolated according to Batsios et al. (2013). The cell pellet was resuspended in 20 ml nuclei lysis buffer and lysed by filtration using a 5 µm Nucleopore polycarbonate filter (Whatman, GE Healthcare, Freiburg) two times. The filtrate was loaded on a chilled sucrose gradient (1 ml of 50% sucrose solution with 2 ml of 30% sucrose solution on top) and centrifuges for 10 min at 3,700× *g* (Hettich 460 R) at 4°C. The nuclei fraction was concentrated at the 50%/30% sucrose boarder and was carefully removed without disturbing the pellet and placed on ice for further analysis.

4.5 Microscopy

4.5.1 Fixation for Immunofluorescence Microscopy

For cell fixation $2 \cdot 10^5$ cells in exponential growth phase were used. Cells settled on cover slips for 20 min and were fixed for 5 min in PHEM buffer and freshly supplemented 0.5% glutaraldehyde and 0.5% Triton X-100. Cells were washed with phosphate buffer and blocked for 10 min with freshly prepared 0.1% $NaBH_4$ in phosphate buffer. Cells were

washed two times with PBS and incubated with the primary antibody. Anti-NE81 or anti-Sun1 were diluted 1:1000 in PBS with 1 % BSA and 0,1 % NaN_3. For labeling with anti-Myc and anti-tubulin the cell culture supernatant was used undiluted. Cover slips were washed three times with PBS and incubated for 1 h with the corresponding secondary antibody (diluted 1:1000). Cells were washed two times with PBS and incubated with 0.1 µg/ml DAPI in PBS for 15 min. Cover slips were mounted on slides with mounting medium.

For light microscopic assembly studies the purified protein was diluted with high salt buffer and dialyzed as described above. 10-25 µg protein were centrifuged onto round 12 mm coverslips (4500x *g*, 10 min, 4°C) followed by incubation in fixative (3.7% formalin in phosphate or Tris buffered saline, pH = 8.0) for 5 min. Specimens were labeled as described.

4.5.2 Analysis of Isolated Nuclei

For immunofluorescence of isolated nuclei (HisMyc-Ce-lamin and HisMyc-Ce-laminΔNLS), 20 µl of the nuclei were diluted in 200 ml gradient buffer and spun down on 12 mm cover slips for 10 min at 2800x g. Nuclei were fixed on coverslips for 5 min in PHEM buffer with freshly supplemented 0.5% glutaraldehyde and with (+detergent) or without (Ø detergent) 0.5% Triton X-100. Remaining fixation steps, antibody labeling and chromatin staining was done as described before.

4.5.3 Widefield Immunofluorescent Microscopy

Widefield fluorescence microscopy was performed as described previously (Kuhnert et al., 2012) using a Zeiss CellObserver HS system equipped with a PlanApo 1.4/100x objective, an Axiocam MRm Rev.3 CCD camera and a piezo stage (Carl Zeiss Mikroskopie GmbH, Jena). For deconvolution of image stacks the iterative algorithm of Axiovision 4.8 (Carl Zeiss Mikroskopie GmbH, Jena) and either a point spread function (PSF) measured with 200 nm Tetraspeck beads (conventional light microscopy; Thermo Fisher) or a theoretical PSF (expansion microscopy) were employed.

4.5.4 Super-resolution Microscopy

Expansion microscopy was carried out according to Chozinski et al. and Tillberg et al. (2016). Fixation was done with glutaraldehyde as described before. Incubation time for labeling was extended and the antibody concentration was higher. Primary antibody was incubated up to 8 h at 4°C with a 1:500 dilutions (anti NE81/anti-Sun1) and the secondary antibodies were incubated up to 4 h and diluted 1:500 in PBS. Instead of DAPI, the chromatin was stained with 10 µg/ml Hoechst 33342 (Thermo Fisher) in PBS. It turned out that DAPI is not stable during expansion microscopy processing. Staining followed by 10 min post-fixation with 0,025% glutaraldehyde in PBS. The cover slip was mounted in gelling solution immediately after post-fixation using 188 µl monomer solution mixed with 4 µl 10% APS, 4 µl 10% TEMED and 4 µl ddH_2O. Gelation occurred in a self-made slide chamber with #4 cover slips as spacer for 30min followed by 45 min proteinase K digestion at 37°C in digestion buffer containing 8 units/ml proteinase K. Gels were cut in trapezoids, measured and expanded for two hours in water followed by 30 min incubation with 50 µg/ml Hoechst 33342 in ddH_2O. The gel was placed in water for 20 min. Then a part of the gel was treated with 5% DABCO (Carl Roth) in ddH_2O and placed on a polylysine-L (Sigma-Aldrich) coated slide with the specimen up. The gel was mounted with a high precision cover slip on top fixed with Twinsil (picodent, Wipperfürth) at the sides. For imaging the same Zeiss CellObserver HS system equipped with a LCI PlanNeo 1.3/63× objective was used.

STED microscopy was carried out essentially as described before (Klauss et al., 2015, Klauss et al., 2017) using a retrofitted confocal microscope based on an Olympus inverted time-resolved confocal scanning microscope (MicroTime 200, PicoQuant, Berlin) equipped with an Olympus UPLSAPO 1.4/100x objective. The incubation time for primary antibody labeling was extended (overnight, 4°C). The cover slip was mounted in Prolong® Gold (Thermo Fisher).

4.5.5 Electron Microscopy

Transmission electronic microscopy was performed with a TEM Philips CM100 electron microscope (Prof. Dr. Otto Baumann) or JEOL JEM1011 (Sibylle Rüstig). For negative staining 4 µl aliquots were absorbed for 2 min to pioloform-coated copper grids, fixed 2min with 2,5% glutaraldehyde in Tris buffer and stained with 1% uranylacetate. Measurement of filaments was done with ImageJ and evaluated in Microsoft Excel.

For feSEM the isolated HisMyc-NE81dNLS and AX2 control nuclei (30 µl and 60 µl) were diluted in 1 ml gradient buffer and spun down onto a silicon chip (Agar Scientific, UK) for 10 min at 2800x g (Heraeus Multifuge 1 S-R). Chips were then fixed in SEM buffer for at least 10 min and placed in a new 1.5 ml reaction tube filled with SEM buffer and shipped to the UK (Prof. Dr. Martin Goldberg). For SEM analysis the chips were washed briefly two times in deionised water, then placed in 0.1% OsO4 for 10 minutes, then washed briefly in water and dehydrated through an ethanol series, and critical point dried (Baltec CPD 030). Samples were then sputter coated with 1-2 nm chromium (Cressington, UK, model 328) and viewed in a Hitachi S-5200 field emission scanning electron microscope at 10kV accelerating voltage. Measurement of filaments was done with ImageJ and evaluated in Microsoft Excel.

5 References

Adam, S. A., **Sengupta, K.** & **Goldman, R. D.** 2008. Regulation of nuclear lamin polymerization by importin alpha. *J Biol Chem,* 283, 8462-8.

Adl, S. M., **Bass, D.**, **Lane, C. E.**, **Lukes, J.**, **Schoch, C. L.**, **Smirnov, A.**, **Agatha, S.**, **Berney, C.**, **Brown, M. W.**, **Burki, F.**, **Cardenas, P.**, **Cepicka, I.**, **Chistyakova, L.**, **Del Campo, J.**, **Dunthorn, M.**, **Edvardsen, B.**, **Eglit, Y.**, **Guillou, L.**, **Hampl, V.**, **Heiss, A. A.**, **Hoppenrath, M.**, **James, T. Y.**, **Karnkowska, A.**, **Karpov, S.**, **Kim, E.**, **Kolisko, M.**, **Kudryavtsev, A.**, **Lahr, D. J. G.**, **Lara, E.**, **Le Gall, L.**, **Lynn, D. H.**, **Mann, D. G.**, **Massana, R.**, **Mitchell, E. A. D.**, **Morrow, C.**, **Park, J. S.**, **Pawlowski, J. W.**, **Powell, M. J.**, **Richter, D. J.**, **Rueckert, S.**, **Shadwick, L.**, **Shimano, S.**, **Spiegel, F. W.**, **Torruella, G.**, **Youssef, N.**, **Zlatogursky, V.** & **Zhang, Q.** 2019. Revisions to the classification, nomenclature, and diversity of eukaryotes. *J Eukaryot Microbiol,* 66, 4-119.

Aebi, U., **Cohn, J.**, **Buhle, L.** & **Gerace, L.** 1986. The nuclear lamina is a meshwork of intermediate-type filaments. *Nature,* 323, 560-4.

Andresen, M., **Schmitz-Salue, R.** & **Jakobs, S.** 2004. Short tetracysteine tags to beta-tubulin demonstrate the significance of small labels for live cell imaging. *Mol Biol Cell,* 15, 5616-22.

Barth, C., **Fraser, D. J.** & **Fisher, P. R.** 1998. A rapid, small scale method for characterization of plasmid insertions in the *Dictyostelium* genome. *Nucleic Acids Research,* 26, 3317 - 3318.

Barton, R. M. & **Worman, H. J.** 1999. Prenylated prelamin A interacts with Narf, a novel nuclear protein. *J Biol Chem,* 274, 30008-18.

Batsios, P., **Baumann, O.**, **Gräf, R.** & **Meyer, I.** 2013. Isolation of *Dictyostelium* nuclei for light and electron microscopy. *Methods Mol Biol,* 983, 283-94.

Batsios, P., **Peter, T.**, **Baumann, O.**, **Stick, R.**, **Meyer, I.** & **Gräf, R.** 2012. A lamin in lower eukaryotes? *Nucleus,* 3, 237-43.

Batsios, P., **Ren, X.**, **Baumann, O.**, **Larochelle, D. A.** & **Gräf, R.** 2016. Src1 is a protein of the inner nuclear membrane interacting with the *Dictyostelium* lamin NE81. *Cells,* 5.

Beck, M. & **Hurt, E.** 2017. The nuclear pore complex: understanding its function through structural insight. *Nat Rev Mol Cell Biol,* 18, 73-89.

Ben-Harush, K., **Wiesel, N.**, **Frenkiel-Krispin, D.**, **Moeller, D.**, **Soreq, E.**, **Aebi, U.**, **Herrmann, H.**, **Gruenbaum, Y.** & **Medalia, O.** 2009. The supramolecular organization of the *C. elegans* nuclear lamin filament. *J Mol Biol,* 386, 1392-402.

Benavente, R., **Krohne, G.** & **Franke, W. W.** 1985. Cell type-specific expression of nuclear lamina proteins during development of *Xenopus laevis*. *Cell,* 41, 177-90.

Chaves, I., **Pokorny, R.**, **Byrdin, M.**, **Hoang, N.**, **Ritz, T.**, **Brettel, K.**, **Essen, L. O.**, **van der Horst, G. T.**, **Batschauer, A.** & **Ahmad, M.** 2011. The cryptochromes: blue light photoreceptors in plants and animals. *Annu Rev Plant Biol,* 62, 335-64.

Chozinski, T. J., **Halpern, A. R.**, **Okawa, H.**, **Kim, H. J.**, **Tremel, G. J.**, **Wong, R. O.** & **Vaughan, J. C.** 2016. Expansion microscopy with conventional antibodies and fluorescent proteins. *Nat Methods,* 13, 485-8.

Davidson, P. M. & **Lammerding, J.** 2014. Broken nuclei--lamins, nuclear mechanics, and disease. *Trends Cell Biol,* 24, 247-56.

de Leeuw, R., **Gruenbaum, Y.** & **Medalia, O.** 2017. Nuclear lamins: thin filaments with major functions. *Trends Cell Biol*.

Dechat, T., **Adam, S. A.**, **Taimen, P.**, **Shimi, T.** & **Goldman, R. D.** 2010. Nuclear lamins. *Cold Spring Harb Perspect Biol,* 2, a000547.

Dechat, T., **Pfleghaar, K.**, **Sengupta, K.**, **Shimi, T.**, **Shumaker, D. K.**, **Solimando, L.** & **Goldman, R. D.** 2008. Nuclear lamins: major factors in the structural organization and function of the nucleus and chromatin. *Genes Dev,* 22, 832-53.

Dhe-Paganon, S., **Werner, E. D.**, **Chi, Y. I.** & **Shoelson, S. E.** 2002. Structure of the globular tail of nuclear lamin. *J Biol Chem,* 277, 17381-4.

Dittmer, T. A. & **Misteli, T.** 2011. The lamin protein family. *Genome Biol,* 12, 222.

Eichinger, L., **Pachebat, J. A.**, **Glockner, G.**, **Rajandream, M. A.**, **Sucgang, R.**, **Berriman, M.**, **Song, J.**, **Olsen, R.**, **Szafranski, K.**, **Xu, Q.**, **Tunggal, B.**, **Kummerfeld, S.**, **Madera, M.**, **Konfortov, B. A.**, **Rivero, F.**, **Bankier, A. T.**, **Lehmann, R.**, **Hamlin, N.**, **Davies, R.**, **Gaudet, P.**, **Fey, P.**, **Pilcher, K.**, **Chen, G.**, **Saunders, D.**, **Sodergren, E.**, **Davis, P.**, **Kerhornou, A.**, **Nie, X.**, **Hall, N.**, **Anjard, C.**, **Hemphill, L.**, **Bason, N.**, **Farbrother, P.**, **Desany, B.**, **Just, E.**, **Morio, T.**, **Rost, R.**, **Churcher, C.**, **Cooper, J.**, **Haydock, S.**, **van Driessche, N.**, **Cronin, A.**, **Goodhead, I.**, **Muzny, D.**, **Mourier, T.**, **Pain, A.**, **Lu, M.**, **Harper, D.**, **Lindsay, R.**, **Hauser, H.**, **James, K.**, **Quiles, M.**, **Madan Babu, M.**, **Saito, T.**, **Buchrieser, C.**, **Wardroper, A.**, **Felder, M.**, **Thangavelu, M.**, **Johnson, D.**, **Knights, A.**, **Loulseged, H.**, **Mungall, K.**, **Oliver, K.**, **Price, C.**, **Quail, M. A.**, **Urushihara, H.**, **Hernandez, J.**, **Rabbinowitsch, E.**, **Steffen, D.**, **Sanders, M.**, **Ma, J.**, **Kohara, Y.**, **Sharp, S.**, **Simmonds, M.**, **Spiegler, S.**, **Tivey, A.**, **Sugano, S.**, **White, B.**, **Walker, D.**, **Woodward, J.**, **Winckler, T.**, **Tanaka, Y.**, **Shaulsky, G.**, **Schleicher, M.**, **Weinstock, G.**, **Rosenthal, A.**, **Cox, E. C.**, **Chisholm, R. L.**, **Gibbs, R.**, **Loomis, W. F.**, **Platzer, M.**, **Kay, R. R.**, **Williams, J.**, **Dear, P. H.**, **Noegel, A. A.**, **Barrell, B.** & **Kuspa, A.** 2005. The genome of the social amoeba *Dictyostelium discoideum*. *Nature,* 435, 43-57.

Evan, G. I., **Lewis, G. K.**, **Ramsay, G.** & **Bishop, J. M.** 1985. Isolation of monoclonal antibodies specific for human c-myc proto-oncogene product. *Mol Cell Biol,* 5, 3610-6.

Fisher, P. R. 2001. Genetic analysis of phototaxis in *Dictyostelium*. *In:* HÄDER, D.-P. A. L., M. (ed.) *Photomovement. ESP Comprehensive Series in Photosciences.* Amsterdam: Elsevier Science Ltd.

Foeger, N., **Wiesel, N.**, **Lotsch, D.**, **Mücke, N.**, **Kreplak, L.**, **Aebi, U.**, **Gruenbaum, Y.** & **Herrmann, H.** 2006. Solubility properties and specific assembly pathways of the B-type lamin from *Caenorhabditis elegans*. *J Struct Biol,* 155, 340-50.

Francione, L. M. & **Fisher, P. R.** 2011. Heteroplasmic mitochondrial disease in *Dictyostelium discoideum*. *Biochem Pharmacol,* 82, 1510-20.

Gao, M., **Maraspini, R.**, **Beutel, O.**, **Zehtabian, A.**, **Eickholt, B.**, **Honigmann, A.** & **Ewers, H.** 2018. Expansion stimulated emission depletion microscopy (ExSTED). *ACS Nano,* 12, 4178-4185.

Goldberg, M. W. & **Allen, T. D.** 1992. High resolution scanning electron microscopy of the nuclear envelope: demonstration of a new, regular, fibrous lattice attached to the baskets of the nucleoplasmic face of the nuclear pores. *J Cell Biol,* 119, 1429-40.

Goldberg, M. W., **Huttenlauch, I.**, **Hutchison, C. J.** & **Stick, R.** 2008. Filaments made from A- and B-type lamins differ in structure and organization. *J Cell Sci,* 121, 215-25.

Gräf, R., **Batsios, P.** & **Meyer, I.** 2015. Evolution of centrosomes and the nuclear lamina: Amoebozoan assets. *Eur J Cell Biol,* 94, 249-56.

Gräf, R., **Euteneuer, U.**, **Ho, T. H.** & **Rehberg, M.** 2003. Regulated expression of the centrosomal protein DdCP224 affects microtubule dynamics and reveals mechanisms for the control of supernumerary centrosome number. *Mol Biol Cell,* 14, 4067-74.

Gräf, R., **Euteneuer, U.**, **Ueda, M.** & **Schliwa, M.** 1998. Isolation of nucleation-competent centrosomes from *Dictyostelium discoideum*. *Eur J Cell Biol,* 76, 167-75.

Grafe, M., **Batsios, P.**, **Meyer, I.**, **Lisin, D.**, **Baumann, O.**, **Goldberg, M. W.** & **Gräf, R.** 2019. Supramolecular structures of the *Dictyostelium* lamin NE81. *Cells,* 8.

Grossman, E., **Dahan, I.**, **Stick, R.**, **Goldberg, M. W.**, **Gruenbaum, Y.** & **Medalia, O.** 2012. Filaments assembly of ectopically expressed *Caenorhabditis elegans* lamin within *Xenopus* oocytes. *J Struct Biol,* 177, 113-8.

Gruenbaum, Y. & **Foisner, R.** 2015. Lamins: nuclear intermediate filament proteins with fundamental functions in nuclear mechanics and genome regulation. *Annu Rev Biochem,* 84, 131-64.

Haas, M. & **Jost, E.** 1993. Functional analysis of phosphorylation sites in human lamin A controlling lamin disassembly, nuclear transport and assembly. *Eur J Cell Biol,* 62, 237-47.

Heitlinger, E., **Peter, M.**, **Haner, M.**, **Lustig, A.**, **Aebi, U.** & **Nigg, E. A.** 1991. Expression of chicken lamin B2 in *Escherichia coli:* characterization of its structure, assembly, and molecular interactions. *J Cell Biol,* 113, 485-95.

Heitlinger, E., **Peter, M.**, **Lustig, A.**, **Villiger, W.**, **Nigg, E. A.** & **Aebi, U.** 1992. The role of the head and tail domain in lamin structure and assembly: analysis of bacterially expressed chicken lamin A and truncated B2 lamins. *J Struct Biol,* 108, 74-89.

Hell, S. W. & **Wichmann, J.** 1994. Breaking the diffraction resolution limit by stimulated emission: stimulated-emission-depletion fluorescence microscopy. *Opt Lett,* 19, 780-2.

Hirth, K. P., **Edwards, C. A.** & **Firtel, R. A.** 1982. A DNA-mediated transformation system for *Dictyostelium discoideum*. *Proc Natl Acad Sci U S A,* 79, 7356-60.

Hofmann, P. 2019. *Lichtsensitive Regulation der Lamin-Polymerisation bei Dictyostelium discoideum.* Bachelor thesis, Universität Potsdam.

Isermann, P. & **Lammerding, J.** 2013. Nuclear mechanics and mechanotransduction in health and disease. *Curr Biol,* 23, R1113-21.

J. W. Strutt, I. L. R. 1989. Investigations in optics, with special reference to the spectroscope. *Philosophical Magazine,* VIII, 261; 403; 477.

Karabinos, A., **Schunemann, J.**, **Meyer, M.**, **Aebi, U.** & **Weber, K.** 2003. The single nuclear lamin of *Caenorhabditis elegans* forms *in vitro* stable intermediate filaments and paracrystals with a reduced axial periodicity. *J Mol Biol,* 325, 241-7.

Klauss, A., **Conrad, F.** & **Hille, C.** 2017. Binary phase masks for easy system alignment and basic aberration sensing with spatial light modulators in STED microscopy. *Sci Rep,* 7, 15699.

Klauss, A., **Konig, M.** & **Hille, C.** 2015. Upgrade of a scanning confocal microscope to a single-beam path STED microscope. *PLoS One,* 10, e0130717.

Kollmar, M. 2015. Polyphyly of nuclear lamin genes indicates an early eukaryotic origin of the metazoan-type intermediate filament proteins. *Sci Rep,* 5, 10652.

Koreny, L. & **Field, M. C.** 2016. Ancient eukaryotic origin and evolutionary plasticity of nuclear lamina. *Genome Biol Evol,* 8, 2663-71.

Kreplak, L., **Richter, K.**, **Aebi, U.** & **Herrmann, H.** 2008. Electron microscopy of intermediate filaments: teaming up with atomic force and confocal laser scanning microscopy. *Methods Cell Biol,* 88, 273-97.

Krohne, G., **Stuurman, N.** & **Kempf, A.** 1998. Assembly of *Drosophila* lamin Dm0 and C mutant proteins studied with the baculovirus system. *Eur J Cell Biol,* 77, 276-83.

Krüger, A., **Batsios, P.**, **Baumann, O.**, **Luckert, E.**, **Schwarz, H.**, **Stick, R.**, **Meyer, I.** & **Gräf, R.** 2012. Characterization of NE81, the first lamin-like nucleoskeleton protein in a unicellular organism. *Mol Biol Cell,* 23, 360-70.

Kuhnert, O., **Baumann, O.**, **Meyer, I.** & **Gräf, R.** 2012. Functional characterization of CP148, a novel key component for centrosome integrity in *Dictyostelium*. *Cell Mol Life Sci,* 69, 1875-88.

Kuspa, A., **Dingermann, T.** & **Nellen, W.** 1995. Analysis of gene function in *Dictyostelium*. *Experientia,* 51, 1116-23.

Lammerding, J., **Fong, L. G.**, **Ji, J. Y.**, **Reue, K.**, **Stewart, C. L.**, **Young, S. G.** & **Lee, R. T.** 2006. Lamins A and C but not lamin B1 regulate nuclear mechanics. *J Biol Chem,* 281, 25768-80.

Laurell, E., Beck, K., Krupina, K., Theerthagiri, G., Bodenmiller, B., Horvath, P., Aebersold, R., Antonin, W. & Kutay, U. 2011. Phosphorylation of Nup98 by multiple kinases is crucial for NPC disassembly during mitotic entry. *Cell,* 144, 539-50.

Levi, S., **Polyakov, M.** & **Egelhoff, T. T.** 2000. Green fluorescent protein and epitope tag fusion vectors for *Dictyostelium discoideum*. *Plasmid,* 44, 231-8.

Lisin, D. 2017. *Reinigung und Analyse von IF-Familie Proteinen aus Dictyostelium Amöben.* Bachelor thesis, Universität Potsdam.

Lochs, S. J. A., **Kefalopoulou, S.** & **Kind, J.** 2019. Lamina associated domains and gene regulation in development and cancer. *Cells,* 8.

Loomis, W. F., Jr. 1971. Sensitivity of *Dictyostelium discoideum* to nucleic acid analogues. *Exp Cell Res,* 64, 484-6.

Manabe, K. & **Poff, K. L.** 1978. Purification and Characterization of the Photoreducible b-type Cytochrome from *Dictyostelium discoideum*. *Plant Physiol,* 61, 961-6.

Maurer, M. & **Lammerding, J.** 2019. The driving force: nuclear mechanotransduction in cellular function, fate, and disease. *Annu Rev Biomed Eng,* 21, 443-468.

Meyer, I., **Kuhnert, O.** & **Gräf, R.** 2011. Functional analyses of lissencephaly-related proteins in *Dictyostelium*. *Semin Cell Dev Biol,* 22, 89-96.

Meyer, I., **Peter, T.**, **Batsios, P.**, **Kuhnert, O.**, **Kruger-Genge, A.**, **Camurca, C.** & **Gräf, R.** 2017. CP39, CP75 and CP91 are major structural components of the *Dictyostelium* centrosome's core structure. *Eur J Cell Biol,* 96, 119-130.

Meyfarth, O.-E. 2017. *Heterologe Expression von Xenopus Lamin LIII in Dictyostelium discoideum.* Bachelor thesis, Universität Potsdam.

Mikhaylova, M., **Cloin, B. M.**, **Finan, K.**, **van den Berg, R.**, **Teeuw, J.**, **Kijanka, M. M.**, **Sokolowski, M.**, **Katrukha, E. A.**, **Maidorn, M.**, **Opazo, F.**, **Moutel, S.**, **Vantard, M.**, **Perez, F.**, **van Bergen en Henegouwen, P. M.**, **Hoogenraad, C. C.**, **Ewers, H.** & **Kapitein, L. C.** 2015. Resolving bundled microtubules using anti-tubulin nanobodies. *Nat Commun,* 6, 7933.

Muñoz-Braceras, S., **Mesquita, A.** & **Escalante, R.** 2013. *Dictyostelium discoideum* as a model in biomedical research. *In:* ROMERALO, M., BALDAUF, S., ESCALANTE, R. (ed.) *Dictyostelids.Evolution, Genomics and Cell Biology.* Berlin/Heiderberg, Germany: Springer.

Nelson, M. D. & **Fitch, D. H.** 2011. Overlap extension PCR: an efficient method for transgene construction. *Methods Mol Biol,* 772**,** 459-70.

Osmani, A. H., **Davies, J.**, **Liu, H. L.**, **Nile, A.** & **Osmani, S. A.** 2006. Systematic deletion and mitotic localization of the nuclear pore complex proteins of *Aspergillus nidulans*. *Mol Biol Cell,* 17**,** 4946-61.

Pang, K. M., **Lynes, M. A.** & **Knecht, D. A.** 1999. Variables controlling the expression level of exogenous genes in *Dictyostelium*. *Plasmid,* 41**,** 187-97.

Peter, A. & **Stick, R.** 2015. Evolutionary aspects in intermediate filament proteins. *Curr Opin Cell Biol,* 32**,** 48-55.

Pitzen, V., **Askarzada, S.**, **Gräf, R.** & **Meyer, I.** 2018. CDK5RAP2 is an essential scaffolding protein of the corona of the *Dictyostelium* centrosome. *Cells,* 7.

Prüfert, K., **Vogel, A.** & **Krohne, G.** 2004. The lamin CxxM motif promotes nuclear membrane growth. *J Cell Sci,* 117**,** 6105-16.

Ralle, T., **Grund, C.**, **Franke, W. W.** & **Stick, R.** 2004. Intranuclear membrane structure formations by CaaX-containing nuclear proteins. *J Cell Sci,* 117**,** 6095-104.

Riemer, D. & **Weber, K.** 1994. The organization of the gene for *Drosophila* lamin C: limited homology with vertebrate lamin genes and lack of homology versus the *Drosophila* lamin Dm0 gene. *Eur J Cell Biol,* 63**,** 299-306.

Sachse, R., **Dondapati, S. K.**, **Fenz, S. F.**, **Schmidt, T.** & **Kubick, S.** 2014. Membrane protein synthesis in cell-free systems: from bio-mimetic systems to bio-membranes. *FEBS Lett,* 588**,** 2774-81.

Sasse, B., **Lustig, A.**, **Aebi, U.** & **Stuurman, N.** 1997. In vitro assembly of *Drosophila* lamin Dm0--lamin polymerization properties are conserved. *Eur J Biochem,* 250**,** 30-8.

Schulz, I., **Baumann, O.**, **Samereier, M.**, **Zoglmeier, C.** & **Gräf, R.** 2009a. *Dictyostelium* Sun1 is a dynamic membrane protein of both nuclear membranes and required for centrosomal association with clustered centromeres. *Eur J Cell Biol,* 88**,** 621-38.

Schulz, I., **Erle, A.**, **Gräf, R.**, **Krüger, A.**, **Lohmeier, H.**, **Putzler, S.**, **Samereier, M.** & **Weidenthaler, S.** 2009b. Identification and cell cycle-dependent localization of nine novel, genuine centrosomal components in *Dictyostelium discoideum*. *Cell Motil Cytoskeleton,* 66**,** 915-28.

Shimi, T., **Kittisopikul, M.**, **Tran, J.**, **Goldman, A. E.**, **Adam, S. A.**, **Zheng, Y.**, **Jaqaman, K.** & **Goldman, R. D.** 2015. Structural organization of nuclear lamins A, C, B1, and B2 revealed by superresolution microscopy. *Mol Biol Cell,* 26**,** 4075-86.

Shimi, T., **Pfleghaar, K.**, **Kojima, S.**, **Pack, C. G.**, **Solovei, I.**, **Goldman, A. E.**, **Adam, S. A.**, **Shumaker, D. K.**, **Kinjo, M.**, **Cremer, T.** & **Goldman, R. D.** 2008. The A- and B-type nuclear lamin networks: microdomains involved in chromatin organization and transcription. *Genes Dev,* 22**,** 3409-21.

Simon, D. N. & **Wilson, K. L.** 2013. Partners and post-translational modifications of nuclear lamins. *Chromosoma,* 122**,** 13-31.

Stick, R. & **Peter, A.** 2017. Evolutionary changes in lamin expression in the vertebrate lineage. *Nucleus,* 8**,** 392-403.

Strelkov, S. V., **Herrmann, H.** & **Aebi, U.** 2003. Molecular architecture of intermediate filaments. *Bioessays,* 25, 243-51.

Su, X. Z., **Wu, Y.**, **Sifri, C. D.** & **Wellems, T. E.** 1996. Reduced extension temperatures required for PCR amplification of extremely A+T-rich DNA. *Nucleic Acids Res,* 24, 1574-5.

Suckau, T. 2016. *Isolierung und Lokalisation von rekombinanten Lamin Mutanten in Dictyostelium discoideum und zellfreien System.* Master thesis. Universität Potsdam.

Sussman, R. & **Sussman, M.** 1967. Cultivation of *Dictyostelium discoideum* in axenic medium. *Biochem Biophys Res Commun,* 29, 53-5.

Tapley, E. C. & **Starr, D. A.** 2013. Connecting the nucleus to the cytoskeleton by SUN-KASH bridges across the nuclear envelope. *Curr Opin Cell Biol,* 25, 57-62.

Tatli, M. & **Medalia, O.** 2018. Insight into the functional organization of nuclear lamins in health and disease. *Curr Opin Cell Biol,* 54, 72-79.

Tillberg, P. W., **Chen, F.**, **Piatkevich, K. D.**, **Zhao, Y.**, **Yu, C. C.**, **English, B. P.**, **Gao, L.**, **Martorell, A.**, **Suk, H. J.**, **Yoshida, F.**, **DeGennaro, E. M.**, **Roossien, D. H.**, **Gong, G.**, **Seneviratne, U.**, **Tannenbaum, S. R.**, **Desimone, R.**, **Cai, D.** & **Boyden, E. S.** 2016. Protein-retention expansion microscopy of cells and tissues labeled using standard fluorescent proteins and antibodies. *Nat Biotechnol,* 34, 987-92.

Torvaldson, E., **Kochin, V.** & **Eriksson, J. E.** 2015. Phosphorylation of lamins determine their structural properties and signaling functions. *Nucleus,* 6, 166-71.

Turgay, Y., **Eibauer, M.**, **Goldman, A. E.**, **Shimi, T.**, **Khayat, M.**, **Ben-Harush, K.**, **Dubrovsky-Gaupp, A.**, **Sapra, K. T.**, **Goldman, R. D.** & **Medalia, O.** 2017. The molecular architecture of lamins in somatic cells. *Nature,* 543, 261-264.

Van Bortle, K. & **Corces, V. G.** 2013. Spinning the web of cell fate. *Cell,* 152, 1213-7.

Vietri, M., **Schink, K. O.**, **Campsteijn, C.**, **Wegner, C. S.**, **Schultz, S. W.**, **Christ, L.**, **Thoresen, S. B.**, **Brech, A.**, **Raiborg, C.** & **Stenmark, H.** 2015. Spastin and ESCRT-III coordinate mitotic spindle disassembly and nuclear envelope sealing. *Nature,* 522, 231-5.

Weeks, G. & **Weijer, C. J.** 1994. The *Dictyostelium* cell cycle and its relationship to differentiation. *FEMS Microbiol Lett,* 124, 123-30.

Wehland, J., **Willingham, M. C.** & **Sandoval, I. V.** 1983. A rat monoclonal antibody reacting specifically with the tyrosylated form of alpha-tubulin. I. Biochemical characterization, effects on microtubule polymerization *in vitro*, and microtubule polymerization and organization *in vivo*. *J Cell Biol,* 97, 1467-75.

Wiegand, S., **Kruse, J.**, **Gronemann, S.** & **Hammann, C.** 2011. Efficient generation of gene knockout plasmids for *Dictyostelium discoideum* using one-step cloning. *Genomics,* 97, 321-5.

Williams, K. L. & **Newell, P. C.** 1976. A genetic study of aggregation in the cellular slime mould *Dictyostelium discoideum* using complementation analysis. *Genetics,* 82, 287-307.

Xie, W., **Chojnowski, A.**, **Boudier, T.**, **Lim, J. S.**, **Ahmed, S.**, **Ser, Z.**, **Stewart, C.** & **Burke, B.** 2016. A-type lamins form distinct filamentous networks with differential nuclear pore complex associations. *Curr Biol,* 26, 2651-2658.

Zhang, Y., **Werling, U.** & **Edelmann, W.** 2012. SLiCE: a novel bacterial cell extract-based DNA cloning method. *Nucleic Acids Res,* 40, e55.

DANKSAGUNG

Ich bedanke mich bei meinem Doktorvater Prof. Dr. Ralph Gräf für das Thema, die große Unterstützung und die Freiheit, uneingeschränkt zu forschen.

Ich bedanke mich bei der gesamten AG Zellbiologie für das angenehme Arbeitsklima und die schöne Zeit.

Dr. Irene Meyer und Dr. Petros Batsios danke ich für die fachkundige Unterstützung.

Kristina Mitic und Valentin Pitzen danke ich für die vergnügliche Zeit in unserem Doktoranden Büro.

Sandra Pauluhn, Anita Guhlan und Cindy Marona danke ich für die Unterstützung.

Prof. Dr. Otto Baumann danke ich für die EM Bilder und die kritische Begutachtung.

Prof. Dr. Martin Goldberg und Sibylle Rüstig danke ich für die EM Bilder.

Dr. Andre Klauss danke ich für die Unterstützung bei der STED Mikroskopie.

Prof. Dr. Georg Krohne und Prof. Dr. Salvatore Chiantia danke ich für die Begutachtung.

Meinen Student(inn)en danke ich für ihr Engagement und ihre Lernbereitschaft.

Anne danke ich für die Durchsicht und die konstruktiven Anmerkungen.